



MAX-PLANCK-INSTITUT
FÜR POLYMERFORSCHUNG



JOHANNES GUTENBERG
UNIVERSITÄT MAINZ

NANOCAPSULES FOR UPTAKE, RELEASE AND SENSING IN CELLS

A dissertation submitted in partial fulfillment of
the requirements for the degree of
Doktor rerum naturalium (Dr. rer. nat.)

Submitted to
THE FACULTY OF BIOLOGY, JOHANNES GUTENBERG UNIVERSITY
Mainz, Germany

The doctoral thesis has been carried out at the
MAX PLANCK INSTITUTE FOR POLYMER RESEARCH
Mainz, Germany

RAWEEWAN THIRAMANAS

Born in Bangkok, Thailand

Mainz, February 2019

Thesis
Entitled

NANOCAPSULES FOR UPTAKE, RELEASE AND SENSING IN CELLS

The thesis was carried out from October 2015 until December 2018 in the department of Prof. Dr. Katharina Landfester in the group of Prof. Dr. Volker Mailänder at the Max Planck Institute for Polymer Research, Mainz, Germany.

Reviewer 1: [REDACTED]
[REDACTED]
[REDACTED]

Reviewer 2: [REDACTED]
[REDACTED]
[REDACTED]

Dean: [REDACTED]
[REDACTED]
[REDACTED]

Date of doctoral defence: March 2019

Content

Abstract.....	1
Introduction.....	4
Chapter A: Nanocapsule as a Nanocarrier for T-cells.....	8
A1: Silica Nanocapsule as a Suitable Nanocarrier: Uptake and Toxicity Study in T-cells.....	19
A2: Cellular Uptake of siRNA Loaded Nanocarrier to Knockdown PD-L1: Strategies to Improve T-cell Functions.....	39
Chapter B: Light-triggered Release from Nanocapsules	50
B1: Upconversion Nano-Carriers Encapsulated with Photoactivatable Ru Complexes for Near-Infrared Light-Regulated Enzyme Activity.....	62
B2: Photoactivation of Anticancer Ru Complexes in Deep Tissue: How Deep Can We Go?	76
B3: Red-Light-Controlled Release of Drug-Ru Complex Conjugates from Metallopolymer Micelles for Phototherapy in Hypoxic Tumor Environments	86
Chapter C: Nanocapsule as a Temperature Sensor in Living Cells.....	99
C1: Temperature Sensing in Cells by Polymeric Upconversion Nanocapsules.....	106
Materials and Methods.....	120
Summary and Outlook.....	132
Zusammenfassung.....	135
Literature.....	138
Declaration	146
Curriculum Vitae.....	147
Publication List.....	149
Acknowledgement.....	150

Abstract

Nanotechnology has emerged as a powerful tool for many biomedical applications including diagnostics, therapy, imaging, and sensing. A wide variety of advanced nanomaterials have been innovatively designed and synthesized to fulfill the requirements according to their applications. Among them, nanocapsules are some of the most interesting nanostructures and known to be commonly used for loading therapeutic agents or fluorescent dyes in order to have curing effects or tracking the capsule, respectively. The main function of the nanocapsule is to protect and transport cargo to target cells. It can also be created to enable release of a functional payload according to the stimuli used for a controlled release platform. Furthermore, responsive stimuli can be used for triggering the sensing unit and then emitting the signal as a reporter in the sensor system. Therefore, critical cytotoxicity must be determined before applying the loaded nanocapsules to the cells. Internalization of the capsule inside the cells must subsequently be investigated by flow cytometry and confirmed by confocal laser scanning microscopy. Finally, the specific functions/properties of the nanocapsules are verified.

With the aim of utilizing silica nanocapsules (SiNCs) to carry siRNA to CD8⁺ T-cell, an immune cell destroying virus-infected cells and cancer, a novel silica core-shell NC with various physicochemical properties including sizes, core hydrophilicities, surface charges, and surface functionalizations as well as serum concentrations in a culture medium were systematically examined for their effect on toxicity and uptake. It was found that different physicochemical characteristics of the SiNCs, especially sizes, and serum concentrations had a strong impact on cytotoxicity and cellular uptake. These findings can be used for the suitable design of nanocarriers and adjustments in culture conditions to avoid toxicity and promote the uptake of nanocarriers for T-cell immunotherapy. Subsequently, the SiNCs loaded with siRNA specific to *Pd-11* mRNA, which translates to a crucial immune checkpoint protein PD-L1 inactivating T-cell, were applied to the CD8⁺ T-cell. The results suggest that these siRNA loaded nanocarriers exhibit the potential for use in the delivery of siRNA into T-cells, enhancement of T-cell survival and functions by decreasing the expression of inhibitory protein PD-L1, increasing cell proliferation and specific T-cell activation

biomarkers CD25 and CD71, and can be applied in adoptive T-cell immunotherapy for the treatment of cancer.

Stimuli-responsive nanocarriers are of great interest for achieving the controlled release of functional payloads at a target site. Near infrared (NIR) light was used to trigger the enzyme inhibitor releasing platform. The system consisted of the upconversion nanoparticles (UCNP) and the ruthenium (Ru)-Cathepsin K enzyme inhibitor complex, which was loaded inside mesoporous silica nanocapsules. NIR light activated UCNPs resulted in the emission of blue light, which can cleave the light sensitive bond of Ru complex, then releasing the inhibitor and finally inhibiting the enzyme activity *in vitro*. In another system, red light was used instead of NIR light to trigger the Ru complex and showed deep penetration through thick tissue, which was still able to cleave the light sensitive bond, uncage the toxic product and finally kill HeLa cancer cells. With the significant potential of a red-light sensitive Ru complex releasing system, a micelles-containing Ru complex conjugated anti-cancer drug chlorambucil was developed. After red light stimulation, the anti-cancer product was cleaved and effectively killed HeLa cells, even under hypoxia simulated *in vitro* conditions and in tumor-bearing mouse *in vivo*. Due to the non-invasive method and spatiotemporal control, the light-responsive controlled release system provides a promising strategy for cancer therapy.

Temperature at the cellular level can be used to determine the metabolic state of cells such as anti-cancer drug metabolism. It could also be used to distinguish between cancer cells and normal cells. To measure intracellular temperature, light activated-polymeric upconversion nanocapsules (UCNCs) based on the temperature dependence of triplet-triplet annihilation upconversion (TTA-UC) phenomenon were developed. A cellular temperature measurement in the range of 22 to 40 °C was successfully obtained after red light activation. The novel nanothermometer exhibited the potential for use in treatment and diagnostics in the medical field.

These studies demonstrate the advantages of recently-developed nanocarrier systems, which can be used for cellular uptake, controlled release and intracellular sensing in living cells. The proof of concept systems reveals the critical factors involved in cytotoxicity and cellular uptake, ideas for innovatively and carefully designing the

delivery or sensing systems and new strategies for cancer therapy that can be applied in various bio-applications.

Introduction

(Note: The literature of the introduction can be found on page 138 at the end of the dissertation.)

According to the IUPAC, nanoparticles (NPs) are tiny materials defined with a size in the range of 1-100 nm.^[Z-1-2] They can be presented as particulate dispersions or as solid powders.^[Z-3] Similarly, the US Food and Drug Administration (USFDA), the International Organization for Standardization (ISO) and American Society for Testing Materials (ASTM) have provided their definitions of nanoparticles which are defined as a nano-object with at least one dimension in the size range from approximately 1 nm to 100 nm.^[Z-2,4] However, the British Standards Institution and the U.K. House of Lords Science and Technology Committee recommended that the definition of nanomaterials are not limited to a size under 100 nm but instead refer to ‘the nanoscale’ to ensure that all materials with a dimension under 1000 nm are considered.^[Z-5-6] Due to the size in nanoscale, NPs present unique physical and chemical properties. They provide a high surface to volume ratio, enhance cellular uptake, deliver water-insoluble drugs and possess size and shape dependent reactivity, as well as toughness and optical properties presented in different colors. These distinct characteristics make NPs suitable candidates for various kinds of applications.^[Z-3-4,7] NPs can be categorized into organic NPs such as polymeric nanospheres, nanocapsules, micelles, liposomes and dendrimers, and inorganic NPs such as silica NPs, carbon nanotubes, iron oxide NPs, gold NPs and quantum dots, as shown in **Figure 1**. Summaries focused on material use, cargo attachments, advantages and disadvantages are presented in **Table 1**.^[Z-8]

Nanocapsules and nanospheres are the two main types of polymeric nanoparticles, which are different in their morphology and architecture (**Figure 2**). Nanocapsules exhibit a typical core-shell structure consisting of a liquid core, in which either the hydrophilic or hydrophobic cargo is entrapped inside the interior cavity surrounded by a polymeric membrane made up of natural or synthetic polymers. Unlike nanocapsules, nanospheres are formed by dense polymers where the drug is homogeneously dispersed in the polymeric matrix.^[Z-9-11]

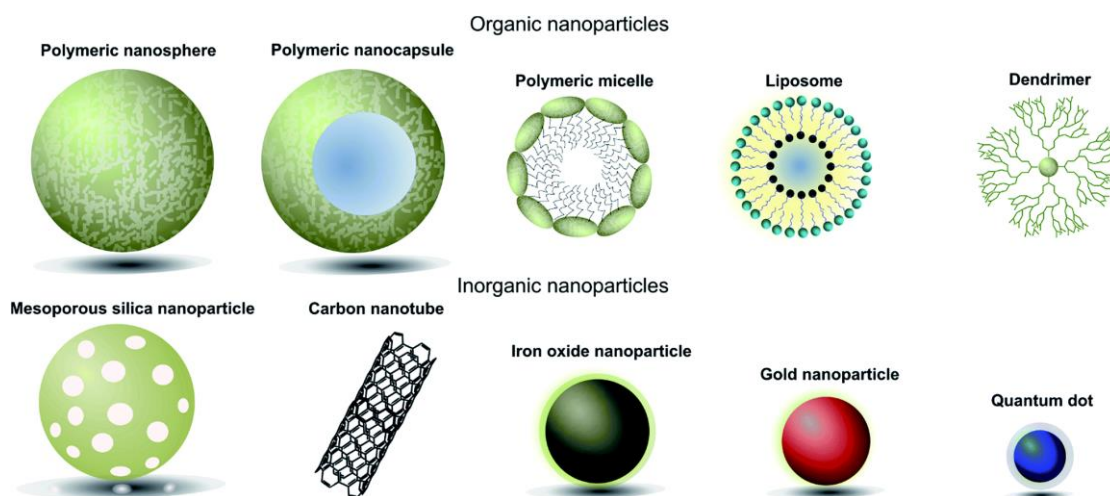


Figure 1. Different types of nanoparticles used in biomedical applications. (Taken from *Ref.* ^[Z-8] *Chemical Science*, 2016, 8(1), 63-77. Copyright © 2017 The Royal Society of Chemistry)

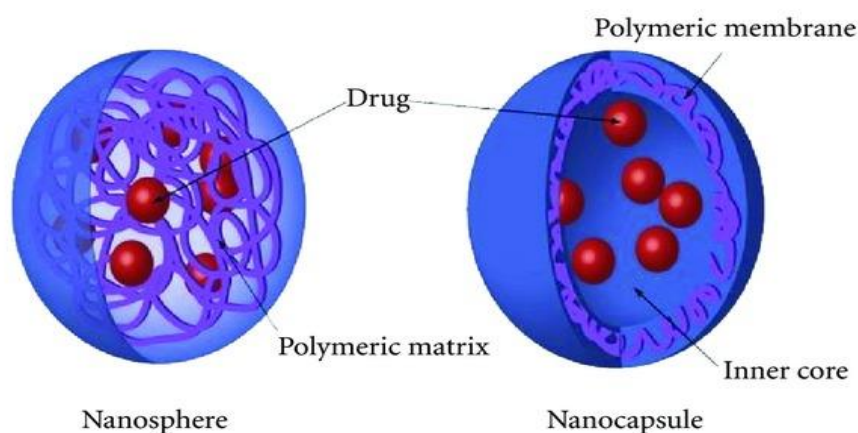


Figure 2. Difference in the morphology and architecture of nanospheres (matrix system) and nanocapsule (reservoir system). (Taken from *Ref.* ^[Z-11] *Mediators of Inflammation*, 2012, 126463. Copyright © 2012 John B. Christoforidis et al., original figure with Courtesy of Nanomedicine (2010) Future Medicine Ltd).

Polymeric nanocapsules have been widely developed for many decades and used as nano-sized carriers to achieve effective internalization, controlled release, and targeting as well as a sensitive cellular reporting system.^[Z-12]

Table 1. Summaries of different types of nanoparticles and their material use, cargo attachments, advantages and disadvantages. (Taken from *Ref.* ^[Z-8] *Chemical Science*, 2016, 8(1), 63-77. Copyright © 2017 The Royal Society of Chemistry)

Nanoparticle	Material(s)	Cargo attachment	Advantages	Disadvantages
Liposomes	Self-assembling lipid bilayer	Encapsulated within the hydrophilic core	Easily synthesised, biocompatible, high internal loading	Highly sensitive to structural changes and nature of payload
Polymeric micelles	Hydrophobic polymer core surrounded by hydrophilic polymeric chains	Encapsulated within the hydrophobic core	Small, biocompatible, able to incorporate highly hydrophobic cargo	Highly sensitive to structural changes, poor release profiles
Polymeric nanospheres/nanocapsules	Solid hydrophobic polymer matrix with optional aqueous core (nanocapsule)	Embedded in the polymer matrix or within the core	High loading capacity, flexible loading capabilities, reliable release profiles	Difficult to purify and poor store properties
Dendrimers	Highly branched polymer matrix	Embedded in the polymer branches	Highly soluble, non-immunogenic, high loading capacity, controlled synthesis	Lacking data on toxicity and biocompatibility
Iron oxide nanoparticles	Iron oxide core surrounded by biocompatible coating	Attached to the surface/ surface coating	Innate magnetic properties	No internal loading capacity
Gold nanoparticles	Solid gold particles typically coated with PEG chains	Attached to the surface/ surface coating	Innate optical and photothermal properties	No internal loading capacity, poor biocompatibility and biodegradability
Mesoporous silica nanoparticles	Mesopores surrounded by a silica framework	Encapsulated within the mesopores	High loading capacity, good biodegradability	Issues with physiological stability, rapid clearance rates
Carbon nanoparticles	Graphite arranged in either a sheet or cylindrical conformation	Attached to the carbon backbone	Innate optical and electrical properties, high surface loading capacities	Poor biodegradability, organ accumulation
Quantum dots	Typically a cadmium selenide core with a zinc selenide cap	Attached to the surface/ surface coating	Innate optical properties, high extinction coefficients	No internal loading capacity, potential toxicity issues

This work consists of three major sections aimed to develop a novel nanocarrier system, especially for nanocapsules which can be used for cellular uptake in **Chapter A**, controlled released in **Chapter B** and intracellular sensing in **Chapter C** for living cells. The recently developed systems demonstrated the potential for use according to their applications and proof of concept *in vitro*.

For **Chapter A**, intensive study of silica nanocapsules (SiNCs) uptake and toxicity was challenged in a well-known, “hard to transfect cell”, the T-cell. The crucial physicochemical properties of SiNCs and the culture component, such as serum concentrations that can form a “protein corona” on SiNC surface and affect cellular uptake as well as toxicity, were systematically investigated in CD8⁺ T-cells” in **Part A1**. Then, SiNCs loaded with siRNA specific to *Pd-11* mRNA translating to PD-L1, an important immune checkpoint protein, were applied to CD8⁺ T-cells and evaluated for knockdown efficiency at mRNA and protein levels, the cell proliferation and specific T-cell function biomarker expression in **Part A2**.

For **Chapter B**, light-responsive nanocarriers draw attention for use in stimuli responsive controlled release of functional payloads at specific target sites due to their non-invasive method and spatiotemporal control. The efficiency of NIR light triggered the inhibitor caging system, consisting of the upconversion nanoparticle (UCNP) and the ruthenium (Ru)-Cathepsin K enzyme inhibitor complex, which was loaded inside mesoporous silica nanocapsules and investigated from enzyme inhibition after NIR irradiation without or through a piece of tissue in **Publication B1**. Instead of NIR light, red light was used to activate the Ru complex and showed deep penetration through the thickness of the tissue, which was then evaluated to answer the question of potential depth, which remains able to uncage the toxic product and kill HeLa cells in **Publication B2**. The red-light sensitive, micelles-containing Ru complex conjugated anti-cancer drug chlorambucil was developed and investigated for the efficiency to kill HeLa cells under hypoxia simulated *in vitro* and tumor-bearing mice *in vivo* in **Publication B3**.

For **Chapter C**, the importance of developing a highly-sensitive, cellular temperature nanosensor that can determine the metabolic state of cells such as anti-cancer drug metabolism and might be used to identify cancer cells from healthy cells, motivated this study. Red-light stimulated-polymeric upconversion nanocapsules (UCNCs) based on the temperature dependence of triplet-triplet annihilation up-conversion (TTA-UC) phenomenon were synthesized and evaluated for potential use as a nanothermometer by measuring intracellular temperature in the range of 22 to 40 °C inside living HeLa cells in **Part C1**.

CHAPTER A

NANOCAPSULE AS A NANOCARRIER FOR T-CELLS

Chapter A combines two different parts. These studies propose the application of silica nanocapsules as suitable nanocarriers in T-cells by investigating the crucial physicochemical characteristics of silica nanocapsules on the impact of cellular uptake and toxicity in T-cells. They likewise demonstrate a strategy to improve T-cell survival and the function for adoptive T-cell immunotherapy for treatment of cancer using silica nanocapsules carrying specific siRNA-mediated gene silencing. A general introduction concerning T-cells, adoptive T-cell immunotherapy and recent advances in nanocarriers applied in T-cells will be described. Afterwards, each study will be presented separately.

(Note: The literature of the introduction can be found on page 138 at the end of the dissertation.)

[A1] **Rawewan Thiramanas,** [REDACTED]
[REDACTED] *Silica Nanocapsule as a Suitable Nanocarrier: Uptake and Toxicity Study in T-cells.* (Manuscript in preparation).

[A2] **Rawewan Thiramanas,** [REDACTED]
[REDACTED] *Cellular Uptake of siRNA Loaded Nanocarrier to Knockdown PD-L1: Strategies to Improve T-cell Functions.* (Manuscript in preparation).

A. Introduction

T-cells, one of the most important cells in an adaptive immune system, possess attractive intrinsic functions that enable the killing of virus-infected cells and cancer, which is highly impactful to the biomedical field. Many researchers have employed T-cells properties in so-called adoptive T-cell immunotherapy for cancer treatment.^[Z-13] The treatment is based on harvesting T-cells from cancer patients, growing and /or genetically modifying them to enhance their killing ability in terms of specificity and efficiency before reinfusing the T-cells back into the patient.^[Z-14] Compared to traditional cancer therapies including surgery, chemotherapy, and radiation therapy, this technique has several advantages such as being highly specific to target cancer cells. Therefore, adverse side effects to healthy tissue can be avoided as well as eliminate immune rejection because the therapeutic cells come from the patient, in addition to overcoming the problems of tumor re-occurrence and metastasis.^[Z-15] However, loss of T-cells viability and function naturally occurs due to time-consuming process and immuno-regulatory mechanism.^[Z-14,16] Therefore, another field of research in parallel to promote T-cells survival and efficacy has been intensively developed. For this purpose, many therapeutic agents such as antibodies, cytokine, and nucleic acids have been applied to T-cells using different methods such as systemic administration, electroporation, and by using nanocarriers.^[Z-17] With the progress in nanotechnology, various types of nanocarriers have been designed and used for the delivery of functional payloads into different kinds of target cells. Nanocarriers provide protection for the cargo from surrounding conditions and facilitating internalization.^[Z-3] Among them, silica nanomaterials exhibit high potential for use in a drug delivery system. Silica nanocarriers have many distinct advantages such as high loading capacity, chemical and physical stability, biocompatibility and biodegradability, and easy surface modification, making them good candidates for delivery to T-cells.^[Z-18] T-cells are well-known to be “the hard to transfect cells”, meaning they are difficult to uptake foreign particles. In addition, they are highly sensitive and easy to exhaust, making it a challenge to choose and design an appropriate nanocarrier.^[Z-19] Lack of study focused on nanocarrier uptake and toxicity in T-cells makes it more difficult to

understand which characteristics of nanocarriers should be carefully considered when applied to T-cells.

In Chapter A, crucial parameters including sizes, cores, charges and surface functionalizations of silica nanocapsules (SiNCs) that have impact on cellular uptake and toxicity in CD8⁺ T-cells were systematically investigated in **Part [A1]** to solve this problem. In addition, the effect of protein corona and serum in culture media on cellular uptake and toxicity were also studied to provide more criteria to consider when applying the nanocarriers in T-cells to achieve high uptake efficiency and low toxicity.

The uptake and toxic profiles were then used for designing the SiNCs carrying the specific siRNA to knockdown PD-L1, a potent inhibitory protein, in CD8⁺ T-cells in order to improve T-cells viability and function in **Part [A2]**. The knockdown efficiency was determined at protein and mRNA levels. The effects of PD-L1 knockdown were demonstrated in terms of cell proliferation and various functional biomarker expressions.

Here, the general background concerning the human immune system is described. The cancer-induced mechanisms for T-cell activation and inhibition, adoptive T-cell immunotherapy and recent advances in nanocarriers applied in T-cells are explained as well.

A.1 Human immune system

The human immune system consists of two major subsystems: innate immunity and adaptive immunity. Innate immunity is the first line of the defense mechanism and is not specific to any particular pathogen in the way that adaptive immune responses are. Although the innate immune system has evolved to quickly detect and destroy a variety of pathogens, the pre-existing set of common pathogenic molecular patterns, which are all established since in the germ line genome that it can recognize, is limited. Excessive variations of antigenic structures and the immune escape-induced mutation of pathogens are the driving forces in the evolution of the adaptive immune system or the acquired immune system, which can be found in vertebrates including birds, fish, amphibians, reptiles, and mammals. The slow response of adaptive immune responses is due to their hallmarks of learning to create highly-specific response and memorizing

processes, which are mediated by white blood cells called lymphocytes. During lymphocyte development, sets of gene segments are rearranged through a process of somatic recombination and assembled to create genes encoding the enormously diverse and specific antigen receptors of T and B lymphocytes to generate highly specific and flexible immune responses capable of recognizing all specific parts of pathogens, known as antigens. There are two major classes of adaptive immunity, humoral and cellular immunity, which are carried out by B-cells and T-cells, respectively.^[Z-20-22]

A.1.1 Adaptive humoral immunity

Adaptive humoral responses or antibody responses are mediated by antibodies, which involve proteins called immunoglobulins produced by plasma cells derived from B-cells. B-cells are so called because they are produced and mature in the bone marrow then travel to the lymphatic system to circulate throughout the body. As a result of somatic recombination, B-cells each carry a set of surface antigen-recognition molecules or membrane-bound antibodies called B-cell receptors (BCR). When B-cells bind an antigen that fits or matches its BCR, they will ingest, process and present digested peptide on MHCII through T-cell receptor (TCR) binding of CD4⁺ T-cells. Activated CD4⁺ T-cells produce stimulatory factors to help B-cells maturation and differentiation to become either a memory B-cell to be reactivated in the future or a plasma cell releasing large amounts of free antibodies specific to its activating-antigen. The antibodies circulate through the bloodstream and body fluids, where they search and bind specifically and directly to the antigens (either presented extracellularly on infected cells or free-floating in the body) that stimulate their production. Antibody binding neutralizes viruses and microbial toxins by blocking their ability to bind to receptors on host cells. In addition, the binding of antibodies also provides notable marking on invaders for targeted-extermination and facilitates engulfment by the phagocytic cells of the innate immune system.^[Z-22-24]

A.1.2 Adaptive cellular immunity

The adaptive cellular-mediated immune response is carried out by T-cells, which are so called because they mature in the thymus. The innate immunity phagocytic cells act by ingestion in the pathogen directly, whereas they serve as antigen-presenting

cells for adaptive immunity. Unlike the B-cells that can directly bind to antigen *via* BCR, T-cells need antigen-presenting cells to process and present small peptides of the antigen to T-cells *via* highly variable T-cell receptors (TCR). This receptor is generated by randomly assorting genes providing T-cells detection and response to a wide range of antigens. Antigen presentation results in the activation of T lymphocytes, the initiation of the adaptive response, and finally the destruction of the target cells *via* induction of apoptosis. T-cells characterized by the CD3 surface marker are categorized into 2 subtypes: the helper cell or regulatory T lymphocyte (T_{reg}) and the effector cell or cytotoxic T lymphocyte (CTL), which can be called $CD4^+$ and $CD8^+$ T-cells according to their unique cell surface markers, respectively. Similar to their names, helper T-cells ‘help’ other cells of the immune system, such as the maturation of B-cells and activation of CTLs, while CTLs kill virus-infected cells and tumors.^[Z-25-26]

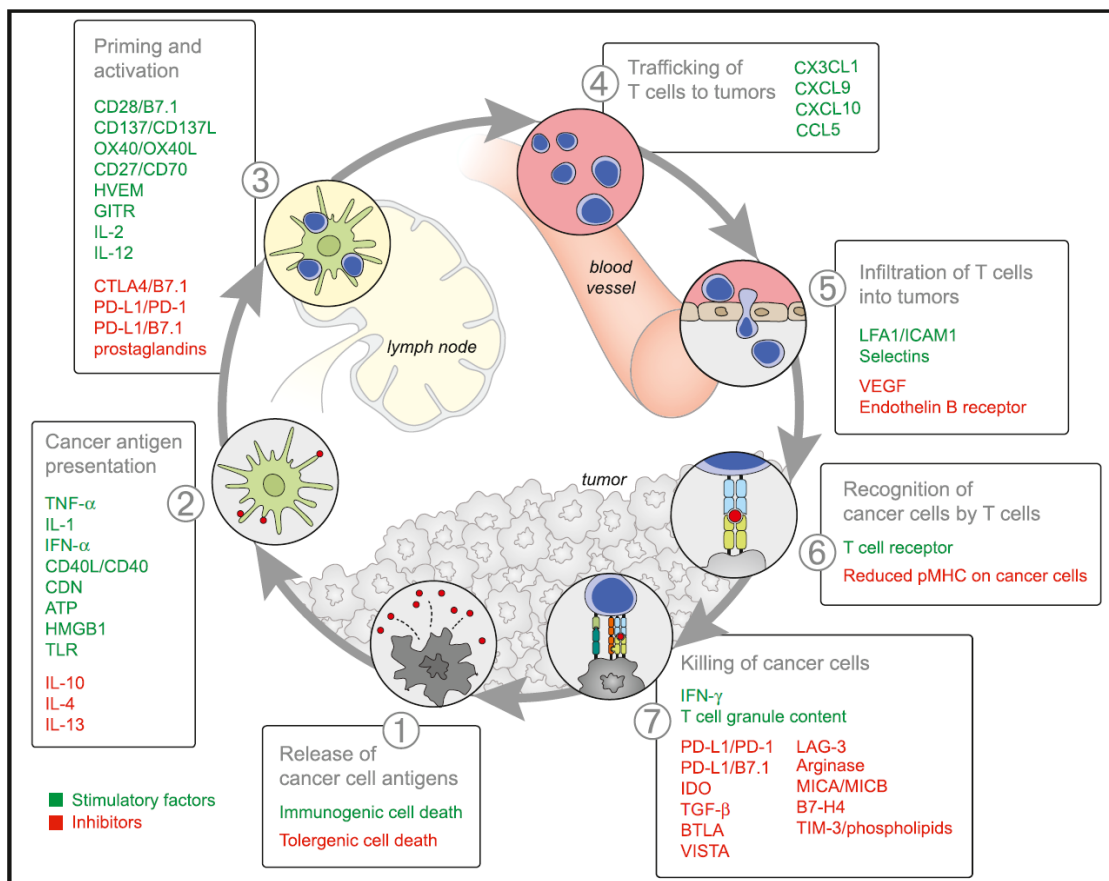


Figure A.1 Stimulatory (present in green) and inhibitory (present in red) factors in the Cancer-Immunity Cycle. Copyright @ 2013 Elsevier Inc. Reprinted with permission from Elsevier. Ref. ^[Z-27] Immunity. 2013, 39(1), 1-10.

A.2 T-cell Activation and the Cancer-Immunity Cycle

For cancer induced immune response, T-cells can be activated through a 7-stepwise complex process called the cancer-immunity cycle, as shown in **Figure A.1**.^[Z-27] In step (1), cancer cell antigens are released from dead cancer cells. Antigen presentation occurs in step (2), after which released antigens are detected, ingested and processed into small peptides by professional antigen-presenting cells (APCs) including dendritic cells (DCs), macrophages and B-cells. During maturation and migration to the lymph node, DCs lose their phagocytic function, but possess high expression of specific molecules called major histocompatibility complex class 1 (MHCI) and class 2 (MHCII) and co-stimulatory molecules such as CD40, CD80, CD83, and CD86 on their surfaces for efficient communication with T-cells.^[Z-28-30] DCs then present the exogenous peptides on MHCI and MHCII to TCR on CD8⁺ (called cross presentation) and CD4⁺ T-cells surfaces, respectively. As a result of mutation, abnormal cells can present endogenous antigens on MHCI which can be detected by CD8⁺ T-cells and stimulate immune response. Antigen presentation through TCR results in step (3) the priming and activation of CTLs that respond to cancer antigens are identified as foreign. Activated CTLs subsequently move through the blood stream (step 4) and infiltrate to the site of the tumor (step 5). After that, CTLs recognize and bind to the stimulating antigens present on MHCI of cancer cells through TCR (step 6), leading to the formation of a channel in order to introduce chemicals including granzymes (serine protease-destroying intracellular protein) and perforin (glycoprotein-forming a pore) as well as the activation of apoptosis and finally the killing of cancer cells (step 7). The dead cancer cells release their antigens and then continue to begin the cycle again to generate stronger immune responses.^[Z-27] Meanwhile, repeated TCR activation also induces proapoptotic pathways *via* the expression of Fas (CD95) ligand, a transmembrane protein that belongs to the tumor necrosis factor family, on the CTL surface, which then binds to Fas receptors on the target cell surface, triggering apoptosis.^[Z-22,31-32]

A.3 T-cell Inactivation and Cancer Immune Escape

Even though T-cells can recognize and efficiently destroy tumors through the Cancer-Immunity Cycle, in many cases the tumor cells are still able to remain,

proliferate and metastasize. These cancer resistance mechanisms are explained based on the concept of “immunoediting”, which consists of 3 phases.^[Z-33] Starting from “immune surveillance”, the immune cells can recognize tumor cells as non-self and progressively eliminate them. If one of the abnormal cells somehow survives immune elimination, scarce cells can generate offspring, which might begin the second phase of “immune equilibrium”, defined as a period during which our immune system and tumors live in a state of balance in the body. This means although the tumors cannot be killed, they cannot grow or metastasize. Because this phase is difficult to identify, the driving forces behind this phase are poorly understood.^[Z-34] During this state plus with immunosuppression in tumor microenvironment such as anaerobic acidic glucose-poor environment, tumor cells accumulate stress, metabolic changes and induced-mutation, leading to the last phase of “immune escape”, when tumors more aggressively progress, invade and metastasize out of control by the immune cells.^[Z-35]

Many chemical factors involved in the cancer-immunity cycle can stimulate or inhibit T-cell activation, as presented in **Figure A.1**.^[Z-27] Stimulatory factors present in green promote immune activity, while inhibitors present in red re-check the process and reduce immune response and/or prevent autoimmunity. Cancer cells smartly take advantage of these major immune checkpoint proteins, such as CTLA-4, PD-1, and PD-L1 to escape the immune system by expression of these checkpoints in order to imitate negative regulatory feedback inhibition when APCs communicate with T-cells.^[Z-36]

Cytotoxic T-lymphocyte associated protein-4 (CTLA-4) can inhibit the T-cell activation step (**Figure A.1**, step 3). Activation of T-cells not only needs the binding between MHC of APCs to TCR, but also co-stimulation between the B7 family, CD80 (B7.1) and CD86 (B7.2), of APCs to CD28 of T-cells. CTLA-4 possesses very high structural homology to the co-stimulatory molecule CD28 and a much higher affinity for both CD80 and CD86 than for CD28. Therefore, its expression on activated T-cells effectively blocks CD28-B7 interaction, resulting in the inactivation of T-cell responses.^[Z-35-37]

Like CTLA-4, programmed cell death 1 (PD-1, CD279) is expressed only in activated T-cells. PD-1 has two ligands which also belong to B7 family, PD-L1 (B7-H1, CD274) and PD-L2 (B7-DC, CD273). PD-L2 is predominantly expressed on APCs

as well as T-cells, whereas PD-L1 can be expressed on many non-hematopoietic and hematopoietic cells including tumor cells, immune cells, epithelial cells, and endothelial cells. T-cells stimulation can be inhibited in the tumor bed (**Figure A.1**, step 7) through PD-1/PD-L1 interaction, in which PD-L1 on the surface of DCs bind to PD-1 on the surface of T-cells, leading to T-cell exhaustion, which might contribute to cancer immune evasion.^[Z-35-37]

The identification of activated T-cell inhibitors, especially CTLA-4, PD-1 and PD-L1, has brought the revolution of checkpoint blockade to a new class of cancer immunotherapy for specifically blocking T-cell inhibition, reinforcing and potentially propagating preexisting anticancer immune responses.^[Z-27] The blockade of the PD-1/PD-L1 pathway was thought to yield greater antitumor activity and fewer side effects compared to CTLA-4 blockade.^[Z-38] Several drugs as checkpoint blockades have been approved and exhibited impressive responses at the clinical level, such as the anti-CTLA-4 antibody ipilimumab, which was approved in 2011 for use against advanced melanoma, and two anti-PD-1 antibodies, pembrolizumab and nivolumab, approved in 2014 for use against metastatic melanoma. Nowadays, these drugs are also under intensive investigation for use in the treatment of other cancers.^[Z-38]

A.4 Adoptive T-cell immunotherapy

Cancer immunotherapy is characterized by using the patient's own immune system to fight against cancer cells. The goal of cancer immunotherapy is to stimulate or restimulate a potential intrinsic cycle of cancer immunity, enabling it to multiply and function as anticancer activity under the optimal immune response to avoid unwanted autoimmune inflammatory response.^[Z-27] Cancer immunotherapy approaches include active immunization, reversal of immunosuppression, nonspecific immune stimulation and adoptive cell therapy (ACT). Among these approaches, ACT has achieved very promising results in cancer clinical trials and therefore is considered to be the most effective cancer immunotherapy.^[Z-15] In ACT, tumor-specific CTLs are collected from and infused into cancer patients with the aim of identifying and destroying tumor cells. CTLs used for ACT can be obtained from tumor-infiltrating lymphocytes (TILs) or peripheral blood lymphocytes, which can then be selected and used either in their natural state or genetically modified cancer-specific T-cells, such as T-cell receptor

(TCR)- and chimeric antigen receptor (CAR)-transduced T-cells.^[Z-14] The key to success of cancer immunotherapy is mainly dependent on the identification of potential cancer antigens that can be used for cancer vaccines, TILs activation and antigen-specific T-cells productions in TCRs and CARs.^[Z-15] TILs production requires 2 critical steps. The first step is the collection and separation of a lymphocyte culture from cancer tissue. This process takes up to 1 month and requires professional decisions by experts. Thus, the automated production process is impossible. The second step is a 14-day large-scale expansion process, which has been accomplished successfully using automated bioreactor. However, modified TCR or CAR cells are much easier to produce and require fewer total cells. Generally, peripheral blood lymphocytes are harvested, transduced with the desired gene and expanded to treatment levels. Because those T-cells are highly active, only low cell numbers are typically required for treatment.^[Z-16] TCR clones can also be produced by co-culturing peripheral blood T-cells with antigen presenting cells that express a specific tumor antigen. To evade immune surveillance, many cancers reduce the expression of MHC, resulting in inefficient T-cells activation due to decreased TCR-MHC interaction. To avoid this interaction, CAR molecules were developed. Combining the advantage of an antibody with a TCR, the CAR structure consists of an extracellular part, which is a ligand-binding domain containing a BCR-derived single-chain variable fragment, and a intracellular signaling domain, which is composed of CD3 ζ and one or more co-stimulatory domains e.g. CD28. Thus, the function of the CAR is independent of MHC interaction or any co-stimulatory signaling.^[Z-15-16,39-40]

A.5 Recent advances in nanocarriers applied in T-cells

Because therapeutic agents including plasmid DNAs, siRNAs, antibodies, enzymes, enzyme inhibitors, and drugs cannot spontaneously cross the cell membrane, delivery approaches are required.

Unfortunately, many of the traditional delivery strategies used in primary immune cells, especially in unstimulated cells and lymphocytes, have shown to be impractical for use due to their undesirable effects either for cell viability or cellular response.^[Z-41] Conventional lipid and cationic transfection reagents result in low transfection efficiencies and induce nonspecific inflammation in these cells because

these agents enter the cells by endocytic pathways. Hence, they trigger the immune response. Similar results also appear when using viral vectors for the same reasons and due to the presence of cytoplasmic viral nucleic acid sensors.^[Z-41] Besides, viral vectors also affect T-cell differentiation.^[Z-42] Electroporation/nucleofection, which allows small molecules such as plasmids, siRNAs or antibodies to pass into the cells through temporary pore formation induced by high voltages, gains satisfactory transfection efficiency. However, cell viability is commonly decreased after electroporation (typically $\approx 60\%$ survival rate), even with optimized voltages and conditions.^[Z-43] Therefore, various kinds of nanocarriers have been developed, used, and reported on as new delivery systems for T-cells with the aim of protecting the cargo, internalizing to the cells and releasing the functional payloads while reducing or eliminating unwanted effects on the cells either for improved T-cells viability and functionality against virus-infected cells or cancers, immunological network study, or for T-cells targeting.

Liu et al. ^[Z-44] modified single-walled carbon nanotubes (SWNT) to enhance hydrophilicity, functionalized with cleavable disulfide bonds conjugated to siRNAs and used to transport siRNA specific to CXCR4 chemokine receptor and CD4 to human T-cells and primary cells with the aim of inhibiting HIV viral entry and minimizing infection. The siRNA mediated these target gene silencing has been observed and exhibited superior performance to that observed with conventional liposome- based non-viral delivery agents.

Lee et al. ^[Z-45] evaluated siRNA delivery to T-cells by chitosan, a derivative of the natural polysaccharide chitin, using nanoparticles which were chemically conjugated to a T-cell-targeting CD7-specific single-chain antibody having a diameter of 320 nm. Silencing of CD4 expression was observed when the Jurkat leukemic T-cell line was incubated with these particles *in vitro*.

Yosef et al. ^[Z-41,46] established new delivery technology by culturing and stabbing primary T-cells on vertical silicon nanowires (NWs) precoated with specific biomolecules including siRNAs, plasmids, peptides, and proteins, which were delivered effectively ($>95\%$) to the cells without stimulation or alteration of viability. Interestingly, the NWs exhibited consistent penetration to the cellular membranes without impacting cell health or morphology. Later, potent silencing of 34 gene targets

was used to simulate a model of the dynamic regulatory network that controls Th17 differentiation.

From the intensive review of Freeley and Long^[Z-19], SWNTs, chitosan nanoparticles and vertical silicon NWs have only been used to answer basic biological questions. However, therapeutic applications in T-cells have not yet been investigated.

Dendrimers, which are highly-branched synthetic polymers, can form with siRNAs through electrostatic interactions. Carbosilane dendrimers by Weber et al. or PAMAM [poly(amidoamine)] dendrimers by Zhou et al.^[Z-47] have been formed with HIV genes-specific siRNAs and shown to inhibit viral replication in T-cell lines and PBMCs *in vitro*.^[Z-48] A strategy to target siRNA delivery was developed by Felber et al.^[Z-49] using antibody-conjugated PAMAM dendrimers, which resulted in enhanced uptake and more potent gene silencing in a prostate cancer cell line, suggesting that antibody-conjugated dendrimers could be a potential T-cell specific siRNA delivery approach.^[Z-19]

The most creative and effective siRNA delivery system described to date for targeting leucocytes and T-cells *in vivo* is I-tsNPs (integrin-targeted stabilized nanoparticles), established by Peer et al.^[Z-19,50] In this system, siRNAs are condensed with the nucleic-acid binding protein protamine and subsequently encapsulated within 100 nm diameter liposome nanoparticles resulting in a ~4000:1 ratio of siRNAs to nanoparticles, which may have significant potential for the improvement of human T-cell function due to their high loading capacity.

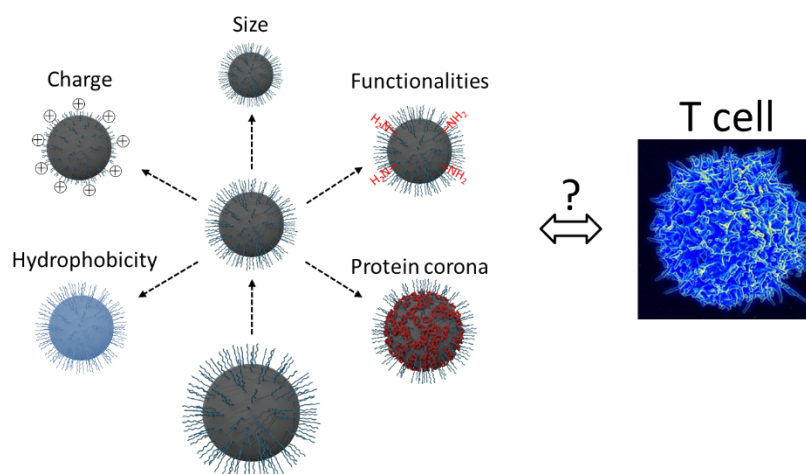
Delivery systems for the targeting of T-cells and avoiding of endocytic activities reduction were developed by Frick et al.^[Z-51] using cytokine interleukin-2 (IL-2) coupled to the surface of hydroxyethyl starch (HES) nanocapsules. The system demonstrated direct and specific T-cell targeting *in vitro* and *in vivo* by IL-2 receptor-mediated internalization. The results suggest that engineering IL-2-functionalized nanocapsules can be used for the efficient targeting of T-cell populations with different IL-2 receptor affinities. It may also be applied to other cytokine-related targeting systems.

A1: SILICA NANOCAPSULE AS A SUITABLE NANOCARRIER: UPTAKE AND TOXICITY STUDY IN T-CELLS

(Note: The literature of the chapter A1 can be found on page 35 at the end of this chapter.)

Permission: The manuscript is under preparation.

Contribution: I carried out the biological part including cytotoxicity, cellular uptake study by flow cytometry, cell imaging by cLSM, and protein corona effect on cellular uptake as well as protein pattern analysis by SDS-PAGE. ██████████ synthesized and characterized the SiNCs. ██████████ performed the cellular uptake progress. The project was supervised by ██████████.



TOC A1: The crucial physico-chemical parameters including sizes, cores, charges and surface functionalizations of silica nanocapsules (SiNCs) as well as the effect of protein corona and serum in culture media were systematically investigated for impact on cellular uptake and toxicity in CD8⁺ T-cells. This study provides the criteria for the suitable design of nanocarriers and the culture conditions to carefully consider when applying the nanocarriers in T-cells *in vitro* to facilitate uptake while avoiding toxicity.

Aim: With the lack of uptake and toxicity profile of SiNCs in T-cells, this study aimed to investigate the effect of physico-chemical characteristics of SiNCs on cellular uptake and toxicity in CD8⁺ T-cells as well as aimed to provide more criteria to consider when applying the nanocarriers in T-cells to achieve high uptake efficiency and minimize toxicity.

Abstract: Adoptive T-cell immunotherapy brings hope to cancer patients. It emerges as a powerful and promising cancer therapy so the problem regarding the immunoreaction between different donors and recipients can be avoided. However, a new problem based on the nature of the T-cell itself is problematic. After long cultivation and expansion under laboratory media conditions, T-cells start to lose their viability and function because of the immune checkpoint proteins, leading to decreased efficiency in killing cancer cells. A new strategy to improve T-cell survival and function is needed. With the advantages of nanotechnology and the biocompatibility of silica-based material, silica nanocapsules (SiNCs) provide an ideal delivery system for the use as nanocarriers to transport therapeutic biomolecules to T-cells. Due to the lack of uptake study concerning T-cells, various physico-chemical properties such as sizes, charges, and surface functionalities of SiNC were systematically studied in this work for their impact on cellular uptake and toxicity in CD8⁺ T-cells. The obtained results are discussed to improve the appropriate design of nanocarriers with low toxicity and high uptake for T-cell immunotherapy. The effect of protein corona from human serum and the serum present in culture medium on the uptake of different SiNCs was also investigated to provide more information to consider for suitable uptake conditions in SiNC in CD8⁺ T-cells.

A1.1. Introduction

Adoptive T-cell immunotherapy (ACT) is the new era of cancer therapy. It can be used to destroy cancer cells by using the immune cells from the patients themselves.^[A1-1] Compared to traditional cancer therapies including surgery, chemotherapy and radiation therapy, immunotherapy has several distinct advantages including no immune reaction (due to the same donors and recipients), high specificity, and high cancer-killing ability (due to intrinsic functionalities of T-cells, which are able to recognize and destroy cancer cells).^[A1-2] It was mentioned that this therapy may overcome the problem of tumor recurrence after surgery and also defeat late-stage cancer, which has very limited options in terms of traditional cancer therapies.^[A1-2] However, the problem of this technique is that we have relied on naturally controlling the mechanism of the immune system. After a certain time of activation, the expression of the immune check

point proteins from either the other immune cells e.g. dendritic cells or T-cell itself will be induced, causing T-cell inactivation and leading to a loss of T-cell survival and function.^[A1-3-5] This situation also occurs in T-cell cultivation for immunotherapy after collection from the patient and activating in culture media, resulting in decreased efficacy for cancer treatment.^[A1-3-5] With significant achievements in ACT and a very promising cancer therapy, research focused on the improvement of T-cell survival and function has been intensively pursued and reported. ^[A1-1-2,4-5] A wide range of therapeutic agents have been used to boost immunity including vaccines,^[A1-6] monoclonal antibodies,^[A1-7] cytokines,^[A1-8,9] siRNAs specific-immune checkpoint proteins such as cytotoxic T lymphocyte-associated molecule 4 (CTLA-4), ^[A1-10] Casitas B-lineage lymphoma b (Cbl-b),^[A1-11] programmed cell death-1 (PD-1), ^[A1-12] and their ligands (PD-L1/PD-L2).^[A1-13] To achieve this goal, an efficient delivery system loaded with specific biomolecules such as drugs, nucleotides, peptides, proteins, and fluorescent dyes is needed in order to obtain the biological effect or track the carrier.

The criteria for an ideal delivery system require abilities to protect the payload against culture environment and low pH in endosome/lysosome. Internalization into the cell without toxicity and without immune response initiation as well as subsequent release of the payload, which is still able to function inside the cell, is also required. ^[A1-14] Due to the rapid development of nanotechnology, a variety of nanocarriers have been designed and widely applied in various fields, especially for biomedical applications. ^[A1-15] Nano-sized carriers provide high surface to volume ratio, protect cargo from the biological environment before encountering the target cell, and facilitate uptake. Among them, silica nanocapsules (SiNCs) have many great advantages including high loading capacity, excellent colloidal and chemical stability, biocompatibility and biodegradability.^[A1-16] With their outstanding properties, silica-based nanocapsules (SiNCs) have been widely used for drug delivery for many decades.^[A1-16-17] SiNCs are not only easy to synthesize in various well-defined controllable sizes, but also facile to modify for different surface functionalities through the rich hydroxyl groups on their surface. Moreover, silicon oxide has been accepted by the U.S. Food and Drug Administration (USFDA) for use in food additives as well as medical care products.^[A1-16-17] Thus, SiNCs seem to be suitable for use as alternative nanocarriers in T-cells.

Due to its nature, a T-cell is a type of cell that is difficult to uptake foreign particles and is highly sensitive to the environment and dies easily.^[A1-18] Few uptake studies of silica nanomaterials in T-cells or related-cells have been reported. Silica nanoparticles (SiNPs) were found to induce oxidative stress and the inflammation of human peripheral blood mononuclear cells (PBMCs). Notably, smaller-sized SiNPs with 10 nm were more cytotoxic and induced more oxidative stress than the bigger SiNPs with 100-nm.^[A1-19] In addition, ultra small SiNPs (<10 nm) were also found to cause T-cell activation by increasing the expression of CD25 and CD69 and the secretion of IFN- γ .^[A1-20] The toxicity of SiNPs was found to be strongly related to their physico-chemical properties, such as size, surface area, and surface features.^[A1-21] Due to the lack of systematic study in terms of various physico-chemical parameters of the silica nanocarriers uptake in T-cell, greater understanding is required concerning the critical properties of SiNC which affect T-cell uptake prior to use of SiNC as a carrier for T-cell immunotherapy.

This study aims to investigate the crucial parameters including different sizes, cores, charges, and surface functionalizations of the SiNCs affecting cellular uptake in CD8⁺ T-cells. For this purpose, novel silica core-shell nanocapsules were synthesized. In general, the therapeutic payload is encapsulated in the SiNC cavity by immersing the SiNCs in a therapeutic solution and allowing the agent to diffuse into its cavity. Here, we used a new one-pot synthesis to facilitate incorporate the payload into the core surrounded with silica shell, which can be beneficial for ensuring the protection of the cargo inside the silica shell. It also provides high loading capacity for the cargo. To avoid interfering with its surface properties, Cy5 dye was incorporated with the shell by using fluorescently labeled silica precursors, which allowed tracking of the capsule inside the cell by flow cytometry and was further confirmed by confocal laser scanning microscopy. Considering *in vivo* uptake for systemic administration, once the nanocarrier faces the biological fluid, the biomolecular components e.g. blood proteins attracted to the carrier surface then create a new identity formed as protein corona, finally impact to cellular uptake.^[A1-22] Not only *in vivo* biological surrounding, but also *in vitro* culture condition needed to be considered. Therefore, further investigation of the effect of protein corona from human serum was carried out, while the effect of

serum in the medium on cellular uptake was studied to provide more criteria to consider for inhibiting or enhancing the uptake of SiNC in CD8⁺ T-cells. The uptake and toxicity of human serum pre-coated SiNCs compared to the uncoated ones were determined by flow cytometry. The SiNCs before and after performing corona were characterized by size-zeta potential analysis. The hard protein corona was demonstrated in the corona pattern on SDS-PAGE and could subsequently be identified by liquid chromatography–mass spectrometry (LC-MS). A better understanding of the consequences of different physico-chemical parameters for SiNCs on cellular uptake in CD8⁺ T-cells will provide information to carefully consider when designing the SiNCs for T-cell immunotherapy.

A1.2. Results and discussion

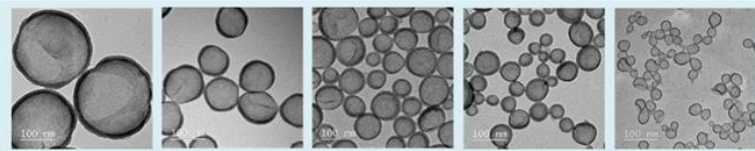
In the following study, we investigated the effect of different characteristics including sizes, surface charges, functional groups, and protein interactions of SiNCs on cellular uptake and toxicity in CD8⁺ T-cells.

A1.2.1 The effect of size

In the first section, we studied the size effect of nanocarriers on cellular uptake in T-cells. Silica nanocarriers (NCs) with hydrodynamic diameters ranging from 400 nm to 50 nm were synthesized by using a mini-emulsion (oil-in-water) polymerization technique.^[A1-23] Cationic surfactant cetyltrimethylammonium chloride (CTAC) was used for stabilizing mini-emulsion droplets against coalescence. The second role of CTAC is to serve as a template agent for confined silica condensation at the nanodroplet-water interface *via* cooperative self-assembly of negatively charged silica species and cationic CTAC. Therefore, positively charged core-shell nanocapsules were obtained with a liquid core that provides a high loading capacity for therapeutic agents. To compare the effect of different charges, Lutensol AT50 (LUT) was chosen as another surfactant to generate differently charged core-shell nanocapsules. Here, we developed a facile dialysis process for the surfactant replacement from CTAC to nonionic surfactant LUT, which has a polyethylene chain as its hydrophilic part. The PEGylated surface could then provide steric stabilization of the nanocapsules. The size of the nanocapsules was tuned by varying the volume ratio of the oil phase and water

phase. NCs with average hydrodynamic diameters ranging from 400 nm (NC-400) to 50 nm (NC-50) are shown in **Table A1.1**. The obtained NCs were characterized in terms of their physico-chemical properties, including hydrodynamic diameter size (D_h) by multi-angle dynamic light scattering (DLS), surface charge by zeta-potential (ζ -potential) measurement, and morphology by transmission electron microscopy (TEM), as listed in **Table A1.1**.

Table A1.1. Characteristics of silica nanocarriers (NCs) with different sizes.

		Hydrophilic core, NC(i)				
		NC-400	NC-200	NC-150	NC-100	NC-50
D_h (H ₂ O) /nm	CTAC	395 ± 232	190 ± 83	144 ± 45	99 ± 40	42 ± 18
	LUT	482 ± 299	148 ± 56	121 ± 47	106 ± 46	56 ± 29
ζ -potential (H ₂ O) /mV	CTAC	-4.4 ± 0.1	-5.0 ± 0.3	4.7 ± 0.2	8.8 ± 0.1	21.5 ± 2.3
	LUT	-4.2 ± 0.2	-6.3 ± 0.3	-4.7 ± 1.0	-3.5 ± 2.5	-11.2 ± 1.6
Morphology by TEM	CTAC					

After 24 h of incubation in CD8⁺ T-cells, the toxicity and uptake of NCs were determined by using flow cytometry. It was found that the toxicity of the capsules was increased when the size decreased, especially for CTAC-stabilized SiNCs (**Figure A1.1a**). A similar trend was also found when SiNPs (1–100 nm) were applied *in vitro* and *in vivo*, leading to cytotoxicity.^[A1-21] When applying the same mass, a distinct size dependent toxicity was clearly observed in CD8⁺ T-cells in this study and also reported in other cell types such as A549 (human type II alveolar epithelial), HaCaT (human keratinocyte), THP-1 (human monocyte), NRK-52E (rat kidney epithelial),^[A1-24] HepG2 (human hepatoma),^[A1-25] Langerhans (dendritic cells of the skin),^[A1-26] and EAHY926 (human endothelial).^[A1-27] It was revealed that the toxicity of SiNPs was strongly related to their physico-chemical properties such as size, surface area, and surface features.^[A1-21,28-31] If there are some features associated with toxicity on the surface, smaller size SiNCs provide more surface area as well as more surface reactivity and higher number of particles per mass, resulting in higher toxicity compared to the

larger size particles, as previously described by others.^[A1-24,31,32] In addition, the higher surface area of small SiNCs can lead to a higher possibility of interaction with cellular biomolecules such as DNA, proteins and sugars.^[A1-30] Another study also demonstrated that small SiNPs (70 nm; 10–90 µg/mL for 24 h) increased the oxidative DNA damage (8-OH-dG levels) in HaCaT cells.^[A1-33] Murugadoss et al. observed that SiNPs could cause overproduction of reactive oxygen species (ROS) resulting in oxidative stress, which could possibly damage the sub-cellular organelles and induce apoptosis in a size- and dose-dependent manner.^[A1-17] The mechanism of SiNPs induced toxicity is still not fully elucidated, but it is believed to be derived from ROS-mediated toxicity.^[A1-17,28,33] This might explain the toxicity of small-sized SiNCs. Moreover, small size NPs may cause toxicity as they pass through the cell membrane and enter the cells.^[A1-29-30,34] Some small NPs (< 50 nm) seem to enter the cells *via* passive diffusion, leading to directly facing cellular components or accumulating in subcellular organelles like mitochondria and nucleus. Another mechanism of small NPs induced toxicity when they are entering to the cells is actin cytoskeleton disruption as a result of NP internalization by endocytosis events, leading to cell deformation and direct cellular injury.^[A1-29-30,34] Even silica-based materials are generally accepted for their biocompatibility and silicon oxide was approved by the USFDA. However, the toxicology of silica nanoparticles (SiNPs) still remains to be reported.^[A1-16-17,28] Besides toxicity, the size-dependent immunological effects of SiNPs in immune cells including monocytes and macrophages were found. It was indicated that nano-sized particles caused a significant increase in pro-inflammatory secretion such as tumor necrosis factor-alpha (TNF- α) compared to sub-micron and micron sized particles.^[A1-17] Since the size of SiNCs was the critical point to induce the cytotoxic effect, the SiNC size was attempted to be controlled at sizes larger than 100 nm for subsequently experiments to avoid toxicity due to the smaller size.

SiNCs with smaller sizes were found to not only be highly toxic, but also have been less taken up by the cells (**Figure A1.1b**). In general, small-sized nanoparticles (< 100 nm) exhibited a stronger ability to be internalized inside cancer cells and were even able to pass through the blood-brain barrier compared to the larger size nanoparticles.^[A1-35] However, small-sized SiNCs they could not be applied in this study

due to their toxicity. The NCs were probably internalized by the cells at high speed, causing cell death.^[A1-24] Not all dead cells were considered for fluorescence positive-cells. The uptake of larger SiNCs (NC-400, NC-200 and NC-150) was further confirmed by cLSM (**Figure A1.1c**). Green dots representing Cy5 labeled-SiNCs were observed inside the cells, indicating efficient cellular uptake. Moreover, the aggregation or clumping pattern of T-cells treated with LUT-stabilized SiNCs was observed indicating healthy cells or the proliferation stage of the cells, which was emphasized by the excellent biocompatibility of LUT-stabilized SiNCs. The result was compared with hydrophobic Cy5 dye (free dye) treated cells to prove that all the results from Cy5-covalented SiNCs in this study were obtained from the dye labeled capsules and not from free dye (**Figure A1.2**). A co-localization assay of the biggest size, NC-400 with lysosome, was also demonstrated (**Figure A1.1d**). The cLSM images showed that the SiNC-Cy5 (green dots) were co-localized with lysosomes (red dots) after 24 h of incubation and appeared as yellow dots, as indicated with white arrows presented in the merged channel, which is a solid proof of cellular uptake. The uptake was confirmed for Cy5 positive-cells. It was also applied through all experiments, which means that all SiNCs were indeed taken up by the cell.

A1.2.2 The effect of core hydrophobicity and surface charges

In the second step, we studied the effect of core hydrophobicity and surface charges of nanocarriers on their cellular uptake in CD8⁺ T-cells. Nanocapsules containing olive oil and water as core materials were synthesized as representative hydrophobic (NC(o)) and hydrophilic (NC(i)) core NCs. Hydrophilic core and hydrophobic core SiNCs can be used to carry water-soluble and water-insoluble therapeutic agents to T-cells, respectively. These NCs are stabilized by using cetyltrimethylammonium chloride (CTAC), Lutensol AT50 (LUT) and Tween (T), as characterized and listed in **Table A1.2**.

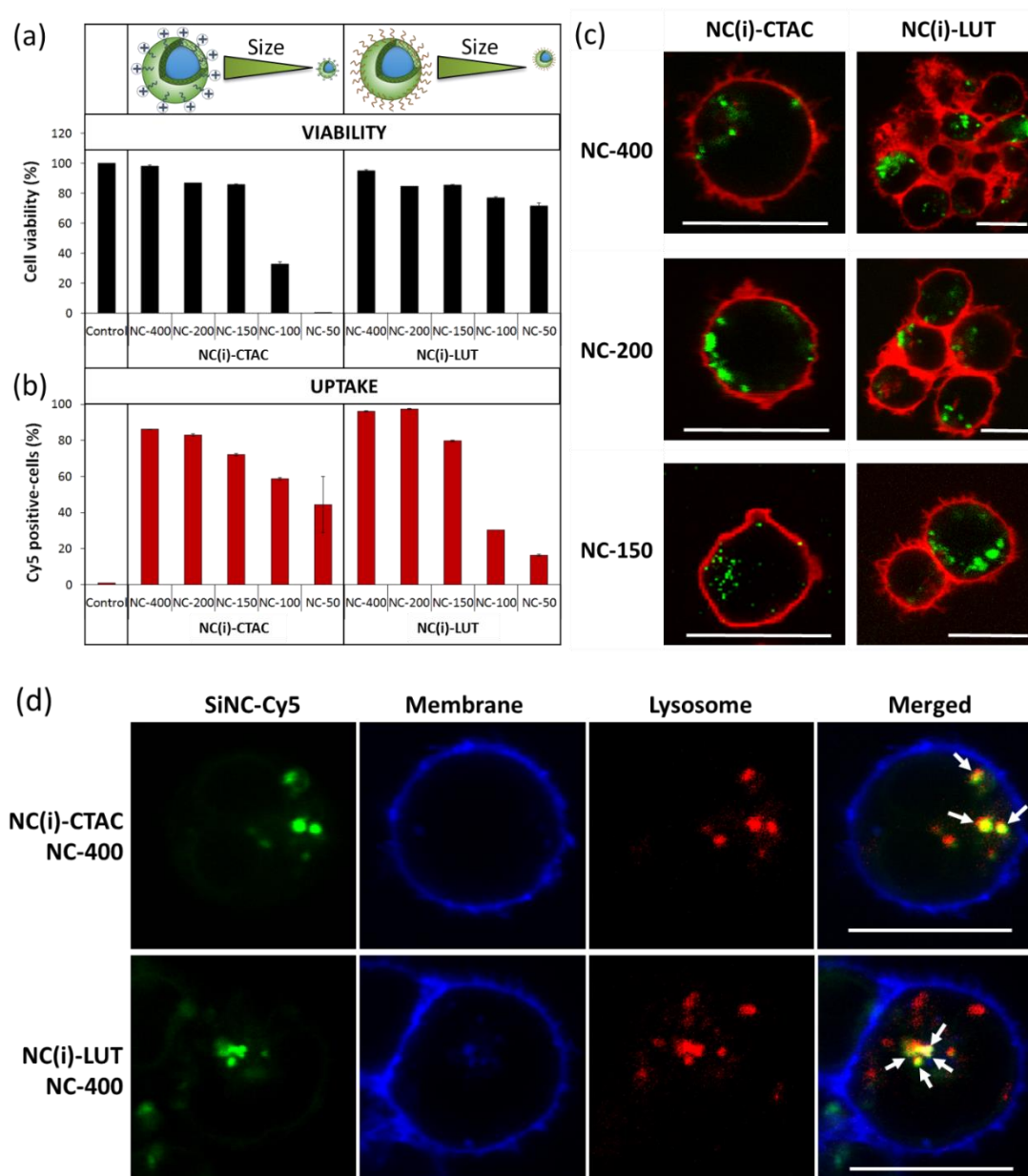


Figure A1.1. Cellular uptake study of SiNCs with different sizes in CD8⁺ T-cells. (a) Cell viability and (b) Cy5 positive-cells of CD8⁺ T-cells after treatment with various kinds of SiNCs (20 μg/mL) in the presence of 1% FBS for 24 h. Confocal laser scanning microscopy images showing (c) the uptake of SiNCs and (d) co-localization with lysosome in CD8⁺ T-cells. Co-localization assay was performed by staining lysosome with LysoTracker® Green DND-26 (red). The membrane was stained with CellMask™ Orange (blue). The SiNC was labeled with Cy5 (green). The merged images of the three channels demonstrated that the SiNCs were co-localized with lysosomes, as indicated with white arrows. The scale bars represent 10 μm.

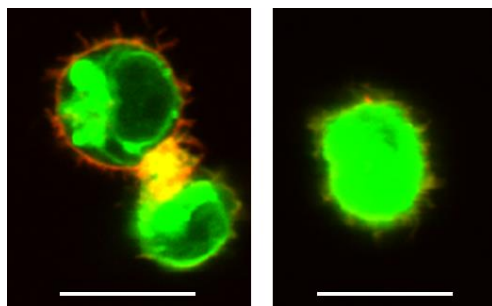


Figure A1.2. cLSM images showing hydrophobic Cy5 dye (0.75 ng/mL) in CD8⁺ T-cells in the presence of 1% FBS for 24 h. The scale bars represent 10 μ m.

Table A1.2. Overview of different functionalized silica nanocapsules.

	Hydrophobic core, NC(o)		Hydrophilic core, NC(i)		Hydrophilic core + amino functionalization		
	NC(o)-CTAC	NC(o)-LUT	NC(i)-CTAC	NC(i)-LUT	NC(i)-LUT -1%NH ₂	NC(i)-LUT -2.5%NH ₂	NC(i)-LUT -5%NH ₂
D_h (H ₂ O) /nm	162 ± 81	157 ± 69	104 ± 48	115 ± 55	128 ± 16	204 ± 95	130 ± 45
ζ -potential (H ₂ O) /mV	12.2 ± 0.5	0.1 ± 0	13.0 ± 0.2	-3.0 ± 0.1	-2.6 ± 0.3	0.7 ± 0.2	4.0 ± 0.5

For the hydrophobic core NCs, the hydrodynamic diameters (D_h) of NC(o)-CTAC and NC(o)-LUT before and after the surfactant exchange were similar; the same was observed for NCs with a hydrophilic core. After functionalization with amino groups with increased densities, the zeta potential of NCs increased due to the deprotonated amino groups. The SiNCs stabilized with CTAC exhibited positive surface charge as presented in positive ζ -potential values (NC(o)-CTAC: 12.2 ± 0.5 mV and NC(i)-CTAC: 13.0 ± 0.2 mV) because of its cationic surfactant property. LUT is a non-ionic surfactant as well as Tween 20 and Tween 80. Normally, LUT stabilized NCs generate nearly neutral surface charge, as found in NC(o)-LUT (0.1 ± 0 mV). However, NC(i)-LUT showed slightly negative ζ -potential (-3.0 ± 0.1 mV) due to the negative charge of silica (at pH above the isoelectric point of silica, \sim pH 2-3). Moreover, the surface charges of SiNCs became more positive when more NH₂ functionalization was applied. It turned from a slightly negative charge in NC(i)-LUT-1%NH₂ (-2.6 ± 0.3 mV) to

nearly neutral in NC(i)-LUT-2.5%NH₂ (0.7 ± 0.2 mV) and became slightly positive in NC(i)-LUT-5%NH₂ (4.0 ± 0.5 mV). In addition, the non-ionic surfactant Tween-stabilized SiNCs also showed negative surface charges like the LUT group (-19.6 ± 1.2 mV for NC(i)-T20 and -11.1 ± 0.6 mV for NC(i)-T80). However, the NC(i)-T20 and NC(i)-T80 were not processed further for cellular uptake studies because of their large sizes (2-6 μ m). TEM micrographs demonstrate the morphology of NC(o)-CTAC and NC(i)-CTAC in **Figure A1.3** showing good capsule formation, which were used as original capsules and subsequently transfer to LUT-stabilized and also amino-functionalized, which were continuously used for the study of cellular uptake.

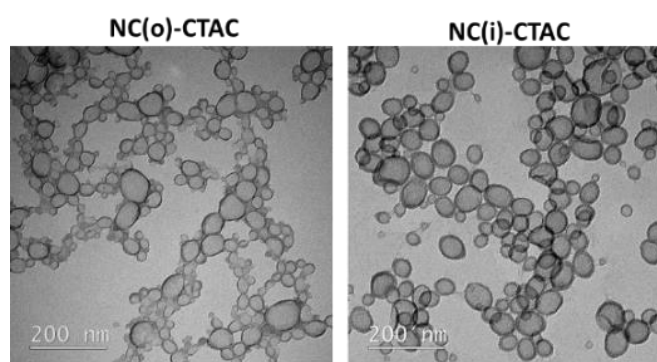


Figure A1.3. TEM micrographs of SiNCs with different cores. (o = hydrophobic core and i = hydrophilic core)

After 24 h of exposure, the cellular uptake of different cores and different surface charges of SiNCs in CD8⁺ T-cells was investigated, as shown in **Figure A1.4**. Toxicity was enhanced in a dose-dependent manner in all capsules, especially at 80 μ g/mL. At 20 and 40 μ g/mL, the hydrophobic and hydrophilic group showed slightly decreased cell viability (**Figure A1.4a**), except for NC(i)-CTAC. The LUT stabilized SiNCs caused less toxicity to the cells compared to the CTAC stabilized SiNCs. Cy5 positive-cells represented the living cells that were supposed to take up the capsule and were analyzed (**Figure A1.4b**). The results showed that the uptake was ~20-35% in all cases, though a low uptake was observed for NC(i)-CTAC due to its high toxicity.

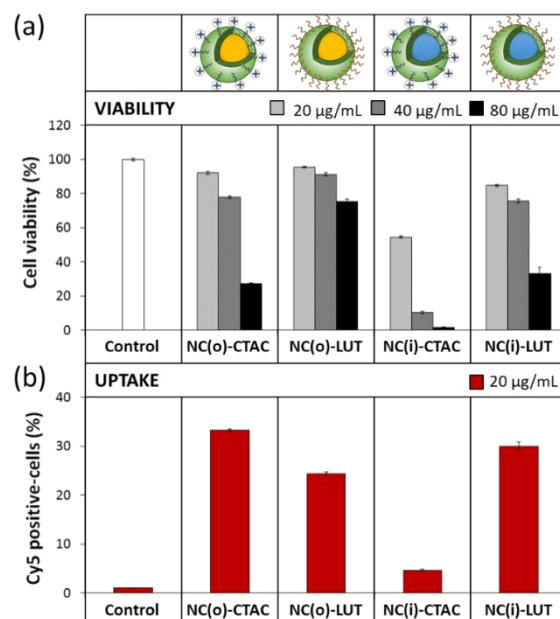


Figure A1.4. Cellular uptake study of SiNCs with different cores (o = hydrophobic core and i = hydrophilic core) and different surfactants (CTAC = Cetyltrimethylammonium chloride and LUT = Lutensol AT50) in CD8⁺ T-cells. (a) Cell viability and (b) Cy5 positive-cells of CD8⁺ T-cells after treatment with various kinds of SiNCs in the presence of 1% FBS for 24 h.

A1.2.3 The effect of functionalizations

Further investigations on the effect of different functionalizations of SiNCs on cellular uptake were carried out in CD8⁺ T-cells (**Figure A1.5**). After 24 h, a dose-dependent toxicity was found. At the same concentration, SiNCs with increasing NH₂ functionalizations did not affect the cell viability compared to unfunctionalized samples. Cy5 positive-cells were slightly decreased when a higher number of NH₂ functionalizations were applied to the cells. Surface functionalization is one of the major parameters contributory to toxicity because it interacts directly with the cells and their compartments.^[A1-31] However, amino functionalization-induced toxicity was not observed in this study.

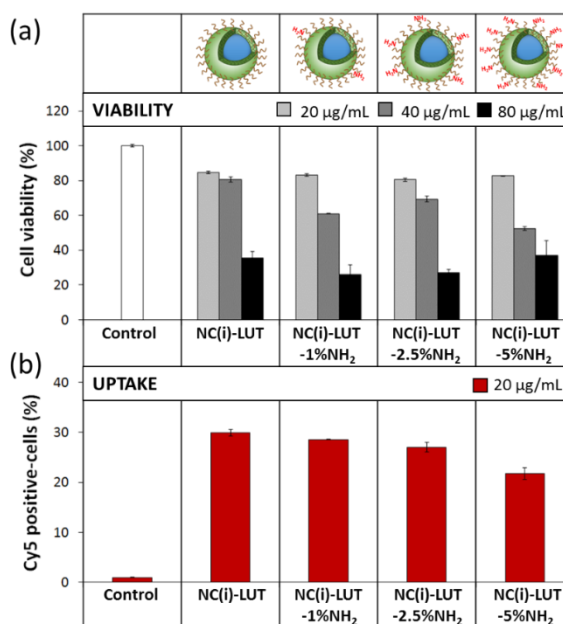


Figure A1.5. Cellular uptake study of SiNCs with different amino-functionalized percentages in CD8⁺ T-cells. (a) Cell viability and (b) Cy5 positive-cells of CD8⁺ T-cells after treatment with various kinds of SiNCs in the presence of 1% FBS for 24 h. (i = hydrophilic core, LUT = Lutensol AT50)

A1.2.4 The effect of protein corona and serum concentrations

After injection into the body, the nanocarriers will travel along the blood stream and face numerous components in the blood, especially proteins. Due to their attractive surface charges, the proteins can be electrostatically adsorbed on the surface of nanocarriers, which is called protein corona, leading to a change in their surface property, covering the targeting moieties and finally impacting cellular uptake.^[A1-22] Therefore, the study of the protein corona effect was performed to understand the uptake behavior by pre-incubating SiNCs with human serum (HS) prior to adding them to CD8⁺ T-cells in medium containing with different percentages of HS. The effect of the protein corona was studied in terms of toxicity, uptake, and protein pattern as well as size-zeta potential analysis, as shown in **Figure A1.6**. The results show that the protein corona reduced the toxicity for all SiNCs compared to uncoated samples

(**Figure A1.6a**). It was also found that the medium containing higher %HS contributed to enhancement of cell viability similar to previous study.^[A1-24] However, the uptake was dramatically decreased in all cases compared to the uncoated samples, together with increasing of %HS in the medium, especially at 10%HS (**Figure A1.6b**). These results suggest that the uptake of SiNCs in CD8⁺ T-cells was inhibited by the adsorbed protein forming protein corona which can be observed from the pre-coated samples. In addition, the different concentration of serum might affect the difference in corona composition resulting in more decrease of the uptake when increasing the serum concentration. The corona inhibited caveolae-mediated endocytosis was mentioned to be a reason for decreasing the uptake of gold nanoparticles in human epidermal keratinocytes.^[A1-36] The protein adsorbed on SiNC surfaces was desorbed and subsequently separated on SDS-PAGE (**Figure A1.6c**). The silver stained gel revealed different corona patterns in 7 different SiNCs. Some small proteins in the size of 6-16 kDa were only found in the corona of NC(i)-LUT with and without NH₂-functionalization. These indicate that the physico-chemical properties of the NCs had a strong effect for corona composition. After forming the protein corona, the SiNCs were subjected to characterization (**Figure A1.6d**). The protein adsorbed amount per m² SiNC was calculated and the size-zeta potential was analyzed. The NC(o) had a higher amount of protein adsorbed on the surface than the NC(i). Among the hydrophilic core, NC(i)-CTAC had the highest amount of protein adsorbed. It can be observed that the protein adsorbed amount was decreased with increasing NH₂-functionalization. The ζ -potential after corona was about -20 mV in all samples because the surface was saturated with a high amount of adsorbed protein. There were no significant differences in the surface charges after corona formation of the various nanoparticles which can be also observed in the literature.^[A1-37] The hydrodynamic size increased by around 20-30% in all SiNCs, except for NC(i)-LUT-5%NH₂ (12%). NC(i)-LUT-2.5%NH₂ showed roughly the same size which likely reflects a particle aggregation.

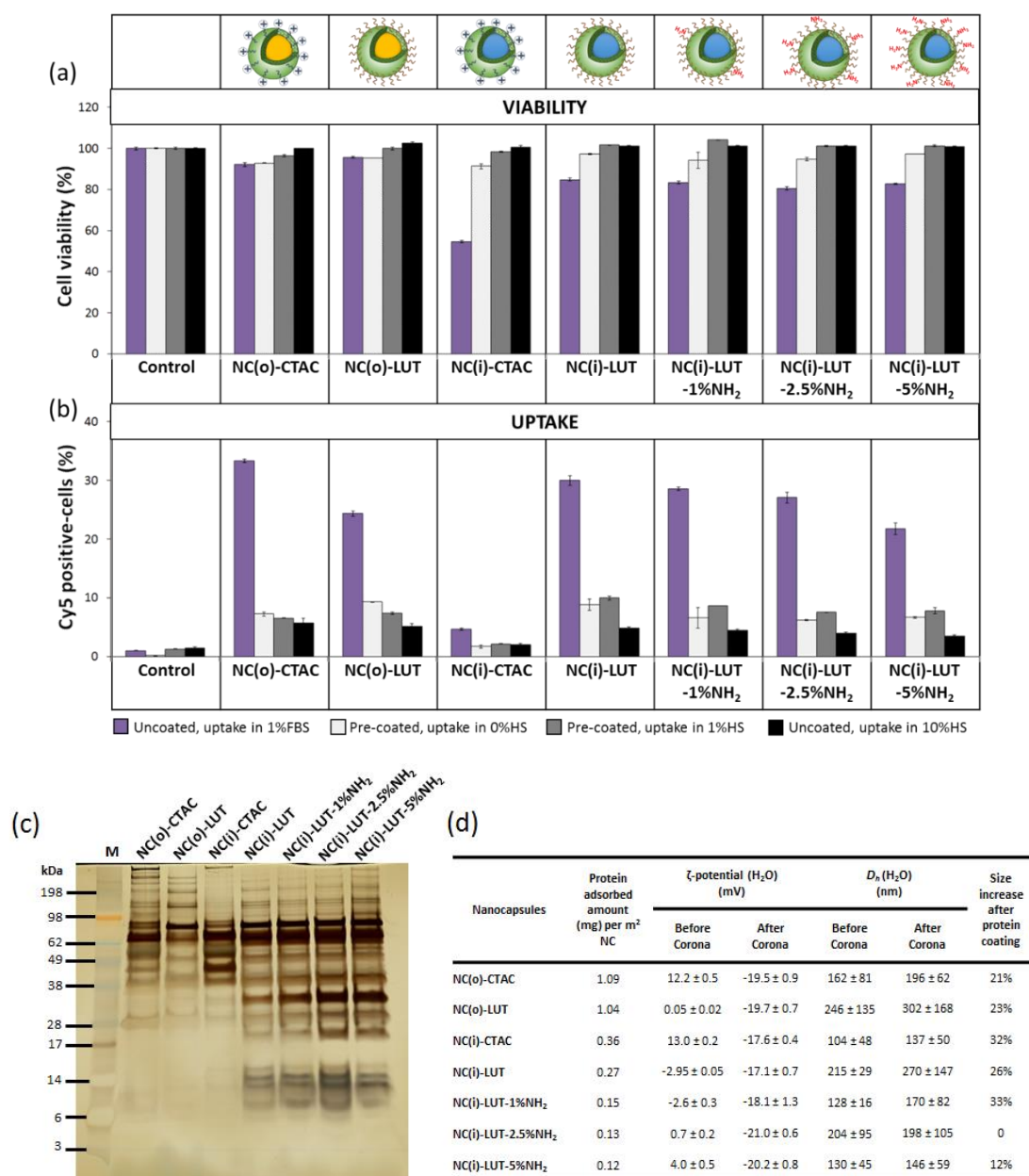


Figure A1.6. Protein corona study of different SiNCs (20 μ g/mL) in CD8⁺ T-cells. (a) Cell viability and (b) Cy5 positive-cells of CD8⁺ T-cells after treatment with 1) uncoated SiNCs in the presence of 1% FBS, 2) HS pre-coated SiNCs in the presence of 0% HS for 6 h. After that, the HS was added to obtain 1% HS, 3) HS pre-coated SiNCs in the presence of 1% HS, and 4) HS pre-coated SiNCs in the presence of 10% HS. (c) Corona pattern of HS pre-coated SiNCs analyzed by SDS-PAGE with 1.5 μ g total protein loading. (d) Characterization of HS pre-coated SiNCs. (o = hydrophobic core, i = hydrophilic core, CTAC = cetyltrimethylammonium chloride, LUT = Lutensol AT50, FBS = fetal bovine serum and HS = human serum).

A1.2.5 The cellular uptake progress

To follow the cellular uptake, NC(o)-LUT covalently bonded with FITC was tracked in Jurkat T-cells with different time points of incubation (**Figure A1.7**). From cLSM images, the capsules were found outside the cells at 2 h, started to get internalized at 4 h, stayed inside at 24 h and were even more internalized at 48 h (**Figure A1.7a**). These observations were quantified by flow cytometry; the uptake was clearly time dependent. When the incubation time was longer, the percentage of fluorescence positive-cells was higher, indicating greater uptake (**Figure A1.7c**). Although it reached a maximum of 100% fluorescence positive-cells after 24 h, the intensity was actually still increased, which can be observed clearly from the median fluorescence intensity (MFI) at 48 h compared to 24 h. It should be noted that cell viability was improved after 4 h (**Figure A1.7b**), which indicates the biocompatibility of the NC(o)-LUT. After the SiNCs were first internalized, cell viability was slightly decreased, but later recovered.

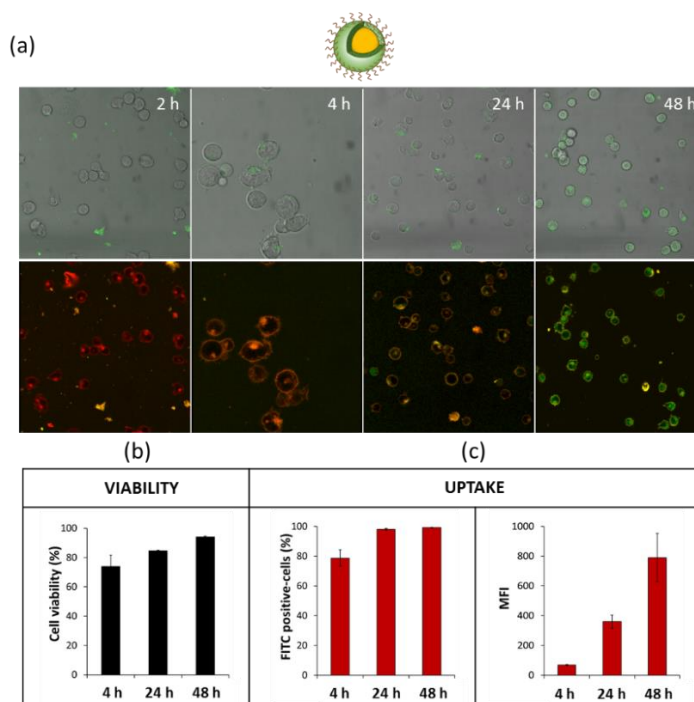


Figure A1.7. Cellular uptake progress of NC(o)-LUT in Jurkat T-cells at various incubation times. (a) cLSM images, (b) Cell viability, (c) FITC positive-cells and median fluorescence intensity (MFI) of Jurkat T-cells after treated with NC(o)-LUT.

A1.3. Conclusion

The different physico-chemical properties of SiNCs led to different toxicities and also affected the uptake behavior. The major impact on cellular uptake and viability was found to be dose- and size-dependent. Smaller size SiNCs than 100 nm caused significant toxicity to the cells, which is probably due to ROS-mediated toxicity. The toxicity of hydrophobic core SiNCs was comparable to the hydrophilic core SiNCs. To select the core, it should correspond to the hydrophilicity or hydrophobicity of the desired payload. The effect of different surface charges on cellular uptake was observed, showing the positive charges of CTAC-stabilized SiNCs decreased the cell viability as well as the uptake more than closely neutral charges of the LUT-stabilized SiNCs. In addition, more amino-functionalizations on SiNC surface slightly decreased the viable cells as well as the uptake. Furthermore, the protein corona study revealed that both protein corona and medium containing serum was able to cover the toxicity of SiNCs, leading to improved viability; however, it inhibited the uptake. Therefore, the concentration of serum in culture condition should be optimized carefully in order to facilitate the uptake, but still keep the cells alive. These findings suggest the appropriate criteria for SiNC designing according concerning their physico-chemical properties for the impact of cellular uptake and toxicity in CD8⁺ T-cells. Because the T-cell is a type of the cell that is difficult to take up foreign particles, it is highly sensitive and not resistant in terms of toxicity.^[A1-18] Therefore, the delivery system that is suitable for use with T-cells has to meet the safety criteria with the ability to protect and deliver the payload without causing toxicity to the T-cell. For SiNC, it is easy to manipulate the structures and surface properties based on these findings in order to avoid toxicity and favor uptake. Therefore, SiNCs are a promising delivery system which can be applied as a nanocarrier in T-cell immunotherapy.

A1.4. References

- [A1-1] Cohen, J. E., Merims, S., Frank, S., Engelstein, R., Peretz, T., & Lotem, M. (2017) Adoptive cell therapy: past, present and future. *Immunotherapy*, 9(2), 183-196.
- [A1-2] Wang, M., Yin, B., Wang, H. Y., & Wang, R. F. (2014). Current advances in T-cell-based cancer immunotherapy. *Immunotherapy*, 6(12), 1265-78.

- [A1-3] Perica, K., Varela, J. C., Oelke, M., & Schneck, J. (2015). Adoptive T cell immunotherapy for cancer. *Rambam Maimonides medical journal*, 6(1), e0004.
- [A1-4] Sathyanarayanan, V., & Neelapu, S. S. (2015). Cancer immunotherapy: Strategies for personalization and combinatorial approaches. *Molecular oncology*, 9(10), 2043-53.
- [A1-5] Baruch, E. N., Berg, A. L., Besser, M. J., Schachter, J., & Markel, G. (2017). Adoptive T cell therapy: An overview of obstacles and opportunities. *Cancer*, 123, 2154-2162.
- [A1-6] Li, A. V., Moon, J. J., Abraham, W., Suh, H., Elkhader, J., Seidman, M. A., Yen, M., Im, E. J., Foley, M. H., Barouch, D. H., & Irvine, D. J. (2013). Generation of effector memory T cell-based mucosal and systemic immunity with pulmonary nanoparticle vaccination. *Science translational medicine*, 5(204), 204ra130.
- [A1-7] Zitvogel, L., & Kroemer, G. (2012). Targeting PD-1/PD-L1 interactions for cancer immunotherapy. *Oncoimmunology*, 1(8), 1223-1225.
- [A1-8] Frick, S. U., Domogalla, M. P., Baier, G., Wurm, F. R., Mailaender, V., Landfester, K., & Steinbrink, K. (2016). Interleukin-2 Functionalized Nanocapsules for T Cell-Based Immunotherapy. *ACS Nano*, 10, 9216-9226.
- [A1-9] Schmid, D., Park, C. G., Hartl, C. A., Subedi, N., Cartwright, A. N., Puerto, R. B., Zheng, Y., Maiarana, J., Freeman, G. J., Wucherpfennig, K. W., Irvine, D. J., & Goldberg, M. S. (2017). T cell-targeting nanoparticles focus delivery of immunotherapy to improve antitumor immunity. *Nature communications*, 8(1), 1747.
- [A1-10] Li, S. Y., Liu, Y., Xu, C. F., et al. (2016). Restoring anti-tumor functions of T cells via nanoparticle-mediated immune checkpoint modulation. *J Control Release*. (231), 17-28.
- [A1-11] Stromnes, I. M., Blattman, J. N., Tan, X., Jeevanjee, S., Gu, H., & Greenberg, P. D. (2010). Abrogating Cbl-b in effector CD8⁺T cells improves the efficacy of adoptive therapy of leukemia in mice. *The Journal of clinical investigation*, 120(10), 3722-34.
- [A1-12] Ligtenberg, M. A., Pico de Coaña Y., Shmushkovich, T., Yoshimoto, Y., Truxova, I., Yang, Y., Betancur-Boissel, M., Eliseev, A. V., Wolfson, A. D., & Kiessling, R. (2018). Self-Delivering RNAi Targeting PD-1 Improves Tumor-Specific T Cell Functionality for Adoptive Cell Therapy of Malignant Melanoma. *Mol Ther*. 26(6), 1482-1493.
- [A1-13] Iwamura, K., Kato, T., Miyahara, Y., Naota, H., Mineno, J., Ikeda, H., & Shiku, H. (2012). siRNA-mediated silencing of PD-1 ligands enhances tumor-specific human T-cell effector functions. *Gene Therapy* (19), 959–966.
- [A1-14] Ding, C., Tong, L., Feng, J., & Fu, J. (2016) Recent Advances in Stimuli-Responsive Release Function Drug Delivery Systems for Tumor Treatment. *Molecules*, 21, 1715.
- [A1-15] Mohanraj, V. J., & Chen, Y. (2006). Nanoparticles – A Review. *Tropical Journal of Pharmaceutical Research*, 5(1), 561-573.
- [A1-16] Zhang, Y., Hsu, B. Y., Ren, C., Li, X., & Wang, J. (2015). Silica-based nanocapsules: synthesis, structure control and biomedical applications. *Chem. Soc. Rev.*, 44, 315-335.

- [A1-17] Murugadoss, S., Lison, D., Godderis, L., Van Den Brule, S., Mast, J., Brassinne, F., Sebaihi, N., & Hoet, P. H. (2017). Toxicology of silica nanoparticles: an update. *Archives of toxicology*, *91*(9), 2967-3010.
- [A1-18] Freeley, M., & Long, A. (2013). Advances in siRNA delivery to T-cells: potential clinical applications for inflammatory disease, cancer and infection. *Biochem J.* *455*(2):133-47.
- [A1-19] Mendoza, A., Torres-Hernandez, J. A., Ault, J. G., Pedersen-Lane, J. H., Gao, D., & Lawrence, D. A. (2014). Silica nanoparticles induce oxidative stress and inflammation of human peripheral blood mononuclear cells. *Cell stress & chaperones*, *19*(6), 777-90.
- [A1-20] Vis, B., Hewitt, R. E., Faria, N., Bastos, C., Chappell, H., Pele, L., Jugdaohsingh, R., Kinrade, S. D., & Powell, J. J. (2018). Non-Functionalized Ultrasmall Silica Nanoparticles Directly and Size-Selectively Activate T Cells. *ACS Nano*. doi: 10.1021/acsnano.8b03363.
- [A1-21] Napierska, D., Thomassen, L. C., Lison, D., Martens, J. A., & Hoet, P. H. (2010). The nanosilica hazard: another variable entity. *Particle and fibre toxicology*, *7*(1), 39.
- [A1-22] Lundqvist, M., Augustsson, C., Lilja, M., Lundkvist, K., Dahlbäck, B., Linse, S., et al. (2017) The nanoparticle protein corona formed in human blood or human blood fractions. *PLoS ONE* *12*(4): e0175871.
- [A1-23] Jiang, S., Lv, L., Li, Q., Wang, J., Landfester, K., & Crespy, D. (2016). Tailoring nanoarchitectonics to control the release profile of payloads. *Nanoscale*, *8* (22), 11511-11517.
- [A1-24] Hsiao, I., Gramatke, A. M., Joksimovic, R., Sokolowski, M., Gradzielski, M., et al. (2014). Size and Cell Type Dependent Uptake of Silica Nanoparticles. *J Nanomed Nanotechnol* *5*, 248.
- [A1-25] Li, Y., Sun, L., Jin, M. H., Du, Z., Liu, X., et al. (2011). Size-dependent cytotoxicity of amorphous silica nanoparticles in human hepatoma HepG2 cells. *Toxicol Vitro* *25*, 1343-1352.
- [A1-26] Nabeshi, H., Yoshikawa, T., Matsuyama, K., Nakazato, Y., Arimori, A., et al. (2010) Size-dependent cytotoxic effects of amorphous silica nanoparticles on Langerhans cells. *Pharmazie* *65*, 199-201.
- [A1-27] Napierska, D., Thomassen, L. C. J., Rabolli, V., Lison, D., Gonzalez, L., et al. (2009) Size-dependent cytotoxicity of monodisperse silica nanoparticles in human endothelial cells. *Small*. *5*, 846-853.
- [A1-28] Yildirimer, L., Thanh, T. K. N., Loizidou, M., & Seifalian, M. A. (2011). Toxicological considerations of clinically applicable nanoparticles. *Nano Today*. *6*, 585-607.
- [A1-29] Bakand, S., & Hayes, A. (2016). Toxicological Considerations, Toxicity Assessment, and Risk Management of Inhaled Nanoparticles. *International journal of molecular sciences*, *17*(6), 929.
- [A1-30] Huang, Y. W., Cambre, M., & Lee, H. J. (2017). The Toxicity of Nanoparticles Depends on Multiple Molecular and Physicochemical Mechanisms. *International journal of molecular sciences*, *18*(12), 2702.
- [A1-31] Buzzea, C., Pacheco, I. I., & Robbie, K. (2007). Nanomaterials and nanoparticles: sources and toxicity. *Biointerphases*. *2*(4), MR17-71.

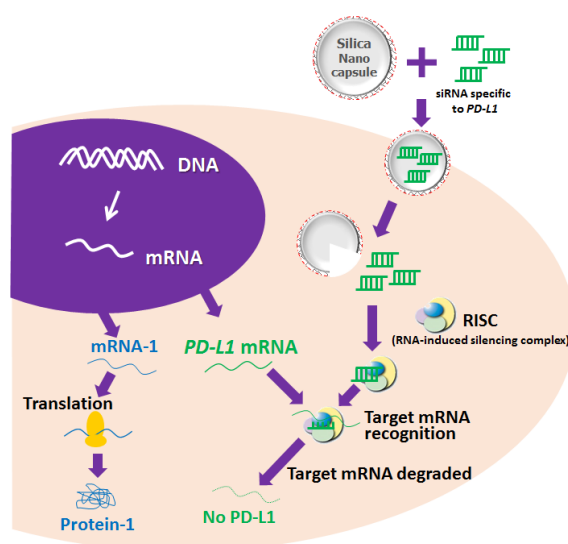
- [A1-32] Kipen, H. M., & Laskin, D. L. (2005) Smaller is not always better: nanotechnology yields nanotoxicology. *Am J Physiol-Lung Cell Mol Physiol.* 289, L696-L697.
- [A1-33] Nabeshi, H., Yoshikawa, T., Matsuyama, K. et al. (2011a). Amorphous nanosilica induce endocytosis-dependent ROS generation and DNA damage in human keratinocytes. *Part Fibre Toxicol* 8:1.
- [A1-34] Accomasso, L., Gallina, C., Turinetto, V., & Giachino, C. (2015). Stem Cell Tracking with Nanoparticles for Regenerative Medicine Purposes: An Overview. *Stem cells international*, 2016, 7920358.
- [A1-35] Betzer, O., Shilo, M., Opoichinsky, R., Barnoy, E., Motiei, M., Okun, E., Yadid, G., & Popovtzer, R. (2017). The effect of nanoparticle size on the ability to cross the blood–brain barrier: an in vivo study. *Nanomedicine*, 12 (13), 1533-1546.
- [A1-36] Li, Y. & Monteiro-Riviere, N. A., Mechanisms of cell uptake, inflammatory potential and protein corona effects with gold nanoparticles. *Nanomedicine* 2016, 11 (24), 3185-3203.
- [A1-37] Mirshafiee, V., Kim, R., Park, S., Mahmoudi, M., & Kraft, M. L. (2016). Impact of protein pre-coating on the protein corona composition and nanoparticle cellular uptake. *Biomaterials*, 75, 295-304.

A2: CELLULAR UPTAKE OF siRNA LOADED NANOCARRIER TO KNOCKDOWN PD-L1: STRATEGIES TO IMPROVE T-CELL FUNCTIONS

(Note: The literature of the chapter A2 can be found on page 48 at the end of this chapter.)

Permission: The manuscript is under preparation.

Contribution: I carried out the biological part including cytotoxicity, cellular uptake study by flow cytometry, cell imaging by cLSM, PD-L1 knockdown study and quantitative polymerase chain reaction (qPCR) analysis. ██████████ synthesized and characterized the SiNCs. The project was supervised by ██████████



TOC A2: The siRNA mediated PD-L1, a potent inhibitory protein, silencing was carried out by using the silica nanocapsules (SiNCs) carrying the PD-L1 specific siRNA to CD8⁺ T-cells in order to inhibit PD-L1 expression resulting in the improvement of T-cells viability and function.

Aim: To inactivate PD-L1 expression, the silica nanocapsules (SiNCs) carrying the PD-L1 specific siRNA were internalized to CD8⁺ T-cells. Knockdown efficiency was determined at protein and mRNA levels. The effects of PD-L1 knockdown were demonstrated in terms of cell proliferation and some functional biomarker expressions.

Abstract: T-cells or T-lymphocytes are a type of lymphocyte (a subtype of white blood cells) that plays a central role in cell-mediated immunity. Nowadays, adoptive T-cell immunotherapy has been researched and developed to fight against cancer. In this therapy, T-cells are harvested from a patient's blood. After several weeks of expansion in culture, tumor-specific T-cells can be reinfused into the same cancer patient. This technique provides high efficiency for cancer treatment. However, several processes exist to suppress anti-cancer responses of T-cells leading to the loss of their functionality and reduction of their viability. Therefore, strategies are needed to improve T-cell survival and functions. Here, small interfering RNA (siRNA) loaded nanocarriers were used to knockdown PD-L1, one of the most important proteins causing loss of functionality in T-cells. Biocompatibility and cellular uptake of siRNA loaded silica nanocapsules (SiNCs) were investigated in CD8⁺ T-cells. Then, PD-L1 expression at protein and mRNA levels of treated cells were evaluated. Furthermore, the effect of PD-L1 knockdown was observed in terms of cell proliferation and the expression of specific biomarkers: CD25 and CD71, which are indicators of T-cell functions. The results suggest that this siRNA loaded nanocarrier exhibits the potential for use in delivery of siRNA into T-cells, enhanced T-cell survival by decreasing the expression of inhibitory protein PD-L1 and can be applied in adoptive T-cell immunotherapy for the treatment of cancer.

A2.1. Introduction

T-cells or T-lymphocytes are some of the most important cells in the immune system. They can be divided into two main subtypes according to their surface markers, CD4⁺ and CD8⁺ T-cells. CD4⁺ T-cells (T-helper cells) involve the maturation of B-cells as well as the activation of CD8⁺ T-cells. CD8⁺ T-cells (cytotoxic T-cells) play a major role in destroying virus-infected cells and tumor cells.^[A2-1-3] With the outstanding ability to kill cancer cells, a technique called adoptive T-cell immunotherapy for cancer treatment using CD8⁺ T-cells has been employed and studied intensively for a past decade with promising results.^[A2-4-5] In the first step for immunotherapy, CD8⁺ T-cells are collected from patient blood, selected and activated under the culture condition to enhance the number of specific T-cells and make them strong enough to fight against

cancer before reinfusion to the patient's body.^[A2-6] However, T-cells start to lose their viability and function after a long expansion and cultivation time, leading to less efficiency to kill cancer cells.^[A2-4-7] The decrease in T-cells survival and killing ability is due to the natural mechanism of the immune system. When antigen presenting cells, for example dendritic cells, present cancer antigen on their surface and then bind to T-cell receptor resulting in T-cell activation, trafficking along the blood stream to the cancer site, recognition of cancer, and finally killing the cancerous cells. After that, the amount of specific T-cells will decrease to ensure that they are inactivated later to avoid chronic inflammation and autoimmune disease. There are several proteins involved in T-cell inactivation, which are called immune check point proteins such as cytotoxic T-lymphocyte antigen 4 (CTLA-4), programmed cell death-1 (PD-1), and their cognate ligands (PD-L1 and PD-L2).^[A2-8-12] One of the well-known T-cell inhibitions occurs through PD-1/PD-L1 interaction by the specific binding of PD-1 receptor on the surface of T-cells through its ligand (PD-L1) on the surface of dendritic cells. Many researches have focused on the inhibition of PD-1 expression with the aim of improving T-cell function.^[A2-12] In fact, PD-L1 is also expressed on the surface of T-cells, which can also cause PD-1/PD-L1 interaction between the T-cell population itself, which finally blocks T-cell activation.^[A2-13] To inhibit the immune check point proteins either PD-1 or PD-L1 expression, it is necessary to pay careful attention to the systemic blocking, which can result in an undetermined effect of over immune reaction. PD-L1 is not only expressed on the surface of hematopoietic cells, but is also found on the surface of non-hematopoietic cells.^[A2-14] As selective inhibition, small interfering RNA (siRNA)-mediated silencing of PD-L1 was used and electroporated into tumor specific CD4⁺ and CD8⁺ human T-cells.^[A2-13] The transfected T-cells successfully increased the interferon- γ production and antigen specific cytotoxicity. These findings suggest that siRNA-mediated PD-L1 silencing is another possible approach to achieve the inhibition of immune check point proteins, leading to enhanced T-cell function. However, it is known that the electroporation technique is harmful to cells due to electric shock, resulting in decreased cell viability after transfection.^[A2-15] With the great advantages of nanotechnology, nanocarriers containing payloads such as drugs, dyes and specific biomolecules have been widely developed and used. Among the various kinds of nanocarriers, silica-based nanocapsules have shown a high loading capacity, ease of

synthesis and surface functionalization. Furthermore, silicon oxide has been approved by the U.S. Food and Drug administration (USFDA) for use in medical care products. Silica-based materials are accepted because their biocompatibility as well as their stability.^[A2-16-17]

This study, therefore, was aimed to inhibit PD-L1 expression on CD8⁺ T-cells using silica core shell nanocapsules as nanocarriers to carry siRNA specific to PD-L1 mRNA. The silica nanocapsules (SiNCs) encapsulated siRNA-Cy5 dye was applied to the cells to track the cell uptake by flow cytometry and further confirmed by confocal laser scanning microscopy. Knockdown efficiencies at protein and mRNA levels were evaluated and the effects of PD-L1 knockdown were investigated in terms of cell proliferation and specific biomarker expression.

A2.2. Results and discussion

To screen for a good candidate of nanocarriers with the ability to deliver highly sensitive biomolecules such as siRNA into T-cells, Cy-5 labeled oligonucleotides (oligo Cy5) were used to encapsulate various kinds of silica nanocapsules (SiNCs), as listed in **Table A2.1** for simulation of siRNA and the tracking of the capsules inside the cells. CD8⁺ T-cells stimulated with anti-CD3 antibody and IL-2 were treated with NC1 and NC2 with different surfactants. The capsules were stabilized with cationic surfactant cetyltrimethylammonium chloride (CTAC) and non-ionic surfactant Lutensol AT50 (LUT) to prevent aggregation, to increase stability and to display different surface charges. The charges of the capsules were determined by the zeta-potential measurements; CTAC stabilized capsules were slightly positive, while LUT stabilized capsules were close to neutral.

Table A2.1. Overview of silica nanocapsules encapsulated Oligo Cy5.

Sample	Diameter (nm)	Zeta potential (mv)	Encapsulation efficiency of Oligo Cy5
NC1-Oligo Cy5-CTAC	237 ± 104	15	39%
NC1-Oligo Cy5-LUT	262 ± 100	-10	21%
NC2-Oligo Cy5-CTAC	231 ± 111	5	63%
NC2-Oligo Cy5-LUT	248 ± 108	-8	44%

Cellular uptake of SiNCs encapsulated oligo-Cy5 in CD8⁺ T-cells was studied in terms of toxicity and uptake after 24 h of incubation. Flow cytometry revealed a slight decrease in cell viability of CD8⁺ T-cells treated with SiNCs up to 80 µg/mL, indicating their biocompatibility with CD8⁺ T-cells (**Figure A2.1a**) and an increase of Cy5 positive-cells with the increasing concentration of SiNCs (**Figure A2.1b**). The cellular uptake of these SiNCs was further confirmed by confocal laser scanning microscopy (cLSM) (**Figure A2.1d**). cLSM images demonstrated green dots, representing SiNC-oligo Cy5 in the cytoplasm and indicating effective uptake by the cells. In the experiments mentioned above, all SiNCs exhibited good potential for use as a nanocarrier of biomolecules into CD8⁺ T-cells; however, the capsule NC2 showed better capsule formation in which the shell structure was formed clearly as observed in TEM images (**Figure A2.1c**). Therefore, the NC2 was chosen for use in subsequent experiments.

To investigate the effect of different surface charges on cellular uptake, anti-CD3 antibody and IL-2 stimulated CD8⁺ T-cells were incubated with NC2-CTAC or -LUT encapsulated siRNA Cy5 for 24 h. The fluorescence-tracking molecule was changed from oligo-Cy5 to siRNA-Cy5 in order to closely imitate the real payload in this study, which is siRNA that aimed to encapsulate inside the capsules and carry to T-cells. Concentrations of SiNCs from 40 to 640 µg/mL were added to the cells to determine the critical toxic concentration. **Figure A2.2a** showed the increase of toxicity to CD8⁺ T-cells in dose-dependent manner of both NC2-siRNA Cy5-CTAC and NC2-siRNA Cy5-LUT. The half maximal effective concentration (EC₅₀) of NC2-siRNA Cy5-CTAC on CD8⁺ T-cells was 379.8 µg/mL, which was lower than that of NC2-siRNA Cy5-LUT (406.3 µg/mL). This result suggested that the LUT stabilized NC2 was more biocompatible with CD8⁺ T-cells than the CTAC stabilized NC2. The cellular uptake of these SiNCs was determined by an increase of Cy5 positive-cells with increasing concentration of the SiNCs using flow cytometry (**Figure A2.2b**) and subsequently confirmed by cLSM (**Figure A2.2c**). Considering the percentages of Cy5 positive-cells, there was no significant difference between CTAC and LUT stabilized NC2, indicating that they are comparable in cellular uptake efficiency. It seems that the charges of the capsule are not only involved in cellular uptake efficiency, but also other parameters

such as the components of capsule formation. cLSM images demonstrated CD8⁺ T-cells were in a clumping or aggregation form with green dots representing NC2-siRNA Cy5 inside the cytoplasm. This result not only proves efficient uptake by the cells, but also indicates the healthy and/or proliferation stage of the cells due to the excellent biocompatibility of the capsules. To provide more evidence for cellular uptake, the co-localization assay was performed. **Figure A2.3** shows the NC2-siRNA Cy5-CTAC and -LUT were co-localized with lysosome, as indicated with white arrows. This evidence provides solid proof of cellular uptake for these SiNCs in CD8⁺ T-cells. Although the EC₅₀ was not significant difference, but the cell morphology from the cLSM image of LUT stabilized SiNC showed more cell clusters indicating more cell healthy NC2-LUT was then selected for use in the next steps for encapsulation of control siRNA, which has no specific sequences to human mRNA and target siRNA containing specific sequences to PD-L1 mRNA.

NC2-LUT encapsulated with siRNA targeted to PD-L1 mRNA (siRNA target SiNC) was added to CD8⁺ T-cells. The PD-L1 knockdown and their knockdown effects were analyzed and compared with NC2-LUT encapsulated with siRNA control, which has no specific sequences to human mRNA (siRNA control SiNC) and cell control (without any capsule), as shown in **Figure A2.4**. Relative PD-L1 protein expression profiles were observed from day 1 to day 3 by flow cytometry analysis (**Figure A2.4a**). Knockdown efficiency of siRNA target SiNC compared to siRNA control SiNC was 30%, 27% and 6%, respectively. Knockdown efficiency of siRNA target SiNC compared to control was 35%, 48% and 40%, respectively. It seems that siRNA control SiNC had a non-specific effect on PD-L1 expression, which was able to also decrease PD-L1 expression. Since the maximum effect of PD-L1 knockdown of siRNA target SiNC compared to the control was found on day 2, the total RNA was extracted. cDNA was synthesized and subsequently used for quantitative PCR analysis. Relative PD-L1 mRNA expression (**Figure A2.4b**) demonstrated the knockdown efficiency at mRNA level of siRNA target SiNC was 28% compared to siRNA control SiNC and was 61% compared to the control. This higher knockdown efficiency at the mRNA level than at the protein level is quite common because the siRNA targets basically direct to the mRNA, then subsequently inhibit protein synthesis. After confirmation of PD-L1

knockdown at both mRNA and protein levels, the effects of PD-L1 knockdown in terms of cell survival and functions were also studied. Cell proliferation assays (**Figure A2.4c**) and relative expression of some specific biomarkers for T-cell functions such as CD25 and CD71 (**Figure A2.4d**) were investigated. The results showed that cell proliferation on day 1 and day 3 of CD8⁺ T-cells treated with siRNA target SiNC was increased significantly compared to the control. Furthermore, the relative expression of CD25 and CD71 on day 2 of CD8⁺ T-cells treated with siRNA target SiNC was also increased significantly compared to the control.

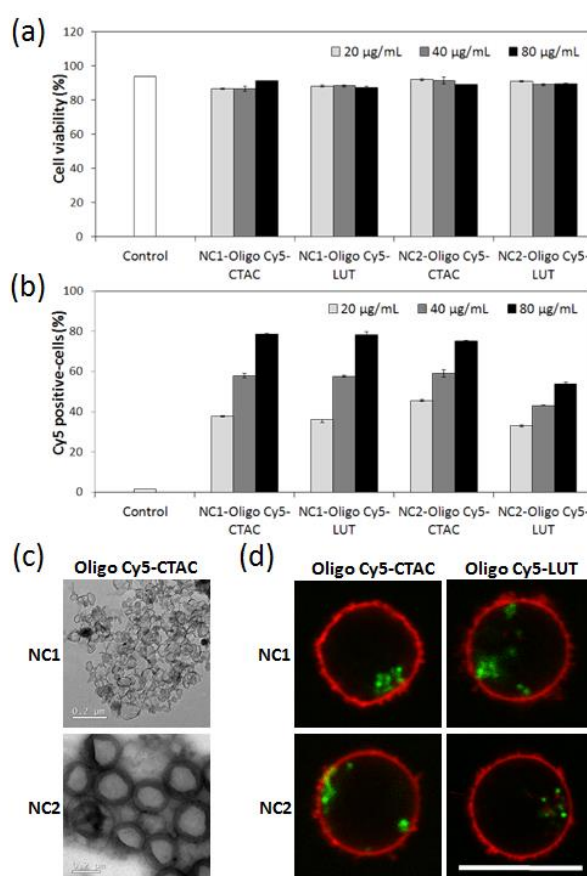


Figure A2.1. Cellular uptake study of SiNCs encapsulated Oligo Cy5 in CD8⁺ T-cells demonstrating (a) Cell viability, (b) Cy5 positive-cells and (d) confocal laser scanning microscopy (cLSM) images of CD8⁺ T-cells after treatment with SiNCs encapsulated Oligo Cy5 for 17 h. The membrane was stained with CellMask™Orange (red). The SiNC was labeled with Oligo Cy5 (green). The scale bars represent 10 µm. (c) TEM micrographs of SiNCs.

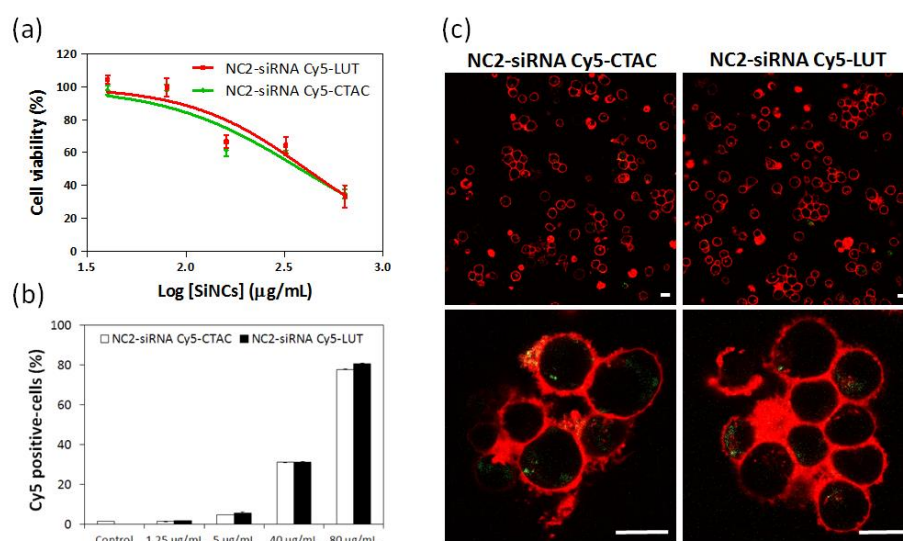


Figure A2.2. Cellular uptake study of SiNCs encapsulated siRNA Cy5 in CD8⁺ T-cells. (a) Cell viability, (b) Cy5 positive-cells and (c) cLSM images of CD8⁺ T-cells after treatment with SiNCs encapsulated siRNA Cy5 for 17 h. The membrane was stained with CellMaskTMOrange (red). The SiNC was labeled with Oligo Cy5 (green). The scale bars represent 10 μm . The EC₅₀ of NC2-siRNA Cy5-CTAC and -LUT were 379.8 and 406.3 $\mu\text{g/mL}$, respectively.

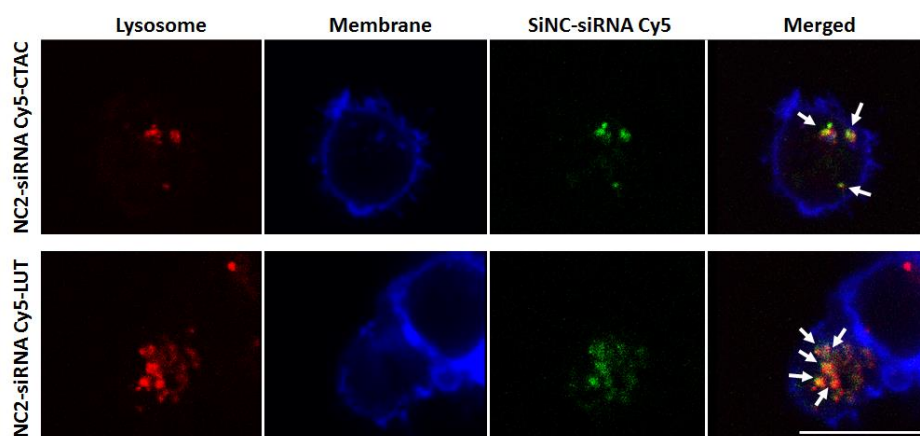


Figure A2.3. cLSM images of SiNCs encapsulated siRNA Cy5 co-localized with lysosomes in CD8⁺ T-cells after 17 h. Co-localization assay was performed by staining lysosome with LysoTracker dye (red). The membrane was stained with CellMaskTMOrange (blue). The SiNC was labeled with siRNA Cy5 (green). The merged images demonstrated that SiNCs encapsulated siRNA Cy5 were co-localized with lysosomes as indicated with white arrows. The scale bars represent 10 μm .

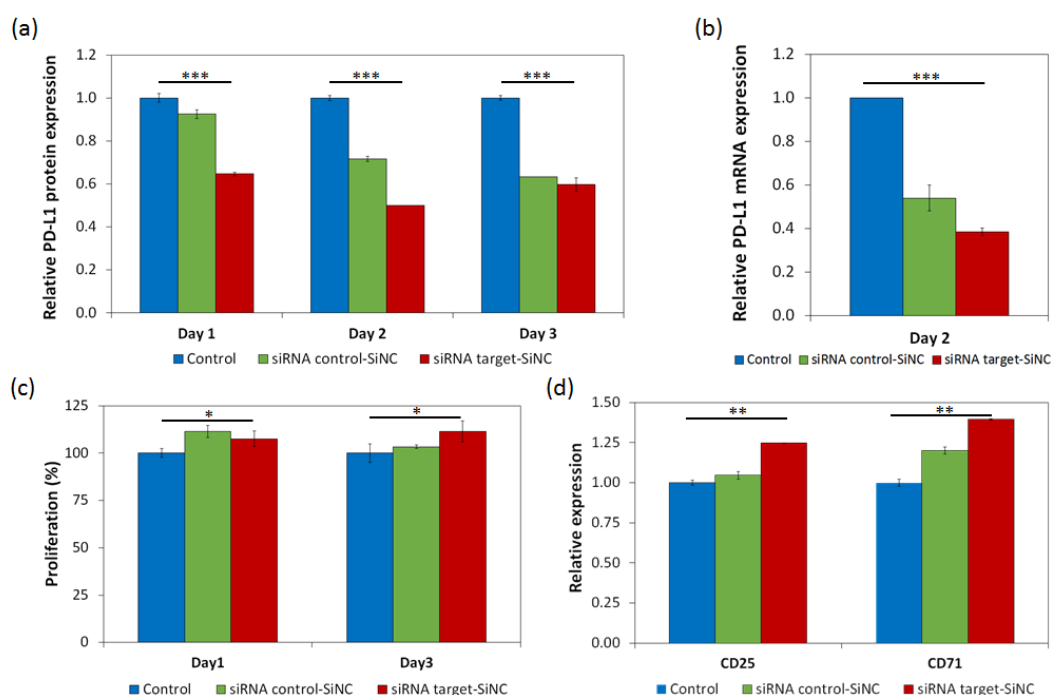


Figure A2.4. PD-L1 expression profiles and the effect of PD-L1 knockdown after treated CD8⁺ T-cells with SiNC encapsulated siRNA target that are specific to PD-L1 compared to those cells treated with SiNC encapsulated siRNA control and control (without any capsules). Relative expression of (a) PD-L1 protein expression from day 1 to day 3 and (b) PD-L1 mRNA expression on day 2, (c) Cell proliferation assay of day 1 and day 3, and (d) Relative expression of CD25 and CD71 on day 2. Statistical significance was calculated by t-test. *p < 0.05, **p < 0.01. ***p < 0.0001.

A2.3. Conclusion

These results indicated that the NC-LUT carried siRNA was able to deliver siRNA target to CD8⁺ T-cells, subsequent release and knockdown PD-L1 both mRNA and protein levels, and finally enhanced T-cell survival and functions. This NC-LUT exhibited excellent potential for use as a nanocarrier for biomolecule delivery and T-cell immunotherapy for the treatment of cancer.

A2.4. References

- [A2-1] Wang, M., Yin, B., Wang, H. Y., & Wang, R. F. (2014). Current advances in T-cell-based cancer immunotherapy. *Immunotherapy*, 6(12), 1265-78.
- [A2-2] Fontenot, A. P. and P. L. Simonian (2016). 13 - Adaptive Immunity. Murray and Nadel's Textbook of Respiratory Medicine (Sixth Edition). V. C. Broaddus, R. J. Mason, J. D. Ernst et al. Philadelphia, W.B. Saunders: 206-224.e203.
- [A2-3] Moticka, E. J. (2016). Chapter 2 - Hallmarks of the Adaptive Immune Responses. In E. J. Moticka (Ed.), *A Historical Perspective on Evidence-Based Immunology* (pp. 9-19). Amsterdam: Elsevier.
- [A2-4] Perica, K., Varela, J. C., Oelke, M., & Schneck, J. (2015). Adoptive T cell immunotherapy for cancer. *Rambam Maimonides medical journal*, 6(1), e0004.
- [A2-5] Cohen, J. E., Merims, S., Frank, S., Engelstein, R., Peretz, T., Lotem, M. (2017) Adoptive cell therapy: past, present and future. *Immunotherapy*. 9(2), 183-196.
- [A2-6] Sathyanarayanan, V., & Neelapu, S. S. (2015). Cancer immunotherapy: Strategies for personalization and combinatorial approaches. *Molecular oncology*, 9(10), 2043-53.
- [A2-7] Baruch, E. N., A. L. Berg, M. J. Besser, J. Schachter and G. Markel (2017). "Adoptive T cell therapy: An overview of obstacles and opportunities." *Cancer* 123(S11): 2154-2162.
- [A2-8] Chen, D. S. and I. Mellman (2013). "Oncology meets immunology: the cancer-immunity cycle." *Immunity* 39(1): 1-10.
- [A2-9] Pitt, J. M., M. Vetizou, R. Daillere, M. P. Roberti, T. Yamazaki, B. Routy, P. Lepage, I. G. Boneca, M. Chamillard, G. Kroemer and L. Zitvogel (2016). "Resistance Mechanisms to Immune-Checkpoint Blockade in Cancer: Tumor-Intrinsic and -Extrinsic Factors." *Immunity* 44(6): 1255-1269.
- [A2-10] Topalian, S. L., C. G. Drake and D. M. Pardoll (2015). "Immune checkpoint blockade: a common denominator approach to cancer therapy." *Cancer Cell* 27(4): 450-461.
- [A2-11] Sharma, P. and J. P. Allison (2015). "Immune checkpoint targeting in cancer therapy: toward combination strategies with curative potential." *Cell* 161(2): 205-214.
- [A2-12] Shin, D. S. and A. Ribas (2015). "The evolution of checkpoint blockade as a cancer therapy: what's here, what's next?" *Curr Opin Immunol* 33: 23-35.
- [A2-13] Iwamura, K., Kato, T., Miyahara, Y., Naota, H., Mineno, J., Ikeda, H., Shiku, H. (2012). siRNA-mediated silencing of PD-1 ligands enhances tumor-specific human T-cell effector functions. *Gene Therapy* (19), 959–966.
- [A2-14] Mueller, S. N., Vanguri, V. K., Ha, S. J., West, E. E., Keir, M. E., Glickman, J. N., Sharpe, A. H., ... Ahmed, R. (2010). PD-L1 has distinct functions in hematopoietic and nonhematopoietic cells in regulating T cell responses during chronic infection in mice. *The Journal of clinical investigation*, 120(7), 2508-15.

- [A2-15] McManus, M. T., B. B. Haines, C. P. Dillon, C. E. Whitehurst, L. van Parijs, J. Chen and P. A. Sharp (2002). "Small Interfering RNA-Mediated Gene Silencing in T Lymphocytes." *The Journal of Immunology* 169(10): 5754.
- [A2-16] Zhang, Y., Hsu, B. Y., Ren, C., Li, X., Wang, J. (2015). Silica-based nanocapsules: synthesis, structure control and biomedical applications. *Chem. Soc. Rev.*,44, 315-335.
- [A2-17] Murugadoss, S., Lison, D., Godderis, L., Van Den Brule, S., Mast, J., Brassinne, F., Sebaihi, N., Hoet, P. H. (2017). Toxicology of silica nanoparticles: an update. *Archives of toxicology*, 91(9), 2967-3010.

CHAPTER B

LIGHT-TRIGGERED RELEASE FROM NANOCAPSULES

Chapter B combines three different **Publications [B1-B3]**. These studies demonstrated new strategies for using nanocapsules in the release of functional payloads for cancer therapy. General introduction concerning recent advances in the controlled release of anti-cancer drugs are described. Afterwards, each study will be presented separately.

(Note: The literature of the introduction can be found on page 138 at the end of the dissertation.)

- [B1] ██████████, Raweewan Thiramanas⁺, ██████████
██████████ *Upconversion Nanocarriers Encapsulated with Photoactivatable Ru Complexes for Near-Infrared Light-Regulated Enzyme Activity.* *Small* **2017**, 13, 1700997. (+ **Shared first**)
- [B2] ██████████, Raweewan Thiramanas⁺, ██████████
██████████. *Photoactivation of Anticancer Ru Complexes in Deep Tissue: How Deep Can We Go?* *Chem. Eur. J.* **2017**, 23, 10832-10837.
(+ **Shared first**)
- [B3] ██████████, Raweewan Thiramanas⁺, ██████████
██████████
██████████
██████████. *Red-Light-Controlled Release of Drug-Ru Complex Conjugates from Metallopolymer Micelles for Phototherapy in Hypoxic Tumor Environments.* *Adv. Funct. Mater.* **2018**, 28, 1804227. (+ **Shared first**)

B. Introduction

Cancer is a serious medical issue that kills many people around the world every year. Many scientists have invested significant efforts to search for a new target and therapy. However, cancer is hard to kill and diagnose due to its ability to escape the immune system, leading to the decrease of treatment efficacy.^[Z-52-53] In addition, it is difficult to detect cancer in the early stages. Once symptoms are detected, cancer is mostly in the 3rd or 4th stage already.^[Z-54] In addition, a tumor site which is far away from blood supply has a unique tumor microenvironment, such as low oxygen (hypoxia), low nutrient, and acidosis (an excessively acid condition).^[Z-55-57] This hypoxic condition hinders drugs or other methods that need oxygen to generate the killing effect, e.g. singlet oxygen production in photodynamic therapy (PDT).^[Z-58] Nowadays, scientists continue to put effort into finding a new strategy for cancer treatment. The main way to treat cancer is still based on surgery because the bulk of the tumor can be eliminated. However, the disseminated part cannot be completely removed because of difficulty in distinguishing the tumor from healthy tissue. Moreover, the most concerning issues are the induction of tumor regrowth and metastatic state.^[Z-59] In addition to surgery, cancer therapy can be divided into two major strategies, chemotherapy and radiotherapy.

Chemotherapy has been investigated and developed to kill cancer over the last century and is currently the main treatment that will be considered by medical oncologists.^[Z-60] Chemotherapy involves the use of medicines and drugs to destroy cancer cells. Many anti-cancer drugs have been approved and used for the treatment of specific kinds of cancer. For example, doxorubicin (DOX) is effective against breast cancer, 5-fluorouracil against colon cancer, epirubicin against stomach cancer and paclitaxel against lung cancer.^[Z-61] However, directly using these drugs *via* oral, parenteral (injection) or transdermal administration can result in reduced cancer treatment efficiency due to drug metabolism, lacking the ability to achieve site-specific activation, and adverse side effects for healthy tissue.^[Z-62] Therefore, a drug delivery system is needed to protect the encapsulated drug from drug metabolism and deliver it to the target area. Furthermore, a stimuli responsive delivery system is required to avoid

unintentional release in order to protect the normal tissue and control release of the functional payload when it reaches the specific site.

Unlike radiotherapy that kills cancer cells by using high-energy rays, phototherapy involves the use of light to destroy cancer cells. Phototherapy can be used for treatment of a specific area, thereby avoiding damage to the rest of the body.^[Z-63] However, the limitation of this technique is based on how deep the desired therapeutic wavelength can penetrate through the tissue, which can be seen clearly from **Figure B1**. The optimal wavelength used for phototherapy is in the region of 650-900 nm, which is called the “therapeutic window”. Therefore, it is a critically important point to consider for designing a wavelength-specific control release strategy to obtain maximum therapeutic efficacy.

In this chapter, the light responsive nanocarriers or compounds were designed to control the release of an inhibitor of enzyme Cathepsin K in **Publication [B1]**, ruthenium complexes in **Publication [B2]**, and anti-cancer drug Chlorambucil in **Publication [B3]** by combining the advantages of chemotherapy and phototherapy into photochemotherapy and demonstrating the *in vitro* therapeutic effect by treatment in cancer cell lines.

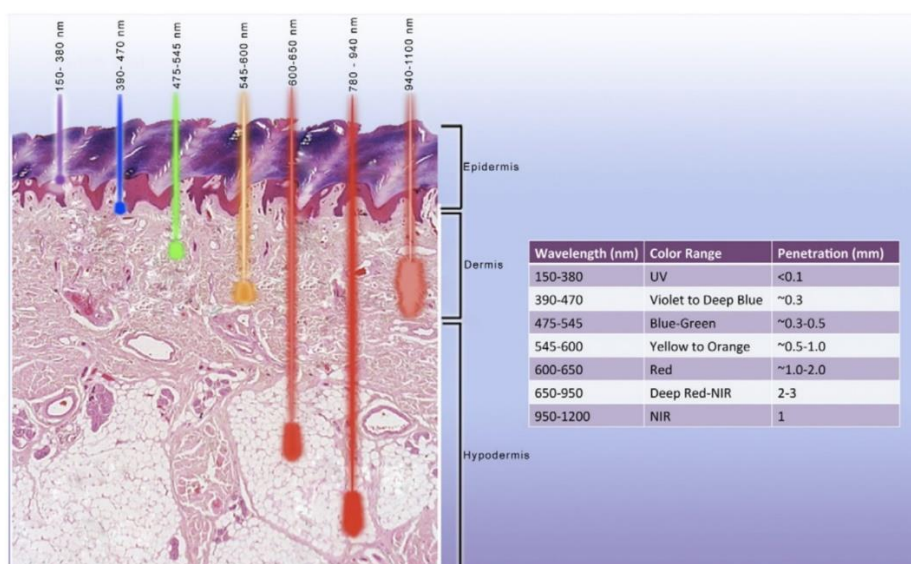


Figure B1. Tissue penetration of various wavelengths. (Taken from *Ref.* ^[Z-64] Semin. Cutan. Med. Surg. 2013, 32, 41-52. Copyright © 2013 Frontline Medical Communications, original figure with Courtesy of Wellman Center for Photomedicine)

In **Publication [B1]**, near-infrared (NIR) light was used to trigger the Cathepsin K inhibitor controllable release system called “photon upconversion enzyme inhibitor (PUEI)”. The system consists of a hollow mesoporous silica nanoparticle used as a nanocarrier encapsulated with upconversion nanoparticles (UCNPs) and ruthenium complex caged inhibitor (RuEI). UCNPs can convert NIR light to blue light, which induces the cleavage of RuEI. The inhibitor is then activated and subsequently released, resulting in the inhibition of Cathepsin K activity as demonstrated in three different cancer cell lines: LNCaP, PC3 and SAOS-2. Cathepsin K is an important enzyme involved in bone resorption and cancer invasion. Thus, the inhibition of this enzyme can impede bone destruction and tumor growth. This system can be used as a model for regulating enzyme activity in deep tissue by using the NIR light responsive control system.

In **Publication [B2]**, a Ru complex was investigated for possible use in photochemotherapy for deep tissue. In fact, NIR light is able to penetrate into the tissue not as deep compared to red light. In addition, the therapeutic window (650-900 nm) is in the region of red light. Therefore, the 671 nm-red light was chosen to activate the Ru complex in this **Publication [B2]** instead of NIR light. With the outstanding property of being photocleavable and ruthenium being an anticancer compound, this makes the Ru complex highly interesting. The complex is less toxic to HeLa cells in the dark condition and becomes more toxic when irradiated with red light (671 nm) passed through 8 mm-thick tissue. The results suggest that red light responsive Ru complex has the potential for use in deep tissue photochemotherapy.

In **Publication [B3]**, from a promising result in **Publication [B2]**, red light in a region of therapeutic window was continued for use in the activation of controlled release of chlorambucil (anticancer drug)-Ru complex conjugates from metallopolymer micelles in hypoxic tumor microenvironment. The hydrophilic block copolymer conjugated with hydrophobic drug-Ru complex can be self-assembled into micelles, thus facilitating the uptake of tumor cells. In deep solid tumors, this area has very low physiological oxygen concentration, leading to reduced cancer treatment efficiency when applying photodynamic therapy, which is critically dependent on local oxygen concentration. With this new dual system using both anticancer drug, toxicity is oxygen

independent and Ru complex, which can be both oxygen dependent- and independent-, the efficiency to kill cancer cells can be overcome, even in hypoxic condition, as demonstrated *in vitro* (in HeLa cells) and *in vivo* (in tumor-bearing mice). This novel red-light responsive drug-Ru complex containing micelles integrates a new powerful system for photochemotherapy and can be applied even in hypoxic tumor microenvironment.

Stimuli responsive drug delivery system can be recognized as on-demand drug delivery system or smart drug delivery system. The system provides an ability to control over the specific place, time, and amount of cargo to be released upon the activation by specific stimuli.^[Z-65] Here, an overview of various stimuli responsive mechanisms that can be applied in the controlled release of payloads is described in general, while light-responsiveness, which is the major controlled release strategy in these studies, is explained in particular.

B.1 stimuli responsive mechanisms

There are various types of stimuli responsive mechanisms used for controlled release, which can be categorized into two major types according to the source of stimuli; intrinsic stimuli and extrinsic stimuli. Considering the huge differences between normal cells and cancerous cells such as cellular pH, redox conditions, specific generated biomolecules types and amounts, all these originally unique characters bring intrinsic stimuli for a controlled release strategy and cell-specific therapy. This type of stimuli employs the internal distinct characters of cancerous cells to switch on the release of the payload. Meanwhile, extrinsic stimuli do not naturally exist inside the human body. Stimuli such as heat, magnetic force and light also share an important role as an ideal stimulus, in which site-, dose- and time-specific release are more precisely controllable from outside of the body.

B.1.1 Intrinsic stimuli

B.1.1.1 pH-responsiveness

pH responsive stimuli is used for control release based on naturally-different pH in various tissues/organs of the body. It generally uses acidic pH to induce drug release. A low pH environment is found not only in cancerous cells, but also in various parts of

the body such as the stomach, skin and vaginal fluid, as shown in **Table B1**. Therefore, the pH responsive delivery system that needs to be used in or passed through these areas has to be carefully designed to avoid the release of the payload before reaching the target site. The mechanisms behind pH induced drug release of the delivery system are based on changing in their structure when they are in different pHs, which can be summarized into three main mechanisms: acid-caused charge reversal, acid-cause dissolution behavior change, and acid-caused hydrolysis reaction and bond breaking.^[Z-66]

Table B1. pH of some fluids, organs and membranes. (Taken from *Ref.* ^[Z-67] J. Environ. Public Health, 2012, 727630. Copyright © 2012 Gerry K. Schwalfenberg)

Organ, fluid or membrane	pH	Function of pH
(1) Skin	Natural pH is between 4 and 6.5 [17]	Barrier protection from microbes
(2) Urine	4.6 to 8.0 [18]	Limit overgrowth of microbes
(3) Gastric	1.35 to 3.5	Break down protein
(4) Bile	7.6 to 8.8	Neutralize stomach acid, aid in digestion
(5) Pancreatic fluid	8.8	Neutralize stomach acid, aid in digestion
(6) Vaginal fluid	<4.7 [13]	Limit overgrowth of opportunistic microbes
(7) Cerebrospinal fluid	7.3	Bathes the exterior of the brain
(8) Intracellular fluid	6.0–7.2 [19]	Due to acid production in cells
(9) Serum venous	7.35	Tightly regulated
(10) Serum arterial	7.4	Tightly regulated

B.1.1.2 Redox-responsiveness

Redox state of cancer cells can be employed for the control release of a drug from its carrier. Many reducing substances are commonly distributed through the human body such as vitamin C, vitamin E, and glutathione (GSH). GSH is one of the most efficient antioxidants naturally produced in the body. It prevents cellular damage from oxidative stress generated by reactive oxygen species (ROS) such as free radicals, peroxides, lipid peroxides, and heavy metals. The concentration of GSH inside the tumor cells is reported at about 2-10 mM, which is an enormous difference from outside by about a thousand-fold. As a reducing agent, GSH reduces disulfide bond within cytoplasmic proteins to cysteines by working as an electron donor. Regarding this disulfide bond cleavage ability, the high concentration of GSH inside the cancer cells can be used to break the carrier formation containing a disulfide bond in its structure, resulting in the release of the payload intracellularly. Based on this strategy, the

functional payload will be released only when the delivery system internalizes the target cancer cells.^[Z-66]

In addition, oxidizing substances can also be used to release the cargo. It has been found that not only GSH is overproduced in cancer cells, but also ROS, especially hydrogen peroxide (H₂O₂). It is proposed that the cancer cells are considered “seeds” that need an appropriate microenvironment considered as “soil” to grow in, develop and metastasize systemically. Cancer cells initially produce and secrete hydrogen peroxide that induces oxidative stress in adjacent cancer-associated fibroblasts, leading to DNA damage, inflammation, cellular aging and cancer metabolism. As a result of providing a paradise-like tumor microenvironment, hydrogen peroxide is considered the “fertilizer”.^[Z-68] Therefore, it is possible to design hydrogen peroxide sensitive materials and employ intracellular hydrogen peroxide to cleave the structure and finally release the cargo inside tumor cells.^[Z-66]

B.1.1.3 Biomolecule-responsiveness

With an increase in knowledge concerning biomolecule generation and distribution, it has become possible to creatively design responsive materials based on specific biomolecules that accumulate higher in the target cancer cells than in normal healthy cells. A wide variety of biological molecules can be used as targets for biomolecule-responsive materials, including nucleic acids, saccharides, peptides, and enzymes. Due to their specificity and excellent biocompatibility, biomolecule-responsive polymers have been widely used in biomedical applications. Importantly, it is also considered as a new generation of material for disease diagnosis and drug controllable release. Because biomolecule-responsive carriers provide better targeting ability compared to traditional extrinsic stimuli, they have gained significant interest for development and application *in vivo*.^[Z-69]

B.1.2 Extrinsic stimuli

B.1.2.1 Thermo-responsiveness

Using thermo-responsive stimuli for the delivery system, thermo-responsive polymers are needed. This type of polymer has a unique characteristic in that its structure can be reversibly transformed relating to the surrounding temperature. It can

be divided into two major types of thermo-responsive polymers: lower critical solution temperature (LCST)-type and upper critical solution temperature (UCST)-type.^[Z-65,70]

For LCST-type polymer, the polymer is more water soluble and swollen when the temperature is below the LCST because of an attractive interaction between polymer chains and water molecules forming hydrogen bonding, which can keep the cargo inside the polymer matrix. In contrast, the polymer is shrunken and collapsed when the temperature is higher than the LCST because of hydrogen bonding breaking, leading to disassembly of the polymer matrix and release of the cargo. The most widely used LCST-type polymers are the family of poly(*N*-isopropylacrylamide)s (PNIPAAms) and poly(2-oxazoline)s (POxs), which comprise naturally derived cellulosic polymers. The LCST of PNIPAAm is about 30-35 °C, which can be beneficial for controlled release because it is very close to the human body. Meanwhile, the LCST of Pox ranges from 23-75 °C depending on the side chain. A critical point to carefully design thermo-responsive stimuli for the delivery system is that the LCST of the polymer should be higher than human body temperature to avoid leakage out of the cargo before reaching the target site. For UCST-type polymers, the behavior is opposite to the LCST-type. When the temperature is below the UCST, the structure becomes heterogeneous. When the temperature is above the UCST, however, its structure becomes homogeneous, as shown in **Figure B2**. In general, heat itself can directly contribute to kill the cancer cell like in phototherapy and can indirectly facilitate the uptake of the drug carrier to cancer cells by increasing the permeability of the cell membrane. Thus, applying thermo-responsive control release drug delivery system to the cell can combine all these benefits.^[Z-65,70]

B.1.2.2 Magnetic field-responsiveness

Because of non-invasive stimuli, the magnetic field-responsive delivery system has been used and widely accepted as a potential carrier for specific drug targeting.^[Z-71] The system needs magnetic nanoparticles such as Fe₃O₄ nanoparticles. In the beginning, nanocarriers loaded with magnetic nanoparticles and drugs are designed to control the direction by applying external magnetic force to accumulate in the site of a tumor. Later, the magnetic field-responsive nanocarriers have been successfully developed based on mechanical deformation or structure rupture under a strong

magnetic field and then release the payload.^[Z-71] Moreover, magnetic nanoparticles can be used as a contrast agent for bio-imaging and can also be applied as a thermo-responsive stimulus in treatment of hyperthermia, resulting in an enhanced extermination effect against cancer cells.^[Z-66]

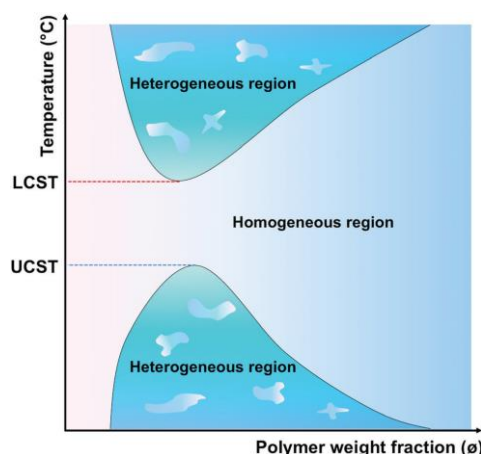


Figure B2. Phase diagrams of LCST- and UCST-type polymer aqueous solutions. Copyright © 2017 Royal Society of Chemistry. Reprinted with permission from Royal Society of Chemistry. Ref. ^[Z-70] *J. Mater. Chem. B*, 2017, 5, 4307-4321.

B.1.2.3 Light-responsiveness

Among different stimuli, light-responsive stimulus is considered to be one of the most promising strategies to control the release of a functional payload from its container due to its distinct advantages. Light is non-invasive, convenient and easy to use.^[Z-65] Importantly, it provides temporal and spatial controllability, which means the release of the payload can be precisely controlled when activating with a specific light at a specific target site. A light-responsive drug delivery system commonly functions based on three major mechanisms: photoisomerization, photocleavage and photo-induced disaggregation of the carriers.^[Z-66] As mentioned previously, the limitation of this stimulus is based on the depth of the desired therapeutic wavelength and its ability to penetrate through tissue, which can be clearly seen from **Figure B1**. The wavelength in the region of 650-900 nm is widely accepted for use in phototherapy, which is called the “therapeutic window”. Therefore, designing a specific wavelength used for control release strategy should be carefully considered to obtain the highest treatment efficiency. The region of specific wavelength that is widely used for triggering the

release includes ultraviolet (UV) light (10-400 nm), visible (Vis) light (400-700 nm), red light (600-700 nm) and near-infrared (NIR) light (780-2526 nm).

UV-Vis light possesses high energy, which can be used to activate the release system efficiently *in vitro*. Many chemicals have been used as UV-Vis light-responsive materials such as azobenzene, spiropyran, pyrenylmethyl, *o*-nitrobenzyl and coumarin family.^[Z-66] However, UV-Vis light is absorbed strongly by the human tissues, leading to low penetration ability. This makes UV-Vis light inappropriate for use in deep tissue. Moreover, UV light can cause photodamage to cells due to its relatively high energy.^[Z-72]

Nowadays, NIR has become more attractive for use in light-triggered control release due to its safety, including no photodamage to cells, weak background fluorescence, high detection sensitivity and high penetration ability in deep tissue.^[Z-72] NIR light has been applied for controlled release based on two-photon absorption, which provides higher excitation and overcomes the poor penetration of UV-Vis light sensitive system.^[Z-73] In fact, however, two-photon absorption requires high-intensity pulsed laser and only occurs at the laser focus. When the laser passes through tissue, it defocuses, which makes the two-photon absorption strategy impractical for use in deep-tissue. In addition, a limitation of NIR light is its low energy, which is not strong enough to activate the photoreaction. To solve this problem, many strategies have been developed such as triplet–triplet annihilation upconversion, upconverting nanoparticles, and the use of NIR photosensitizers.^[Z-65] The recent development of up-conversion nanomaterials makes NIR light an alternative approach to trigger the photosensitive drug releasing system. Upconversion materials are synthesized using lanthanide-based substances. Lanthanide ions such as Tm^{3+} , Er^{3+} and Ho^{3+} possess the distinct ladder-like energy level structures. Lanthanide-doped upconverting nanoparticles (UCNPs) can absorb NIR light and convert it into high energy in a region of UV-Vis emission, which enables activation of the subsequent UV-light responsive system.^[Z-72] Another advantage compared to two-photon absorption strategy is that UCNP-assisted photochemistry does not require a high-intensity pulsed laser. NIR light-triggered photoreactions based on lanthanide-doped upconverting nanoparticles is the controlled release strategy used in **Publication [B1]**.

Similar to NIR light, red light is suitable for use in controlled release in biomedical applications due to its high penetration ability in deep tissue.^[Z-64] In fact, trigger of light responsive therapeutic materials by direct irradiation with red or NIR light *via* a one-photon process is more efficient to obtain a maximum therapeutic effect than nonlinear optical processes such as two-photon absorption and photon upconversion.^[Z-65] For this purpose, photo-sensitive therapeutic agents that can be directly activated by red or NIR light *via* a one-photon process are required. Photosensitizer drugs are commonly used in photodynamic therapy (PDT) and photoactivated chemotherapy (PACT). PDT uses specific light or laser to induce singlet oxygen generation from photosensitizer drugs, leading to oxidative stress in cancer cells and finally kill the cancer cells by reactive oxygen species (ROS)-mediated toxicity. This therapy requires specific light to activate photosensitizer drugs and also physiological oxygen to produce singlet oxygen. Meanwhile, PACT, an oxygen-independent therapy, uses specific light or laser to release the toxic unit from photosensitizer drugs.

A wide variety of exciting strategies employing light-responsive drug delivery systems have been developed to achieve therapeutic efficacy at the clinical level. Many of them have gained proof of concept successfully *in vitro*, while others have demonstrated promising results *in vivo*. However, there has not been any report for light-responsive drug delivery system at clinical trials. Currently, the stimuli-responsive drug delivery systems that have been reported with high progress are the temperature-responsive drug delivery system (ThermoDox, Doxorubicin containing liposome) at clinical trials Phase III targeting to liver cancer and Phase II targeting to lung cancer and redox (GSH concentration) -responsive drug delivery system (T-DM1[®], paclitaxel or docetaxel containing antibody conjugate) targeting to metastatic breast cancer already approved by FDA.^[Z-66]

This is partly due to the complex design of many stimuli-responsive drug delivery systems, including light responsive systems. Therefore, it was suggested that “it will be advantageous to keep the KISS principle in mind: keep it simple and straightforward”.^[Z-65] Some advantages and limitations of each stimuli-responsive drug delivery system have been summarized in **Table B2**.

Table B2. Advantages and limitations of some stimuli-responsive drug delivery systems. (Taken from *Ref.* ^[Z-65] *Therapeutic delivery*, 2017, 8(2), 89-107. Copyright © 2017 Future Science Ltd.)

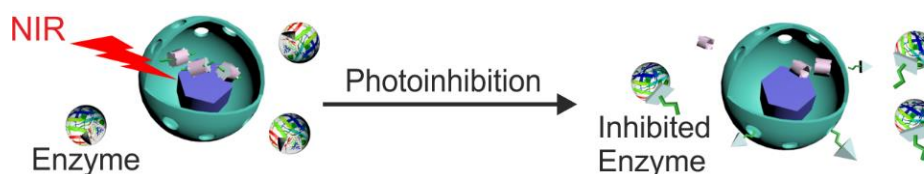
Stimulus	Advantage(s)	Limitation(s)
Biomarker	High target specificity	Stability, potential leakage and possible immunogenicity of enzymes or antibodies used in the delivery system
pH	Small changes in pH can result in significant chemical and physical changes in drug carrier	Limited to the clinical conditions that alter local pH
Electrical	Iontophoresis devices make electrical fields accessible in the clinic Safe levels of electrical field strengths have been extensively studied	Risk of damage to healthy tissue from electric source needed for deep tissue penetration (attenuation of stimulus) Electroresponsiveness is affected by many environmental factors (e.g., composition of aqueous medium, concentrations of electrolytes, presence of ionizable molecules)
Heat	Cancer cells are sensitive to hyperthermia (i.e., apoptosis, increased sensitivity to radiation and chemotherapeutics) Thermally responsive drug-delivery systems are in clinical trials	Risk of superficial tissue damage from external heating source needed for deep tissue penetration (attenuation of stimulus)
Light	Ability to sequentially trigger multiple payloads High degree of spatiotemporal precision	Questionable safety and/or biodegradability of materials Safety risks and low tissue penetration for UV-Vis light
Magnetic	In addition to triggered delivery, capable of magnetically guided drug targeting and can act as a contrast agent for imaging Magnetically responsive drug-delivery systems are in clinical trials	Potential toxicity from iron oxide Requires complex equipment set-up for adequate focusing, intensity and penetration depth
Ultrasound	Minimal safety risks with low intensity and short exposures High degree of spatiotemporal precision	Risk of damage to tissues with high intensity and long exposures Low drug carrier stability

B1: UPCONVERSION NANO-CARRIERS ENCAPSULATED WITH PHOTOACTIVATABLE RU COMPLEXES FOR NEAR-INFRARED LIGHT-REGULATED ENZYME ACTIVITY

(Note: The literature of the chapter B1 can be found on page 73 at the end of this chapter.)

Permission: The following part [B1] is based on a publication in *Small* 2017, 13, 170099. Presented materials are reprinted with permission from John Wiley and Sons. Copyright © 2017, John Wiley and Sons

Contribution: [REDACTED] and I contributed equally to this work. I carried out the biological part including cell toxicity, Cathepsin K activity assay, Cathepsin K inhibition assay, lysosome co-localization assay, cellular uptake study by flow cytometry and cLSM. [REDACTED] synthesized and characterized the Cathepsin K inhibitor controllable release system. [REDACTED] performed upconversion luminescence cell imaging. The project was supervised by [REDACTED]



TOC B1: Photon upconversion enzyme inhibition is employed to regulate enzyme activity using NIR light. Upconverting nanoparticles and caged enzyme inhibitors are encapsulated in hollow mesoporous silica nanoparticles. Upconverting nanoparticles convert near-infrared light to blue light, which activates caged enzyme inhibitors. The activated enzyme inhibitors are released and inhibit the enzyme activity in living cells.

Aim: Cathepsin K is a key enzyme that plays an important role in bone remodeling and cancer metastasis. Therefore, inhibition of this enzyme can prevent bone digestion and tumor invasion. To achieve this goal, the Cathepsin K inhibitor controllable release system responsive to the near infrared (NIR) light was developed and applied to inhibit three different sources of Cathepsin K: purified (commercial) enzyme, lysate and live

cells. Three different cell lines including LNCaP, PC3 cells (prostate cancer cell lines) and SAOS-2 cells (osteosarcoma cell line) were chosen to demonstrate the enzymatic inhibition of the new controlled release platform) due to their ability to exhibit overexpression of Cathepsin K.

Abstract: Enzyme activity is important for metabolism, cell functions, and treating diseases. However, remote control of enzyme activity in deep tissue remains a challenge. Here, we demonstrate near-infrared (NIR) light-regulated enzyme activity in living cells based on upconverting nanoparticles (UCNPs) and a photoactivatable Ru complex. The Ru complex is a caged enzyme inhibitor that can be activated by blue light. To prepare a nano-carrier for NIR photoinhibition of enzyme activity, a UCNP and the caged enzyme inhibitors were encapsulated in a hollow mesoporous silica nanoparticle. In such a nano-carrier, the UCNP can harvest NIR light and convert it into blue light, which can activate the caged enzyme inhibitors. This photoactivation process is feasible in deep tissue because of the tissue penetration ability of NIR light. The nano-carrier was compatible to LNCaP, PC3, and SAOS-2 cells, which showed high enzyme expression. NIR irradiation induced release of the inhibitors and inhibition of enzyme activity in living cells. NIR light provides high spatiotemporal resolution to regulate enzyme activity in deep tissue.

B1.1. Introduction

Enzymes are important macromolecular biological catalysts that enable chemical reactions in biological systems. Controlling enzyme activity can regulate metabolism, manipulate cell functions, kill pathogens, and treat diseases.^[B1-1] Due to the great importance of enzymes in biological systems, the use of external stimuli, such as pH,^[B1-2] temperature,^[B1-3] ATP,^[B1-4] cations,^[B1-5] and light,^[B1-6] to control enzyme activity has been developed. Among these stimuli, light provides high spatiotemporal resolution for controlling enzyme activity. UV or visible light can control photoresponsive compounds, such as photocages and photoswitchable molecules.^[B1-7] The photoproducts from these photoresponsive compounds can then regulate enzyme activities.^[B1-6a, 6e, 8] However, UV light may damage biological systems. Additionally,

both UV and visible light cannot penetrate deeply into tissue. In contrast, near-infrared (NIR) light can penetrate deeply into tissue and causes less photodamage to biological systems.^[B1-9]

NIR light has been applied for controlling enzyme activities based on two-photon absorption.^[B1-8a, 10] However, two-photon absorption requires high-intensity pulsed lasers (typical pulse intensity: $>10^6$ W cm⁻²)^[B1-11] and is inefficient even when femtosecond lasers are employed. Two-photon absorption only occurs at the laser focus. Because the laser defocuses as it passes through tissue, the two-photon absorption strategy is impractical for deep-tissue applications.

Recently, NIR light-triggered photoreactions based on lanthanide-doped upconverting nanoparticles (UCNPs) have been developed.^[B1-9b, 12] UCNPs can convert NIR light into UV and visible light.^[B1-13] Then, the upconverted UV or visible emission can trigger photoreactions of traditional UV- or visible light-responsive compounds. This process is referred to as UCNP-assisted photochemistry.^[B1-9b, 14] UCNP-assisted photochemistry can be triggered by continuous wave laser diodes with intensities that are several orders of magnitude lower than that required for two-photon absorption.^[B1-9b, 15] UCNPs have assisted different photoreactions including photoisomerization,^[B1-14c, 16] photocleavage,^[B1-17] photopolymerization,^[B1-14d, 18] and photo-coupling.^[B1-19] These UCNP-assisted photoreactions have been applied to NIR-controlled drug delivery,^[B1-14c, 15b] biointerfaces,^[B1-15a, 16] uncaging enzymes,^[B1-17c] catalysis,^[B1-20] pH,^[B1-21] and actuators.^[B1-14e] However, inhibition of enzyme activity using NIR light assisted by UCNPs has not been investigated.

Here, we use NIR light to regulate enzyme activity based on UCNP-assisted photochemistry (**Figure B1.1**). We refer to this new method as photon upconversion enzyme inhibition (PUEI). To construct a platform for PUEI, a NaYF₄:TmYb@NaYF₄ UCNP and caged enzyme inhibitors (RuEI) are encapsulated in a hollow mesoporous silica nanoparticle (hmSiO₂) (**Figure B1.1b**). RuEI can be activated by blue light to release the enzyme inhibitor (EI). Our group^[B1-9b, 15, 21-22] and others^[B1-14f] have demonstrated that NIR light can efficiently uncage Ru complexes that are similar to RuEI with the assistance of UCNPs. With RuEI&UCNP@hmSiO₂ in this study, UCNPs can convert NIR light to blue light, which can uncage EI from RuEI (**Figure**

B1.1). After NIR photoactivation, the released EI can inhibit the activity of the cathepsin K enzyme (**Figure B1.1b**). Cathepsin K is an important enzyme that is critical for osteoclastic bone resorption, macrophage invasion, and tumor growth.^[B1-23] Cathepsin K is involved in the resorption of bone tissue in osteoclasts and therefore responsible for the remodeling of bone.^[B1-24] Resorption of bone should be inhibited under some circumstances, such as bone loss in elderly patients or during the regeneration of new bone after a fracture. For the treatment of cancers and tumor metastases, cathepsin K is a key factor that affects the invasiveness of tumors into healthy tissue.^[B1-25] Therefore, the inhibition of cathepsin K is important. NIR photoinhibition of the activity of cathepsin K allows for new routes for manipulating cell functions, regenerative medicine, and treating the spread of malignant diseases in deep tissue. PUEI also provides a general platform for regulating enzyme activity in deep tissue.

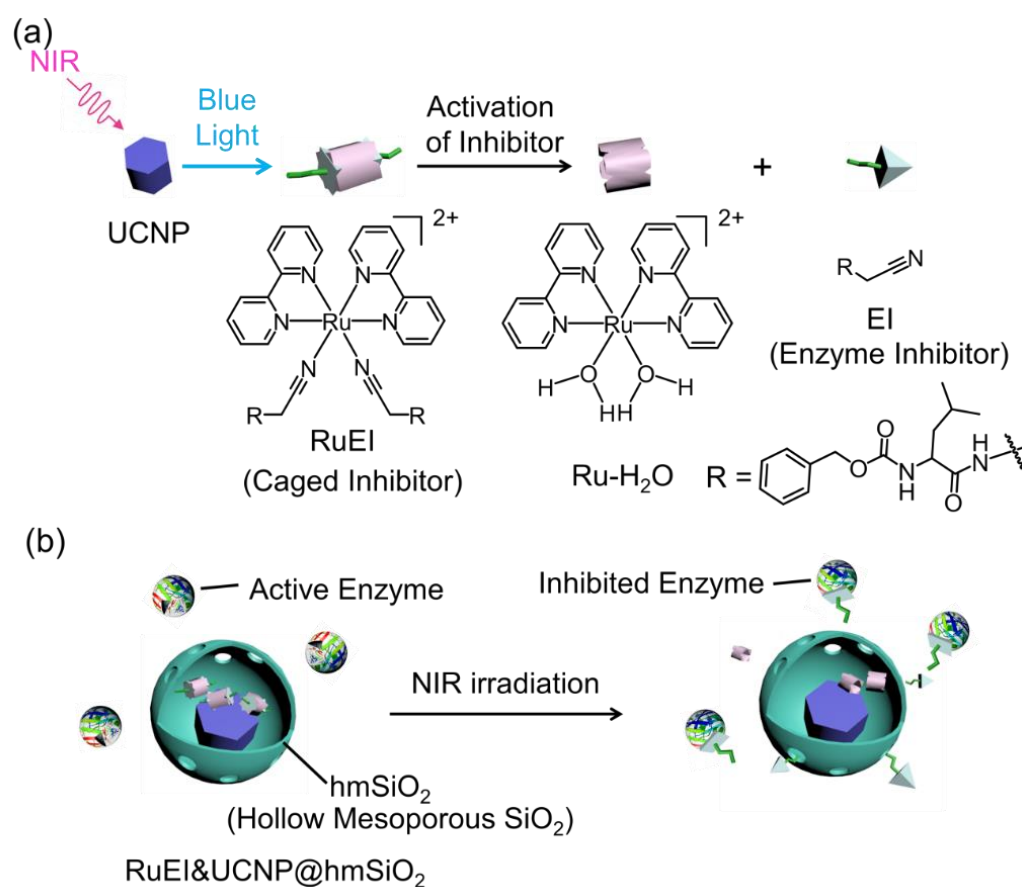


Figure B1.1. Schematic illustration of photon upconversion enzyme inhibition (PUEI). (a) Activation of the enzyme inhibitor using near-infrared (NIR) light with the assistance of UCNPs. UCNPs convert NIR light to blue light, which induces the cleavage of the caged inhibitor (RuEI) and activation of the enzyme inhibitor (EI). (b) NIR irradiation of RuEI&UCNP@hmSiO₂ activates EI, which inhibits enzyme activity.

B1.2. Results and discussion

B1.2.1. NIR photoinhibition of enzyme activity

RuEI&UCNP@hmSiO₂ provides a platform for NIR light-induced inhibition of enzyme activity in deep tissue (**Figure B1.2a**). The half maximal inhibitory concentration (IC₅₀) of the activated EI was only 1/6 of that of the caged inhibitor RuEI for the inhibition of cathepsin K (**Figure B1.3**). Therefore, photoactivation of EI can efficiently inhibit cathepsin K. NIR irradiation of cathepsin K in the presence of RuEI&UCNP@hmSiO₂ triggered photocleavage of RuEI. Released EI can react with thiol moieties of cathepsin K,^[B1-8b] which irreversibly inhibited its activity significantly (**Figure B1.2b, blue bars**). Irradiation for 7, 15, and 30 min reduced the enzyme activity to 30%, 17%, and 13%, respectively (**Figure B1.2b, blue bars**). For comparison, control experiments in the absence of RuEI&UCNP@hmSiO₂ after NIR irradiation (**Figure B1.2b, black bars**) and the presence of RuEI&UCNP@hmSiO₂ without NIR irradiation (**Figure B1.2b, red bars**) were performed. Enzyme activities in these control samples did not decrease. These results demonstrated that the inhibition of enzyme activity was caused by activation of the EI using NIR light. Moreover, the feasibility of using NIR light to inhibit enzyme activity after passing through tissue was investigated, which is important for clinical applications in the future. A piece of chicken tissue was placed between the NIR light and the sample. The NIR light passed through the tissue and inhibited the enzyme activity (**Figure B1.2b, magenta bars**).

B1.2.4. Evaluation of biocompatibility of RuEI&UCNP@hmSiO₂

Before enzyme inhibition in living cells was studied, the biocompatibility of RuEI&UCNP@hmSiO₂ was studied via cellular experiments. LNCaP, PC3 cells (prostate cancer cell lines) and SAOS-2 cells (osteosarcoma cell line) were used in our study. These cell lines were chosen because they have a high cathepsin K expression

rate for their invasiveness, which results in metastases in the prostate cancer cell lines and the osteosarcoma cell line. To test the biocompatibility, RuEI&UCNP@hmSiO₂ was incubated with all three cell lines for 24 h. Only a minor decrease in the cell viability was observed in the presence of a high concentration (150 µg/mL) of RuEI&UCNP@hmSiO₂ (**Figure B1.4**). After NIR irradiation (1 W/cm²) on LNCaP cells in the presence or absence of RuEI&UCNP@hmSiO₂ (150 µg/mL), the cell viability was higher than 90% (**Figure B1.5a**). The biocompatibility tests on PC3 and SAOS-2 cells showed similar results to that of LNCaP cells (**Figure B1.5b, c**). These results suggested that RuEI&UCNP@hmSiO₂ provides a biocompatible platform for NIR photoinhibition of enzyme activity in living cells.

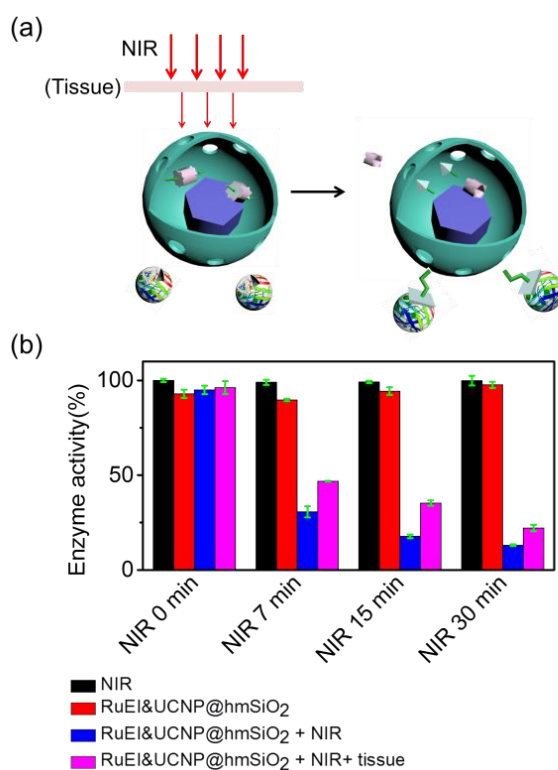


Figure B1.2. (a) Schematic illustration of NIR photoinhibition of enzyme activity using RuEI&UCNP@hmSiO₂. (b) NIR photoinhibition of the activity of cathepsin K. Black bars: activities of cathepsin K in the absence of RuEI&UCNP@hmSiO₂ under NIR irradiation; Red bars: activities of cathepsin K in the presence of RuEI&UCNP@hmSiO₂ without irradiation; Blue bars: activities of cathepsin K in the presence of RuEI&UCNP@hmSiO₂ under NIR irradiation. Magenta bars: activities of cathepsin K in the presence of RuEI&UCNP@hmSiO₂ under NIR irradiation through

a piece of 1 mm thick tissue. The concentration of RuEI&UCNP@hmSiO₂ was 10 µg/mL. The intensity of the 974 nm laser was 1 W/cm².

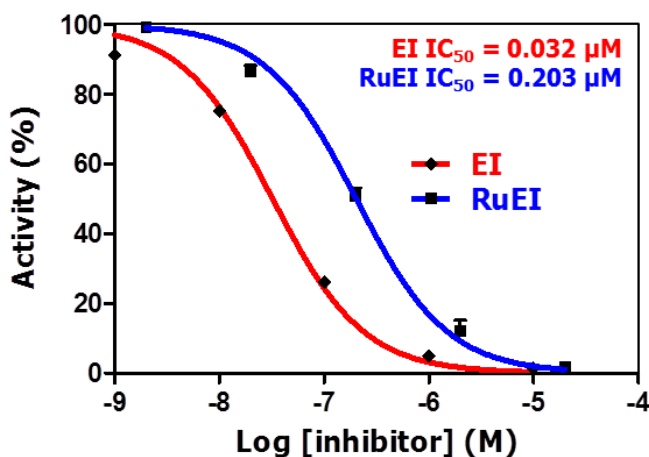


Figure B1.3. Cathepsin K inhibition assay of commercial enzyme in the presence of EI or RuEI determined with hydrolysis of the fluorogenic substrate Z-GPR-AMC. The IC₅₀ of EI and RuEI were 0.032 and 0.203 µM, respectively. This result indicates EI generated by photoactivation of RuEI can efficiently inhibit the activity of cathepsin K.

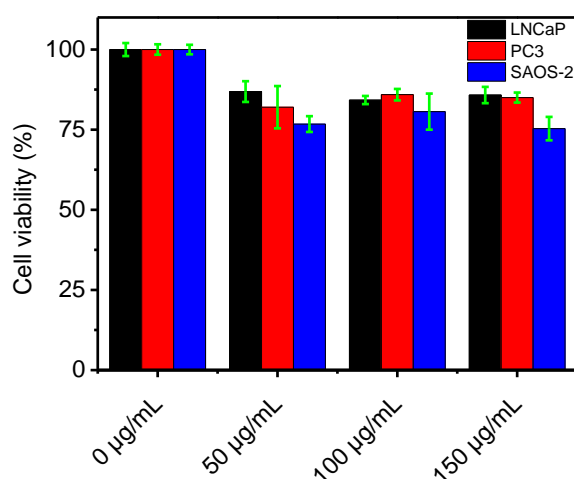


Figure B1.4. Cytotoxicity of RuEI&UCNP@hmSiO₂ in LNCaP, PC3, and SAOS-2 cells. Cell viability was determined by MTS assay after treatment for 24 h. The results indicate that RuEI&UCNP@hmSiO₂ has good biological compatibility with these cells.

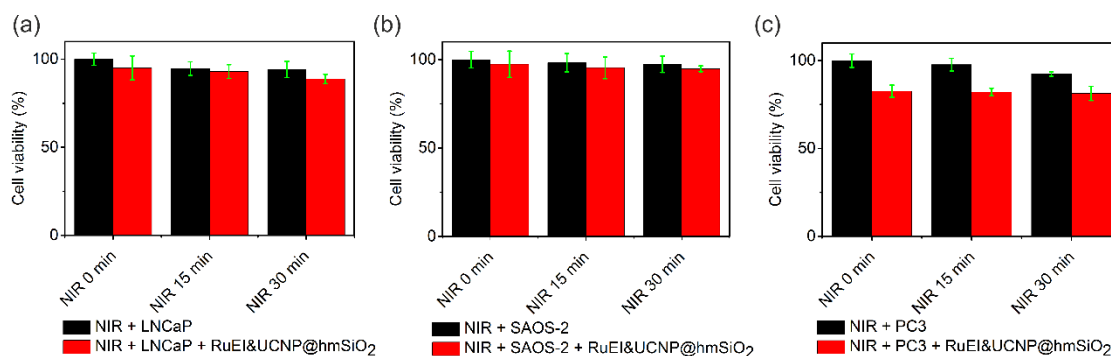


Figure B1.5. Cytotoxicity of RuEI&UCNP@hmSiO₂ in LNCaP, PC3, and SAOS-2 cells upon NIR irradiation. Cell viability was determined by MTS assay after treatment for 24 h.

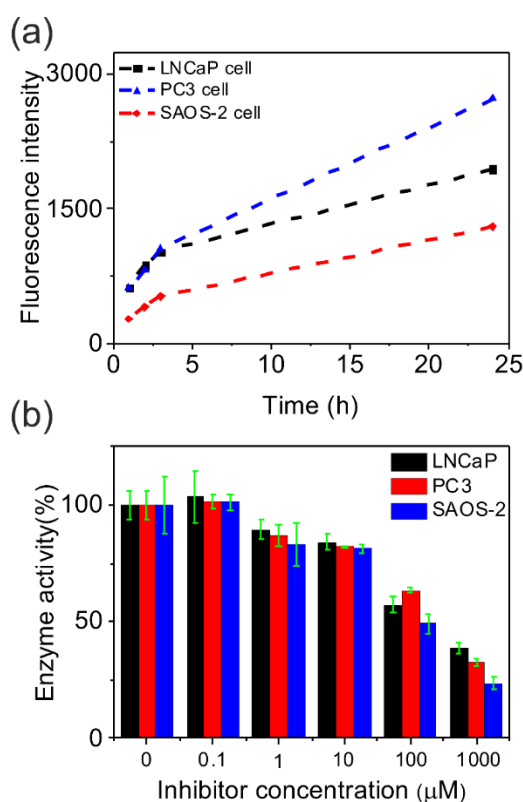


Figure B1.6. (a) Cathepsin K activity assay of LNCaP, PC3 and SAOS-2 live cells determined with hydrolysis of cathepsin K fluorogenic substrate Abz-HPGGPQ-EDDnp. (b) Cathepsin K inhibition assay of LNCaP, PC3 and SAOS-2 cell lines in the presence of EI determined with hydrolysis of cathepsin K fluorogenic substrate Abz-HPGGPQ-EDDnp.

B1.2.5. Cathepsin K activities in live cells

To study cathepsin K activities in the three used cell lines, cathepsin K fluorogenic substrate Abz-HPGGPQ-EDDnp was incubated with LNCaP, PC3, and SAOS-2 live cells at 37 °C. Time-dependent fluorescence increase was observed, which indicated the cleavage of the fluorescent substrate by the active enzyme in the live cells (**Figure B1.6a**). This result confirmed that cathepsin K expressed activity in all three investigated cell lines. To study effects of EI on the activities of cathepsin K in the three cell lines, EI was incubated with these cell lines. Addition of EI decreased the cathepsin K activity in all three cell lines (**Figure B1.6b**), which encouraged us to explore NIR light-induced inhibition of enzyme activity in live cells.

B1.2.6. NIR photoinhibition of enzyme activity in live cells

To study photoinhibition of enzyme activity in live cells, fluorescence-labeled UCNP@hmSiO₂ was incubated with LNCaP, PC3, and SAOS-2 cells, separately. The samples were then imaged using confocal laser scanning microscopy (CLSM). CLSM images indicated that UCNP@hmSiO₂ was taken up by the cells (**Figure B1.7a-c**). Moreover, the co-localization of UCNP@hmSiO₂ with endosome/lysosome in the CLSM image demonstrated the nanoparticles were taken up by cells via endocytosis after incubation for 1 h (**Figure B1.8**). The upconversion luminescence imaging was also performed to prove the cellular uptake of RuEI&UCNP@hmSiO₂. Furthermore, flow cytometry analysis after incubating RuEI&UCNP@hmSiO₂ with PC3 cells for 1 h showed that fluorescence-positive cells was more than 60% compared to the control (**Figure B1.9**). This result further confirms that part of RuEI&UCNP@hmSiO₂ was taken up by the cells. Cathepsin K is typically located in the lysosome and it can also work extracellularly for facilitating tumor invasion. Therefore, it is desirable to inhibit the enzyme activity both inside the cells where cathepsin K is originally accumulated and out of the cells where it commonly functions. Moderate incubation time in our experiment is helpful for the inhibition of intracellular and extracellular cathepsin K.

Irradiating LNCaP, PC3, and SAOS-2 cells, which were incubated with RuEI&UCNP@hmSiO₂ (150 µg/mL) for 1 h, significantly decreased the activities of cathepsin K in the cells (**Figure B1.7d, NIR 7 min and NIR 15 min**). For comparison,

control experiments in the absence of RuEI&UCNP@hmSiO₂ without NIR irradiation (**Figure B1.7d, Control 1**) and in the absence of RuEI&UCNP@hmSiO₂ after NIR irradiation for 15 min (**Figure B1.7d, Control 2**) were performed. The enzyme activities in these control samples did not decrease. In another control experiment, cathepsin K activities in the three cell lines incubated with RuEI&UCNP@hmSiO₂ without NIR irradiation were also measured (**Figure B1.7d, NIR 0 min**). The cathepsin K activities did not change, showing the enzyme inhibition was controlled by light. These experiments demonstrated that RuEI&UCNP@hmSiO₂ enabled NIR photoinhibition of enzyme activities in live cells.

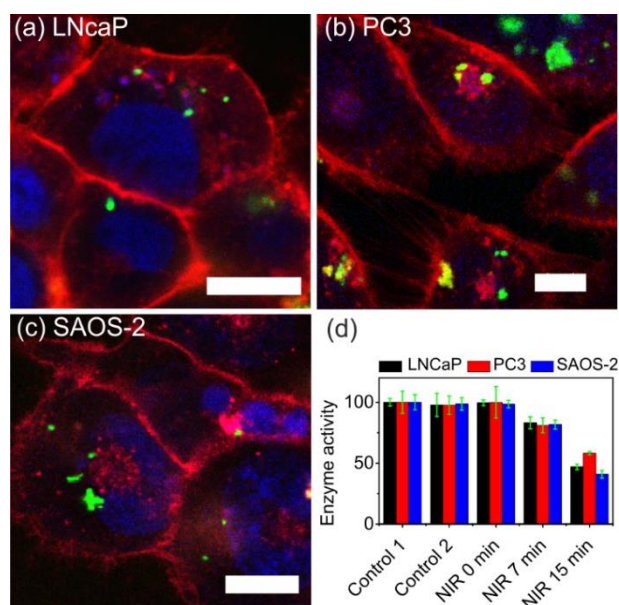


Figure B1.7. CLSM images: fluorescence-labeled UCNP@hmSiO₂ was taken up by (a) LNCaP, (b) PC3, and (c) SAOS-2 cells. The scale bars represent 10 μm. The plasma membranes were stained with CellMask™Orange (red), the DNA was stained with Draq@5 (blue), and UCNP@hmSiO₂ was labeled with FITC (green). FITC was used to label the nanoparticles because FITC can be excited by a laser on the confocal laser scanning microscope but UCNPs cannot be excited by any laser on the microscope. (d) Photoinhibition of the cathepsin K activity in living LNCaP, PC3, and SAOS-2 cells using 974 nm light (1 W/cm²) in the presence of RuEI&UCNP@hmSiO₂ (150 μg/mL). Control 1: cells in the absence of RuEI&UCNP@hmSiO₂ without NIR irradiation. Control 2: cells in the absence of RuEI&UCNP@hmSiO₂ after NIR irradiation for 15 min.

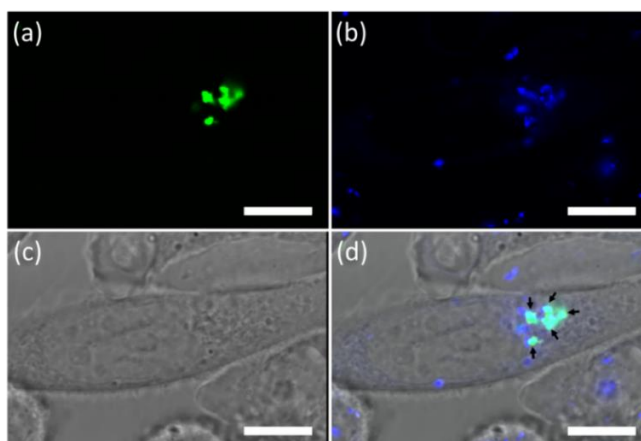


Figure B1.8. Confocal laser scanning microscopy images: FITC-labeled UCNP@hmSiO₂ (150 μg/mL) was taken up by PC3 cells after incubation for 1 h. Single channel pictures of (a) UCNP@hmSiO₂ labeled with FITC (green), (b) the lysosome stained with LysoTracker® Red DND-99 (blue), (c) the bright-field image, and (d) the merged images of three channel demonstrated that FITC-labeled UCNP@hmSiO₂ was co-localized with lysosome as indicated with black arrows. The scale bars represent 10 μm. FITC was used to label the nanoparticles because it fits to the excitation wavelength of the confocal laser scanning microscope.

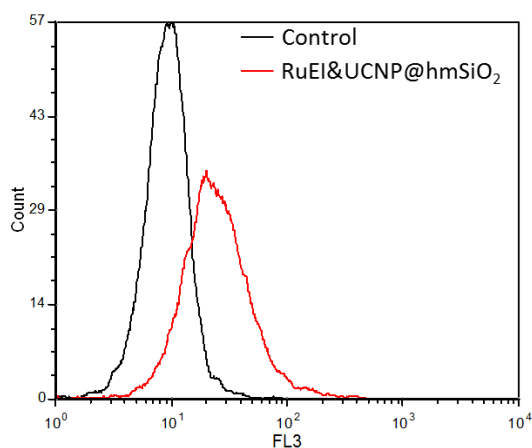


Figure B1.9. Flow cytometry analysis of RuEI&UCNP@hmSiO₂ (150 μg/mL) taken up by PC3 cells after incubation for 1 h (red line). The black line shows the control experiment. The percentage of fluorescence-positive cells was more than 60%. This result together with confocal laser scanning microscopy images (**Figure B1.S3**) and upconversion luminescence images demonstrated cellular uptake of RuEI&UCNP@hmSiO₂.

B1.3. Conclusion

In conclusion, we developed the new method PUEI that can be applied to controlling enzyme activities in living cells with NIR light. In PUEI, UCNP converted NIR light to blue light, which activated caged enzyme inhibitors. The activated enzyme inhibitors can inhibit enzyme activity in living cells. Because NIR light can penetrate deeper into tissue, PUEI is useful for deep-tissue biomedical applications. Because NIR light can activate different photocaged enzyme inhibitors *via* UCNP-assisted photochemistry, RuEI and many other photocaged enzyme inhibitors can be combined with UCNP for NIR light-regulated enzyme activity in deep tissue. Therefore, PUEI is a general approach for regulating activities of different types of enzymes. Controlling enzyme activities by NIR light provides a novel platform for regulating metabolism, manipulating cell functions, and treating diseases in deep tissue.

B1.4. References

- [B1-1] J. M. Berg, J. L. Tymoczko, L. Stryer, *Biochemistry*, W.H. Freeman, New York, USA **2002**.
- [B1-2] T. Stoisser, M. Brunsteiner, D. K. Wilson, B. Nidetzky, *Sci. Rep.* **2016**, *6*, 1
- [B1-3] M. E. Peterson, R. M. Daniel, M. J. Danson, R. Eisenthal, *Biochem. J.* **2007**, *403*, 615.
- [B1-4] K. Okuro, M. Sasaki, T. Aida, *J. Am. Chem. Soc.* **2016**, *138*, 5527.
- [B1-5] M. Wiechen, I. Zaharieva, H. Dau, P. Kurz, *Chem. Sci.* **2012**, *3*, 2330.
- [B1-6] a) P. R. Westmark, J. P. Kelly, B. D. Smith, *J. Am. Chem. Soc.* **1993**, *115*, 3416; b) I. Willner, S. Rubin, A. Riklin, *J. Am. Chem. Soc.* **1991**, *113*, 3321; c) A. Leonidova, C. Mari, C. Aebbersold, G. Gasser, *Organometallics* **2016**, *35*, 851; d) H. Kaufman, Vratsano.Sm, B. F. Erlanger, *Science* **1968**, *162*, 1487; e) T. Respondek, R. N. Garner, M. K. Herroon, I. Podgorski, C. Turro, J. J. Kodanko, *J. Am. Chem. Soc.* **2011**, *133*, 17164.
- [B1-7] a) E. Blasco, B. V. K. J. Schmidt, C. Barner-Kowollik, M. Pinol, L. Oriol, *Macromolecules* **2014**, *47*, 3693; b) E. Blasco, M. Pinol, L. Oriol, B. V. K. J. Schmidt, A. Welle, V. Trouillet, M. Bruns, C. Barner-Kowollik, *Adv. Funct. Mater.* **2013**, *23*, 4011; c) N. Abeyrathna, Y. Liao, *J. Am. Chem. Soc.* **2015**, *137*, 11282; d) S. Bonnet, B. Limburg, J. D. Meeldijk, R. J. M. K. Gebbink, J. A. Killian, *J. Am. Chem. Soc.* **2011**, *133*, 252.
- [B1-8] a) H. J. Montgomery, B. Perdicakis, D. Fishlock, G. A. Lajoie, E. Jervis, J. G. Guillemette, *Bioorgan. Med. Chem.* **2002**, *10*, 1919; b) T. Respondek, R. Sharma, M. K. Herroon, R. N. Garner, J. D. Knoll, E. Cueny, C. Turro, I. Podgorski, J. J. Kodanko, *ChemMedChem* **2014**, *9*, 1306.

- [B1-9] a) R. T. Xing, K. Liu, T. F. Jiao, N. Zhang, K. Ma, R. Y. Zhang, Q. L. Zou, G. H. Ma, X. H. Yan, *Adv. Mater.* **2016**, *28*, 3669; b) S. Wu, H. J. Butt, *Adv. Mater.* **2016**, *28*, 1208; c) N. Zhang, F. Zhao, Q. Zou, Y. Li, G. Ma, X. Yan, *Small* **2016**, *12*, 5936.
- [B1-10] P. Anstaett, V. Pierroz, S. Ferrari, G. Gasser, *Photochem. Photobiol. Sci.* **2015**, *14*, 1821.
- [B1-11] a) M. Álvarez, A. Best, S. Pradhan-Kadam, K. Koynov, U. Jonas, M. Kreiter, *Adv. Mater.* **2008**, *20*, 4563; b) M. Álvarez, A. Best, A. Unger, J. M. Alonso, A. del Campo, M. Schmelzeisen, K. Koynov, M. Kreiter, *Adv. Funct. Mater.* **2010**, *20*, 4265.
- [B1-12] a) B. Yan, J.-C. Boyer, D. Habault, N. R. Branda, Y. Zhao, *J. Am. Chem. Soc.* **2012**, *134*, 16558; b) C.-J. Carling, J.-C. Boyer, N. R. Branda, *J. Am. Chem. Soc.* **2009**, *131*, 10838; c) Z. Y. Cheng, J. Lin, *Macromol. Rapid. Comm.* **2015**, *36*, 790; d) G. Chen, H. Qiu, P. N. Prasad, X. Chen, *Chem. Rev.* **2014**, *114*, 5161.
- [B1-13] a) G. Chen, J. Damasco, H. Qiu, W. Shao, T. Y. Ohulchanskyy, R. R. Valiev, X. Wu, G. Han, Y. Wang, C. Yang, *Nano lett.* **2015**, *15*, 7400; b) E. M. Chan, G. Han, J. D. Goldberg, D. J. Gargas, A. D. Ostrowski, P. J. Schuck, B. E. Cohen, D. J. Milliron, *Nano lett.* **2012**, *12*, 3839; c) X. Wu, Y. Zhang, K. Takle, O. Bilsel, Z. Li, H. Lee, Z. Zhang, D. Li, W. Fan, C. Duan, E. M. Chan, C. Lois, Y. Xiang, G. Han, *ACS nano* **2016**, *10*, 1060; d) K. Huang, N. M. Idris, Y. Zhang, *Small* **2016**, *12*, 836; e) C. Li, D. Yang, P. a. Ma, Y. Chen, Y. Wu, Z. Hou, Y. Dai, J. Zhao, C. Sui, J. Lin, *Small* **2013**, *9*, 4150; f) G. Tian, W. Ren, L. Yan, S. Jian, Z. Gu, L. Zhou, S. Jin, W. Yin, S. Li, Y. Zhao, *Small* **2013**, *9*, 1929.
- [B1-14] a) Y. M. Yang, Q. Shao, R. R. Deng, C. Wang, X. Teng, K. Cheng, Z. Cheng, L. Huang, Z. Liu, X. G. Liu, B. G. Xing, *Angew. Chem. Int. Edit.* **2012**, *51*, 3125; b) M. L. Viger, M. Grossman, N. Fomina, A. Almutairi, *Adv. Mater.* **2013**, *25*, 3733; c) D. Yang, P. Ma, Z. Hou, Z. Cheng, C. Li, J. Lin, *Chem. Soc. Rev.* **2015**, *44*, 1416; d) S. Beyazıt, S. Ambrosini, N. Marchyk, E. Palo, V. Kale, T. Soukka, B. T. S. Bui, K. Haupt, *Angew. Chem. Int. Edit.* **2014**, *53*, 8919; e) W. Wu, L. Yao, T. Yang, R. Yin, F. Li, Y. Yu, *J. Am. Chem. Soc.* **2011**, *133*, 15810; f) E. Ruggiero, A. Habtemariam, L. Yate, J. C. Mareque-Rivas, L. Salassa, *Chem. Commun.* **2014**, *50*, 1715; g) P. T. Burks, J. V. Garcia, R. GonzalezIrias, J. T. Tillman, M. Niu, A. A. Mikhailovsky, J. Zhang, F. Zhang, P. C. Ford, *J. Am. Chem. Soc.* **2013**, *135*, 18145; h) J. A. Liu, W. B. Bu, L. M. Pan, J. L. Shi, *Angew. Chem. Int. Edit.* **2013**, *52*, 4375; i) J. Shen, G. Y. Chen, T. Y. Ohulchanskyy, S. J. Kesseli, S. Buchholz, Z. P. Li, P. N. Prasad, G. Han, *Small* **2013**, *9*, 3213.
- [B1-15] a) Z. J. Chen, S. Q. He, H. J. Butt, S. Wu, *Adv. Mater.* **2015**, *27*, 2203; b) S. Q. He, K. Krippes, S. Ritz, Z. J. Chen, A. Best, H. J. Butt, V. Mailänder, S. Wu, *Chem. Commun.* **2015**, *51*, 431.
- [B1-16] W. Li, J. Wang, J. Ren, X. Qu, *J. Am. Chem. Soc.* **2014**, *136*, 2248.
- [B1-17] a) B. Yan, J.-C. Boyer, N. R. Branda, Y. Zhao, *J. Am. Chem. Soc.* **2011**, *133*, 19714; b) L. Z. Zhao, J. J. Peng, Q. Huang, C. Y. Li, M. Chen, Y. Sun, Q. N. Lin, L. Y. Zhu, F. Y. Li, *Adv. Funct. Mater.* **2014**, *24*, 363; c) H. D. Gao, P. Thanasekaran, C. W. Chiang, J. L. Hong, Y. C. Liu, Y. H. Chang, H. M. Lee, *ACS Nano* **2015**, *9*, 7041.

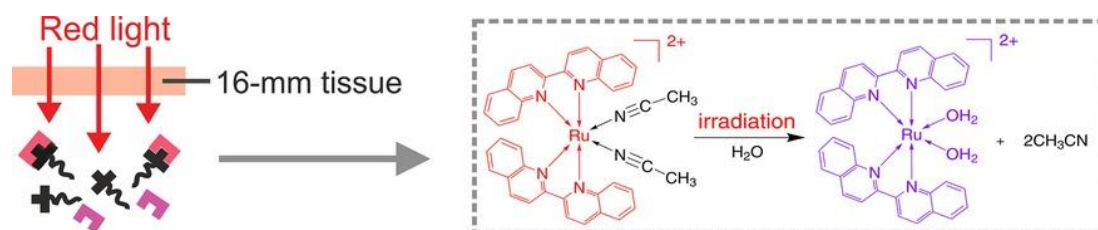
- [B1-18] A. Stepuk, D. Mohn, R. N. Grass, M. Zehnder, K. W. Kramer, F. Pelle, A. Ferrier, W. J. Stark, *Dent. Mater.* **2012**, *28*, 304.
- [B1-19] P. Lederhose, Z. J. Chen, R. Müller, J. P. Blinco, S. Wu, C. Barner-Kowollik, *Angew. Chem. Int. Edit.* **2016**, *55*, 12195.
- [B1-20] Z. Chen, L. Zhou, W. Bing, Z. Zhang, Z. Li, J. Ren, X. Qu, *J. Am. Chem. Soc.* **2014**, *136*, 7498.
- [B1-21] Z. Chen, Y. Xiong, R. Etchenique, S. Wu, *Chem. Commun.* **2016**, **52**, 13959.
- [B1-22] Z. Chen, W. Sun, H. J. Butt, S. Wu, *Chem. Eur. J.* **2015**, *21*, 9165.
- [B1-23] K. D. Brubaker, R. L. Vessella, L. D. True, R. Thomas, E. Corey, *J. Bone. Miner. Res.* **2003**, *18*, 222.
- [B1-24] L. J. Raggatt, N. C. Partridge, *J. Biol. Chem.* **2010**, *285*, 25103.
- [B1-25] M. M. Mohamed, B. F. Sloane, *Nat. Rev. Cancer* **2006**, *6*, 764.

B2: PHOTOACTIVATION OF ANTICANCER RU COMPLEXES IN DEEP TISSUE: HOW DEEP CAN WE GO?

(Note: The literature of the chapter B2 can be found on page 83 at the end of this chapter.)

Permission: The following part [B2] is based on a publication in Chem. Eur. J. 2017, 23, 10832 – 10837. Presented materials are reprinted with permission from John Wiley and Sons. Copyright © 2017, John Wiley and Sons.

Contribution: [REDACTED] and I contributed equally to this work. I carried out the biological part including cell viability. [REDACTED] synthesized and characterized the Ru complex. The project was supervised by [REDACTED].



TOC B2: Anticancer ruthenium (Ru) complexes can be photoactivated by 671-nm light after passing through a 16-mm-thick tissue. The photoactivated Ru complexes can inhibit the growth of cancer cells. These results suggest that Ru complexes are promising anticancer agents for deep-tissue phototherapy.

Aim: Ru complexes have gained intensive interest because of their photoactive and anticancer properties. It is known that different wavelengths of the light are able to penetrate different distances into the external skin. Only the light in the therapeutic window (650-950 nm), which is in a region of red light and NIR, is optimal for use in phototherapy. However, the important question is how deep the red light can penetrate through the skin and still be able to activate Ru complex. Therefore, 671 nm-red light was used to activate the Ru complex passed through the tissue with different thicknesses to clarify this question and demonstrate the efficiency to kill cancer cells.

Abstract : Activation of anticancer therapeutics such as ruthenium (Ru) complexes is currently a topic of intense investigation. The success of phototherapy relies on photoactivation of therapeutics after the light passes through skin and tissue. In this paper, the photoactivation of anticancer Ru complexes with 671-nm red light through tissue of different thicknesses was studied. Four photoactivatable Ru complexes with different absorption wavelengths were synthesized. Two of them (Ru3 and Ru4) were responsive to wavelengths in the “therapeutic window” (650–900 nm) and could be activated using 671-nm red light after passing through tissue up to 16-mm-thick. The other two (Ru1 and Ru2) could not be activated using red light. Additionally, activated Ru4 caused inhibition of cancer cells. These results suggest that photoactivatable Ru complexes are promising for applications in deep-tissue phototherapy.

B2.1. Introduction

Phototherapy based on phototherapeutic agents and light irradiation is a promising strategy for cancer treatment.^[B2-1] Phototherapeutic agents are usually non-toxic or less toxic in the dark, until light converts them to toxic species that kill cancer cells (**Figure B2.1a**). Phototherapy causes minimal side effects for normal tissues because light provides high spatial resolution and allows activation of the phototherapeutic agents at target sites only.^[B2-1-4] Most photoresponsive materials,^[B2-5, 6] such as photoactivated platinum,^[B2-7, 8] coumarin-caged^[B2-9, 10] and pyrenecaged^[B2-11] prodrugs are sensitive to UV or short-wavelength visible light. However, UV or short-wavelength visible light is problematic for biomedical applications, because these wavelengths cannot penetrate deeply into tissue.^[B2-12] Furthermore, UV light can also damage biological systems. In contrast, red or near-infrared (NIR) light is better-suited to biomedical applications, because red or NIR light has a deeper tissue penetration depth (**Figure B2.1b**).^[B2-12, 13]

Simultaneous two-photon absorption is one way to activate photoresponsive materials using NIR light.^[B2-14-17] However, two photon absorption is inefficient and only occurs at the focus of high-intensity pulsed lasers.^[B2-18, 19] Considering that a laser beam will defocus while passing through tissue, a two-photon absorption strategy is impractical for deep-tissue applications. Another method for activating phototherapeutic agents

using NIR light is based on photon upconversion. NIR light can be converted by upconverting nanoparticles or some organic dyes to UV or visible light, which then activates phototherapeutic agents.^[B2-12, 20–23] This process is referred to as upconversion-assisted photochemistry.^[B2-12] Compared to simultaneous two-photon excitation, one advantage of upconversion-assisted photochemistry is that it does not require high-intensity pulsed lasers. However, upconversion is still a non-linear optical process and requires high-intensity laser excitation (at least several hundred mW cm^{-2}), which may damage biological systems.^[B2-12, 24] Furthermore, although NIR light can penetrate into tissue deeply, passing through tissue still attenuates its intensity. Thus, the NIR light intensity may be too low to excite upconversion after NIR light passes through relatively thick tissue.

Activation of phototherapeutic agents by directly using red or NIR light via a one-photon process is more efficient than nonlinear optical processes such as two-photon absorption and photon upconversion. Some phototherapeutics that can be directly activated by red or NIR light via a one-photon process already exist.^[B2-25–29] Previous studies have demonstrated that Ru complexes are photoresponsive molecules and have been applied for biological applications.^[B2-30–33] In particular, our group and others showed that some Ru complexes can be directly activated by low-intensity ($30\text{--}720 \text{ mW cm}^{-2}$) red or NIR light.^[B2-34–37] Ru complexes, analogues of platinum anticancer drugs, are importantly proposed to also be promising anticancer agents.^[B2-26, 38, 39] One advantage of photoactivated Ru complexes is that they are usually less toxic to non-irradiated tissues, only becoming more toxic in tumor cells through photoactivation.^[B2-14, 26, 39–47] Photoactivated Ru-containing materials have already shown anticancer effects in a tumor-bearing mouse model.^[B2-34, 37, 48] Furthermore, photoactivated Ru complexes are promising for deep-tissue phototherapy due to their high photoresponsiveness (e.g. several mW cm^{-2}). However, red or NIR light will eventually be completely attenuated while passing through thick tissue, which means photoactivation of therapeutics via one-photon processes has a certain depth limit. The understanding of this photoactivation of therapeutics in deep tissue will thus help provide guidelines for phototherapy.

Here, we systematically investigated the photoactivation of anticancer Ru complexes after light passes through tissue with different thicknesses. We demonstrated that light is able to pass through 16-mm-thick tissue and activate two Ru complexes. Our results thus indicate phototherapy using Ru complexes is a promising for biological systems with a tissue thickness on the order of 16 mm.

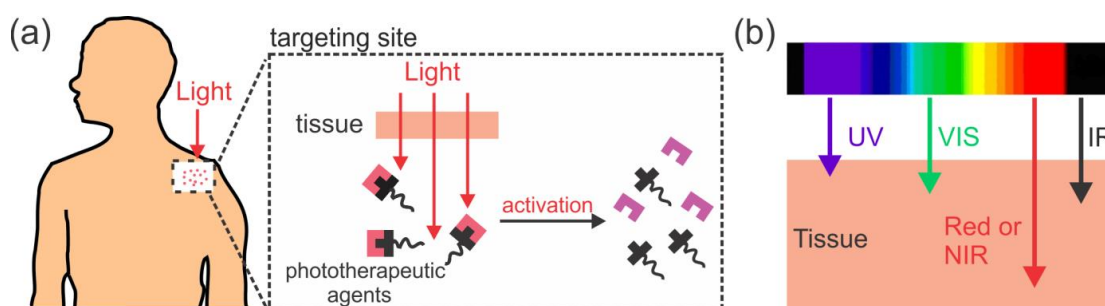


Figure B2.1. Schematic illustrations: (a) Light passes through tissue and activates phototherapeutic agents. (b) Tissue penetration depth of light with different wavelengths. Red or NIR light has a deeper tissue penetration depth than UV and visible light. However, when the light wavelength further shifts to the IR region, the penetration depth decreases again because water absorbs IR light.

B2.2. Results and discussion

To study photoactivation, we synthesized four photocleavable Ru complexes (**Figure B2.2a**): $[\text{Ru}(\text{bpy})_2(\text{CH}_3\text{CN})_2]^{2+}$ (Ru1), $[\text{Ru}(\text{tpy})(\text{bpy})(\text{CH}_3\text{CN})]^{2+}$ (Ru2), $[\text{Ru}(\text{tpy})(\text{biq})(\text{CH}_3\text{CN})]^{2+}$ (Ru3) and $[\text{Ru}(\text{biq})_2(\text{CH}_3\text{CN})_2]^{2+}$ (Ru4). (bpy = 2,2'-bipyridine; tpy = 2,2':6',2''-terpyridine; biq = 2,2'-biquinoline). The Ru-acetonitrile coordination bonds in all the complexes are photocleavable. However, the wavelengths for the photocleavage of these Ru complexes are different because their metal-to-ligand charge transfer (MLCT) bands are located at different wavelengths (**Figure B2.2b**). The absorption maxima of Ru1 (black line) and Ru2 (blue line) were 425 nm and 455 nm, respectively, whereas the absorption tails of Ru1 and Ru2 terminated at ~550 nm and ~605 nm, respectively. Therefore, red to NIR light in the “therapeutic window” (e.g., 650–900 nm) was unable to trigger the photocleavage of Ru1 and Ru2. The absorption maxima of Ru3 (green line) and Ru4 (red line) were located at 515 nm and

535 nm with absorption tails up to ~ 750 nm and ~ 780 nm, respectively. Furthermore, the MLCT bands of Ru3 and Ru4 did not change when they were kept in the dark for an hour, indicating both complexes were thermally stable within the experimental time period. Red light irradiation (671 nm, 110 mW cm^{-2}) successfully induced the photocleavage of Ru3 and Ru4. These results showed that Ru3 and Ru4 are good model compounds to investigate photoactivation in deep tissue.

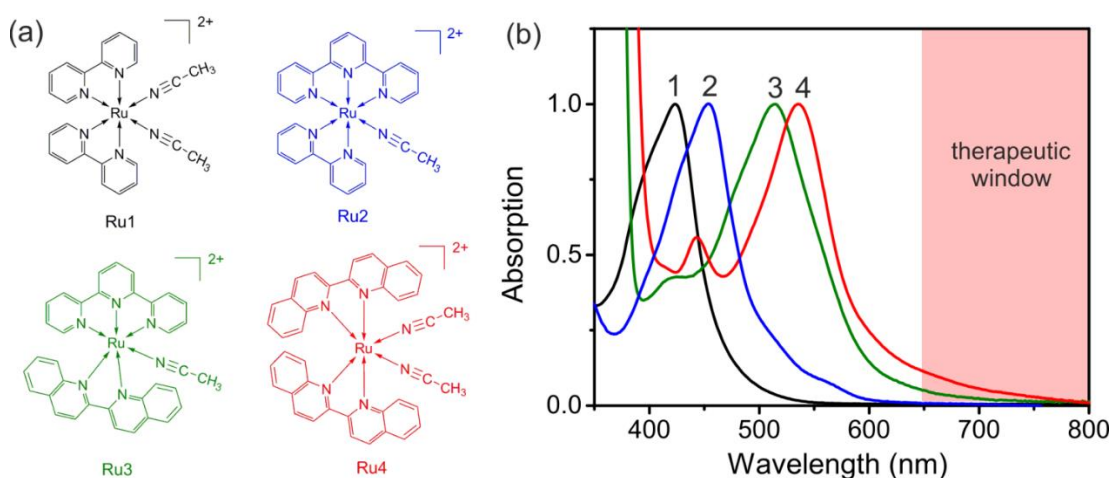


Figure B2.2. (a) Chemical structures of four photocleavable Ru complexes **Ru1-Ru4**. (b) UV-Vis absorption spectra of **Ru1-Ru4**. Red region represents the “therapeutic window”.

We first characterized the ability of 671-nm light to penetrate tissue, which was used for photoactivation of Ru3 and Ru4. We measured the laser power after the laser passed through tissue with different thicknesses, using the setup in **Figure B2.3a**. A DPSS (diode pumped solid state) laser at 671 nm was used as the light source. A tissue holder with a circular hole in the center was placed vertically below the laser. The laser was a parallel beam with an intensity 110 mW cm^{-2} (**Figure B2.3**). This light intensity was chosen for our experiments because the maximum permissible exposure for skin at 671 nm is 0.2 W cm^{-2} according to the American National Standard for Safe Use of Lasers.^[B2-49] Thus, we want to use such an intensity to enable activation of Ru complexes while preventing photodamage to tissues. After passing through a 4-mm-

thick pork tissue, the luminance of the laser spot became weak due to strong light scattering, reflection, and a little absorption (**Figure B2.3c**). The luminance of the laser spot gradually decreased when the tissue thickness increased (8 mm and 12 mm in **Figure B2.3d** and **e**, respectively). When the tissue was as thick as 16 mm, the luminance of laser spot was comparable to that of the surrounding (reflected and scattered light) and the laser spot was nearly invisible to “the naked eye” (**Figure B2.3f**). These results clearly demonstrated thickness strongly influenced laser power after passage through the tissue (**Figure B2.3b–f**). To quantify this intuitive observation, we used a power meter to measure the laser power after passing through tissues (**Figure B2.3g**). The laser power was 60, 38, 23, 10, 6, 2, and 1 mW after passage through 1, 2, 4, 6, 8, 12, and 16 mm thick pork tissue, respectively. Thus, although 671 nm light can penetrate deeply into tissue, only low laser powers can be obtained deep inside the tissue. Therefore, highly photosensitive materials, which are responsive to low-intensity red light, are best-suited for deep-tissue phototherapy.

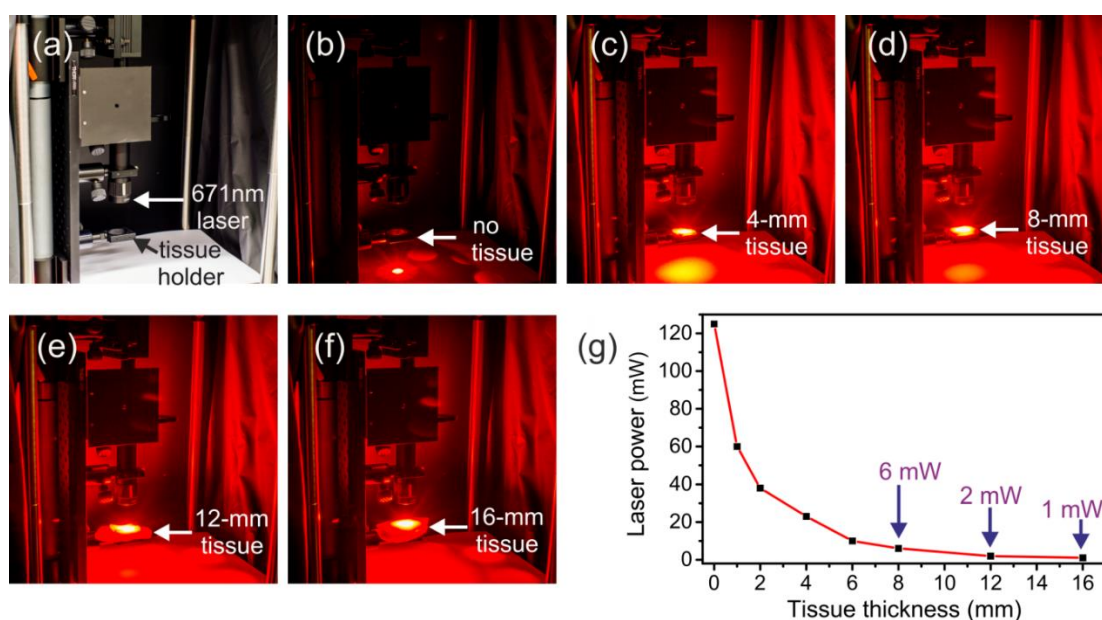


Figure B2.3. (a) Photograph of the laser setup. (b)–(f) Photographs after the laser (671 nm, 125 mW) passing through pork tissue with different thicknesses: (b) no tissue, (c) 4-mm tissue, (d) 8-mm tissue, (e) 12-mm tissue and (f) 16-mm tissue. (g) Laser power after the laser (671 nm, 125 mW) passing through pork tissue with different thicknesses.

The studies on Ru3 and Ru4 demonstrated that red light (671 nm, 125 mW) can pass through tissue up to 16 mm and still activate them. It was reported that photoproducts from Ru complexes similar to Ru3 and Ru4 were more toxic than the Ru complexes before irradiation because the photoproducts may bind to DNA, resulting in apoptosis of cancer cells. Additionally, singlet oxygen, which is also toxic to cancer cells, can be generated during irradiation. Therefore, the combination of phototoxicity and deep-tissue photoactivation of Ru complexes is promising for deep-tissue phototherapy.

As a proof of concept, we used light passing through a piece of 8-mm-thick tissue to inhibit the growth of cancer cells in the presence of Ru4. A piece of 8-mm pork tissue was placed between the laser and HeLa cells incubated in the presence of Ru4 (**Figure B2.4a**). Without Ru4, light irradiation ($\lambda = 671 \text{ nm}$, 110 mW cm^{-2} , 30 min) only caused a little decrease in cell viability (**Figure B2.4b**, $0 \mu\text{g mL}^{-1}$).^[B2-50] Light irradiation (671 nm, 110 mW cm^{-2} , 30 min) in the presence of Ru4 caused significant cell death compared to the mere irradiation and dark condition (**Figure B2.4b**). Hence, Ru4 can be photoactivated in the presence of an 8-mm-thick tissue to inhibit the growth of cancer cells.

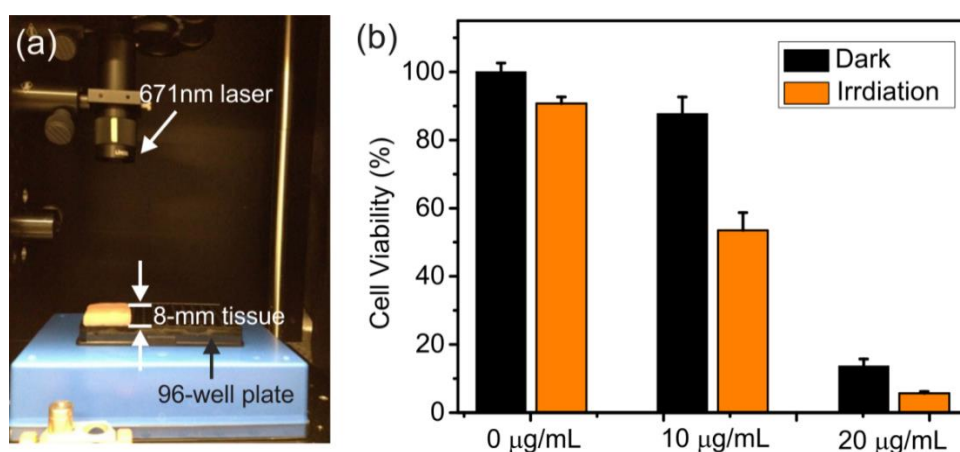


Figure B2.4. (a) Photograph of the setup for cell viability test. (b) Viability of HeLa cells treated with **Ru4** at different concentrations in the dark and after light irradiation ($\lambda = 671 \text{ nm}$, 110 mW cm^{-2} , 30 min). Light irradiation was performed after incubation with Ru4 for 4 h.

B2.3. Conclusion

We studied the photoactivation of anticancer Ru complexes in the presence of tissues with different thicknesses. Anticancer Ru complexes (Ru1–Ru4) were irradiated using a 671-nm laser. Ru1 and Ru2 could not be activated by 671-nm light because their photoresponsive wavelengths are too short. However, Ru3 and Ru4 were activated by 671-nm light due to their long responsive wavelengths. Although only 1% of the laser power remained after passing through a 16-mm-thick tissue, the intensity of the light was still able to activate Ru3 and Ru4. Furthermore, phototoxicity of Ru4 was successfully induced by 671-nm light in cancer cells after passing through an 8-mm-thick tissue. Our results thus suggest that photoactivatable Ru complexes are promising for deep-tissue biomedical applications. Further red shifting the responsive wavelength of Ru complexes would be helpful for phototherapy in deeper tissue. Ru complexes responsive to 800-nm light, the best wavelength for tissue penetration, are expected to be realized in the future.

B2.4. References

- [B2-1] L. Cheng, C. Wang, L. Feng, K. Yang, Z. Liu, *Chem. Rev.* **2014**, *114*, 10869-10939.
- [B2-2] C. Alvarez-Lorenzo, L. Bromberg, A. Concheiro, *Photochem. Photobiol.* **2009**, *85*, 848-860.
- [B2-3] Y. Zhao, *Chem. Rec.* **2007**, *7*, 286-294.
- [B2-4] P. Rai, S. Mallidi, X. Zheng, R. Rahmanzadeh, Y. Mir, S. Elrington, A. Khurshid, T. Hasan, *Adv. Drug. Deliv. Rev.* **2010**, *62*, 1094-1124.
- [B2-5] K. Hildebrandt, K. Elies, D. R. D'Hooge, J. P. Blinco, C. Barner-Kowollik, *J. Am. Chem. Soc.* **2016**, *138*, 7048-7054.
- [B2-6] J. O. Mueller, F. G. Schmidt, J. P. Blinco, C. Barner-Kowollik, *Angew. Chem. Int. Ed.* **2015**, *54*, 10284-10288.
- [B2-7] P. J. Bednarski, F. S. Mackay, P. J. Sadler, *Anticancer Agents Med. Chem.* **2007**, *7*, 75-93.
- [B2-8] J. A. W. Fiona S. Mackay, Pavla Heringová, Jana Kašpárková, Ana M. Pizarro, Stephen A. Moggach, Simon Parsons, Viktor Brabec, Peter J. Sadler, *Proc. Natl. Acad. Sci. USA* **2007**, *104*, 20743-20748.
- [B2-9] W. Fan, X. Tong, Q. Yan, S. Fu, Y. Zhao, *Chem. Commun.* **2014**, *50*, 13492-13494.
- [B2-10] Q. Lin, C. Bao, S. Cheng, Y. Yang, W. Ji, L. Zhu, *J. Am. Chem. Soc.* **2012**, *134*, 5052-5055.

- [B2-11] G. Yu, W. Yu, Z. Mao, C. Gao and F. Huang, *Small* **2015**, *11*, 919-925.
- [B2-12] S. Wu and H. J. Butt, *Adv. Mater.* **2016**, *28*, 1208-1226.
- [B2-13] R. Weissleder, V. Ntziachristos, *Nature Med.* **2003**, *9*, 123-128.
- [B2-14] H. Huang, B. Yu, P. Zhang, J. Huang, Y. Chen, G. Gasser, L. Ji and H. Chao, *Angew. Chem. Int. Ed. Engl.* **2015**, *54*, 1-5.
- [B2-15] X. Zhuang, X. Ma, X. Xue, Q. Jiang, L. Song, L. Dai, C. Zhang, S. Jin, K. Yang, B. Ding, P. C. Wang, X. J. Liang, *ACS Nano* **2016**, *10*, 3486-3495.
- [B2-16] V. Nikolenko, R. Yuste, L. Zayat, L. M. Baraldo, R. Etchenique, *Chem. Commun.* **2005**, 1752-1754.
- [B2-17] R. Araya, V. Andino-Pavlovsky, R. Yuste and R. Etchenique, *ACS Chem. Neurosci.* **2013**, *4*, 1163-1167.
- [B2-18] T. Furuta, S. S.-H Wang, J. L. Dantaker, T. M. Dore, W. J. Bybee, E. M. Callaway, W. Denk, and R. T. Tsien, *Proc. Natl. Acad. Sci. USA* **1999**, *96*, 1193-1200.
- [B2-19] M. Álvarez, A. Best, S. Pradhan-Kadam, K. Koynov, U. Jonas, M. Kreiter, *Adv. Mater.* **2008**, *20*, 4563-4567.
- [B2-20] Y. Dai, H. Xiao, J. Liu, Q. Yuan, P. Ma, D. Yang, C. Li, Z. Cheng, Z. Hou, P. Yang, J. Lin, *J. Am. Chem. Soc.* **2013**, *135*, 18920-18929.
- [B2-21] B. Yan, J.-C. Boyer, N. R. Branda, Y. Zhao, *J. Am. Chem. Soc.* **2011**, *133*, 19714-19717.
- [B2-22] F. Wang, D. Banerjee, Y. Liu, X. Chen, X. Liu, *Analyst* **2010**, *135*, 1839-1854.
- [B2-23] E. Ruggiero, A. Habtemariam, L. Yate, J. C. Mareque-Rivas and L. Salassa, *Chem. Commun.* **2014**, *50*, 1715-1718.
- [B2-24] Z. Chen, W. Sun, H. J. Butt, S. Wu, *Chem. Eur. J.* **2015**, *21*, 9165-9170.
- [B2-25] E. D. Anderson, A. P. Gorka and M. J. Schnermann, *Nat. Commun.* **2016**, *7*, 13378
- [B2-26] C. Mari, V. Pierroz, S. Ferrari and G. Gasser, *Chem. Sci.* **2015**, *6*, 2660-2686.
- [B2-27] K. Liu, R. Xing, Q. Zou, G. Ma, H. Mohwald and X. Yan, *Angew. Chem. Int. Ed. Engl.* **2016**, *55*, 3036-3039.
- [B2-28] N. Zhang, F. Zhao, Q. Zou, Y. Li, G. Ma and X. Yan, *Small* **2016**, *12*, 5936-5943.
- [B2-29] G. Lv, W. Guo, W. Zhang, T. Zhang, S. Li, S. Chen, A. S. Eltahan, D. Wang, Y. Wang, J. Zhang, P. C. Wang, J. Chang, X. J. Liang, *ACS Nano* **2016**, *10*, 9637-9645.
- [B2-30] D. V. Pinnick, B. Burham, *Inorg. Chem.* **1984**, *23*, 1440-1445
- [B2-31] L. Zayat, C. Calero, P. Alborés, L. Baraldo, R. Etchenique, *J. Am. Chem. Soc.*, **2003**, *125*, 882-883.
- [B2-32] R. N. Garner, J. C. Gallucci, K. R. Dunbar, C. Turro, *Inorg. Chem.*, **2011**, *50*, 9213-9215.
- [B2-33] T. Respondek, R. N. Garner, M. K. Herroon, I. Podgorski, C. Turro, J. J. Kodanko, *J. Am. Chem. Soc.*, **2011**, *133* (43), pp 17164–17167
- [B2-34] W. Sun, S. Li, B. Haupler, J. Liu, S. Jin, W. Steffen, U. S. Schubert, H. J. Butt, X. J. Liang, S. Wu, *Adv. Mater.* **2017**, *29*, 1603702.

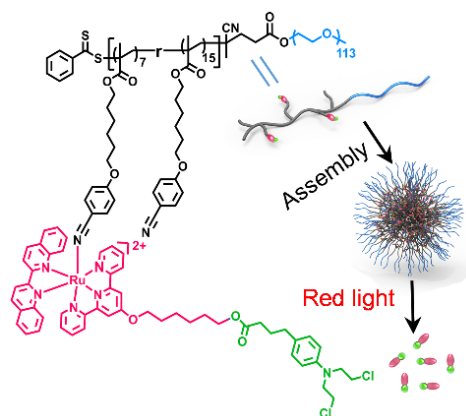
- [B2-35] W. Sun, M. Parowatkin, W. Steffen, H. J. Butt, V. Mailander, S. Wu, *Adv. Healthc. Mater.* **2016**, *5*, 467-473.
- [B2-36] E. Wachter, D. K. Heidary, B. S. Howerton, S. Parkin, E. C. Glazer, *Chem. Commun.* **2012**, *48*, 9649-9651.
- [B2-37] P. Kaspler, S. Lazic, S. Forward, Y. Arenas, A. Mandel and L. Lilje, *Photochem. Photobiol. Sci.* **2016**, *15*, 481-495.
- [B2-38] R. Trondl, P. Heffeter, C. R. Kowol, M. A. Jakupec, W. Berger, B. K. Keppler, *Chem. Sci.* **2014**, *5*, 2925-2932.
- [B2-39] J. D. Knoll and C. Turro, *Coord. Chem. Rev.*, 2015, 282-283, 110-126.
- [B2-40] J. K. White, R. H. Schmehl and C. Turro, *Inorg. Chim. Acta* **2017**, *454*, 7-20.
- [B2-41] N. Karaoun and A. K. Renfrew, *Chem. Commun.* **2015**, *51*, 14038-14041.
- [B2-42] M. A. Sgambellone, A. David, R. N. Garner, K. R. Dunbar, C. Turro, *J. Am. Chem. Soc.* **2013**, *135*, 11274-11282.
- [B2-43] B. Siewert, V. H. van Rixel, E. J. van Rooden, S. L. Hopkins, M. J. Moester, F. Ariese, M. A. Siegler, S. Bonnet, *Chem. Eur. J.* **2016**, *22*, 10960-10968
- [B2-44] B. A. Albani, B. Peña, N. A. Leed, N. A. de Paula, C. Pavani, M. S. Baptista, K. R. Dunbar, C. Turro, *J. Am. Chem. Soc.* **2014**, *136*, 17095-17101.
- [B2-45] V. H. S. van Rixel, B. Siewert, S. L. Hopkins, S. H. C. Askes, A. Busemann, M. A. Siegler, S. Bonnet, *Chem. Sci.* **2016**, *7*, 4922-4929.
- [B2-46] O. Filevich, L. Zayat, L. M. Baraldo and R. Etchenique, *Strut. Bond* **2015**, *165*, 47-68.
- [B2-47] L. N. Lameijer, S. L. Hopkins, T. G. Breve, S. H. Askes and S. Bonnet, *Chem. Eur. J.* **2016**, *22*, 18484-18491.
- [B2-48] P. Zhang, H. Huang, J. Huang, H. Chen, J. Wang, K. Qiu, D. Zhao, L. Ji and H. Chao, *ACS Appl. Mater. Interfaces* **2015**, *7*, 23278-23290.
- [B2-49] American National Standard for Safe Use of Lasers, Laser Institute of America: Orlando, FL . **2000**.
- [B2-50] A. A. Can, G. Bölükbaşıateş, H. Solmaz, ö. Kaya, M. Gülsoy, *International Journal of Oncology and Cancer Therapy* 2016, *1*, 7-11.
- [B2-51] Y. Liu, D. B. Turner, T. N. Singh, A. M. Angeles-Boza, A. Chouai, K. R. Dunbar, C. Turro, *J. Am. Chem. Soc.* **2009**, *131*, 26-27.
- [B2-52] C. R. Hecker, P. E. Fanwick, D. R. McMillin, *Inorg. Chem.* **1991**, *30*, 659-666.
- [B2-53] B. A. Albani, C. B. Durr, C. Turro, *J. Phys. Chem. A* **2013**, *117*, 13885-13892.
- [B2-54] V. S. Miguel, M. Álvarez, O. Filevich, R. Etchenique, A. del Campo, *Langmuir* **2012**, *28*, 1217-1221.
- [B2-55] A. Petroni, L. D. Slep, R. Etchenique, *Inorg. Chem.* **2008**, *47*, 951-956.
- [B2-56] J. P. Marcolongo, T. Weyhermüller, L. D. Slep, *Inorg. Chim. Acta* **2015**, *429*, 174-182.

B3: RED-LIGHT-CONTROLLED RELEASE OF DRUG-RU COMPLEX CONJUGATES FROM METALLOPOLYMER MICELLES FOR PHOTOTHERAPY IN HYPOXIC TUMOR ENVIRONMENTS

(Note: The literature of the chapter B3 can be found on page 97 at the end of this chapter.)

Permission: The following part [B3] is based on a publication in *Adv. Funct. Mater.* 2018, 28, 1804227. Presented materials are reprinted with permission from John Wiley and Sons. Copyright © 2018, John Wiley and Sons.

Contribution: [REDACTED] and I contributed equally to this work. I carried out the *in vitro* biological part including cell viability of HeLa treated with drug-Ru complex conjugates and micelles under normoxia and hypoxia (both in dark and light conditions). [REDACTED] synthesized and characterized the Ru complex. [REDACTED] performed *in vivo* assay and cLSM imaging. The project was supervised by [REDACTED]



TOC B3: Metallopolymers against hypoxic tumors! Amphiphilic metallopolymers, which contain photocleavable drug-Ru complex conjugates, self-assemble into micelles. The micelles are biocompatible and carry the conjugates into tumor cells. Subsequent red-light irradiation induces intracellular release of the drug-Ru complex conjugates. Because the photo-induced release is oxygen-independent, the novel metallopolymer provides a new platform for phototherapy against hypoxic tumors *in vivo*.

Aim: In a deep solid tumor, which is far away from oxygen diffusion distance supplied by blood vessels, the area has a special tumor microenvironment comprised of low oxygen (hypoxia), low nutrients, and acidosis (an excessively acid condition). This hypoxic condition interferes with photodynamic therapy (PDT), which has cancer killing ability significantly dependent on the local oxygen concentration. Therefore, this study aimed to develop a dual-therapy system that can function under both normoxic and hypoxic conditions as oxygen independent toxicity using anticancer drug Chlorambucil Ru complex conjugate self-assemble into micelles. Furthermore, the system was designed to be able to control the release of the drug-Ru complex conjugate from micelles via red-light stimulation. The red-light control release system was proof of concept to kill cancer cells *in vitro* in HeLa and further confirmed the potential to use for phototherapy against hypoxic tumor microenvironments *in vivo* in tumor-bearing mice.

Abstract: Traditional photodynamic phototherapy is not efficient for anticancer treatment because solid tumors have a hypoxic microenvironment. The development of photoactivated chemotherapy based on photoresponsive polymers that can be activated by light in the “therapeutic window” would enable new approaches for basic research and allow for anticancer phototherapy in hypoxic conditions. This work synthesizes a novel Ru-containing block copolymer for photoactivated chemotherapy in hypoxic tumor environment. The polymer has a hydrophilic poly(ethylene glycol) block and a hydrophobic Ru-containing block, which contains red-light-cleavable (650–680 nm) drug–Ru complex conjugates. The block copolymer self-assembles into micelles, which can be efficiently taken up by cancer cells. Red light induces release of the drug–Ru complex conjugates from the micelles and this process is oxygen independent. The released conjugates inhibit tumor cell growth even in hypoxic tumor environment. Furthermore, the Ru-containing polymer for photoactivated chemotherapy in a tumor-bearing mouse model is applied. Photoactivated chemotherapy of the polymer micelles demonstrates efficient tumor growth inhibition. In addition, the polymer micelles do not cause any toxic side effects to mice during the treatment, demonstrating good biocompatibility of the system to the blood and healthy tissues. The novel red-light-

responsive Ru-containing polymer provides a new platform for phototherapy against hypoxic tumors.

B3.1. Introduction

The success of metal complexes such as platinum (Pt) complexes for anticancer applications encourages the development of new metallodrugs.^[B3-1-5] Recent fundamental research and clinical trials showed that ruthenium (Ru) complexes are promising alternatives for Pt drugs.^[B3-1,2] In particular, photoactivatable Ru complexes have been proposed for anticancer phototherapy, which can increase selectivity between tumor and healthy cells.^[B3-1,2,6,7] These complexes are generally nontoxic to nonirradiated normal cells and become highly toxic in tumor cells via selective irradiation of tumors. Phototoxicity of Ru complexes arises from two different mechanisms. One mechanism is singlet oxygen ($^1\text{O}_2$) sensitization using Ru complexes for photodynamic therapy (PDT).^[B3-8-16] The other mechanism is uncaging cytotoxic ligands or Ru species via ligand photosubstitution reactions for photoactivated chemotherapy (PACT).^[B3-17-25] The therapeutic effects of PDT are critically dependent on the local concentration of oxygen.^[B3-26,27] Because solid tumors have a hypoxic microenvironment especially in the areas far away from the blood vessels ($>70\ \mu\text{m}$),^[B3-28] PDT does not work in hypoxic tumor environment. In contrast, PACT using Ru complexes is better suited than PDT for hypoxic tumor treatment because ligand photosubstitution is oxygen independent.^[B3-29-32] Thus, PACT represents a promising approach against hypoxic tumors. We and other groups have shown photoinhibition of tumor cell growth using photoactivatable Ru complexes based on combined PDT and PACT.^[B3-8,33-37] True PACT in hypoxic cancer cells is difficult to achieve due to insufficient anticancer efficiencies of uncaged ligands and Ru species. Recently, Bonnet and co-workers reported PACT against hypoxic cancer cells *in vitro* using a Ru complex caged with a cytotoxic ligand.^[B3-20] The strategy was based on photo-uncaging of cytotoxic ligands, which inhibited the growth of hypoxic cancer cells *in vitro*. The next challenge is the further development of new Ru complexes for PACT *in vivo*. Besides photo-uncaging of efficient anticancer ligands or Ru species, PACT *in vivo* requires that photoactivatable Ru complexes have neglectable side effects to healthy

tissues, can accumulate in tumor cells, and can be photoactivated in the body.^[B3-33,35] However, none of the reported photoactivatable Ru-containing materials has shown therapeutic effects for PACT *in vivo*. Therefore, it is a challenge to design photoactivatable Ru-containing materials for PACT *in vivo*.

Herein, we demonstrate the design of a red-light-responsive Ru-containing block copolymer (PEG-*b*-P(CPH-*co*-RuCHL)) for phototherapy against hypoxic tumors *in vivo* (**Figure B3.1**). The polymer contains a hydrophilic poly(ethylene glycol) (PEG) block. PEGylation is an efficient way to reduce non-specific protein adsorption of drug carriers and improve biocompatibility.^[B3-38-40] Importantly, the hydrophobic block of the polymer contains newly synthesized drug-Ru complex conjugates on the polymer side chains (**Figure B3.1a**). The commercial anticancer drug chlorambucil (CHL) was conjugated with the Ru complex. This novel design, for the first time, results in the release of drug-Ru complex conjugate with enhanced anticancer efficiency, which is different from the design of other systems for photoinduced delivery Ru complexes.^[B3-35,41] CHL-Ru complex conjugates were further grafted to the polymer via the photocleavable Ru-N coordination bond. Red light triggered the cleavage of the CHL-Ru complex conjugates from the polymer chains and subsequent aquation resulted in release of the efficient anticancer CHL-Ru complex conjugate $[\text{Ru}(\text{CHLtpy})(\text{biq})(\text{H}_2\text{O})]^{2+}$. The block copolymer PEG-*b*-P(CPH-*co*-RuCHL) self-assembled into micelles, which carried the CHL-Ru complex conjugates to the tumor site and were taken up by hypoxic cancer cells via endocytosis (**Figure B3.1b**). Red light passed through skin and tissue and then induced the release of $[\text{Ru}(\text{CHLtpy})(\text{biq})(\text{H}_2\text{O})]^{2+}$ for PACT. Red-light-responsive PEG-*b*-P(CPH-*co*-RuCHL) is better suited than conventional UV or short-wavelength visible light-responsive polymers for biomedical applications because red light can penetrate deeper into tissue.^[B3-27] We have demonstrated that red light activated Ru complexes with similar responsive wavelengths to PEG-*b*-P(CPH-*co*-RuCHL) after red light passed through tissue with a thickness up to 16 mm.^[B3-48] Because PEG-*b*-P(CPH-*co*-RuCHL) exhibits improved biocompatibility via PEGylation, enhanced anticancer efficiency via drug conjugation, facilitated endocytosis via micellization, and deep-tissue activation

via red light irradiation, PEG-*b*-P(CPH-*co*-RuCHL) is a promising candidate for PACT against hypoxic tumors *in vivo*.

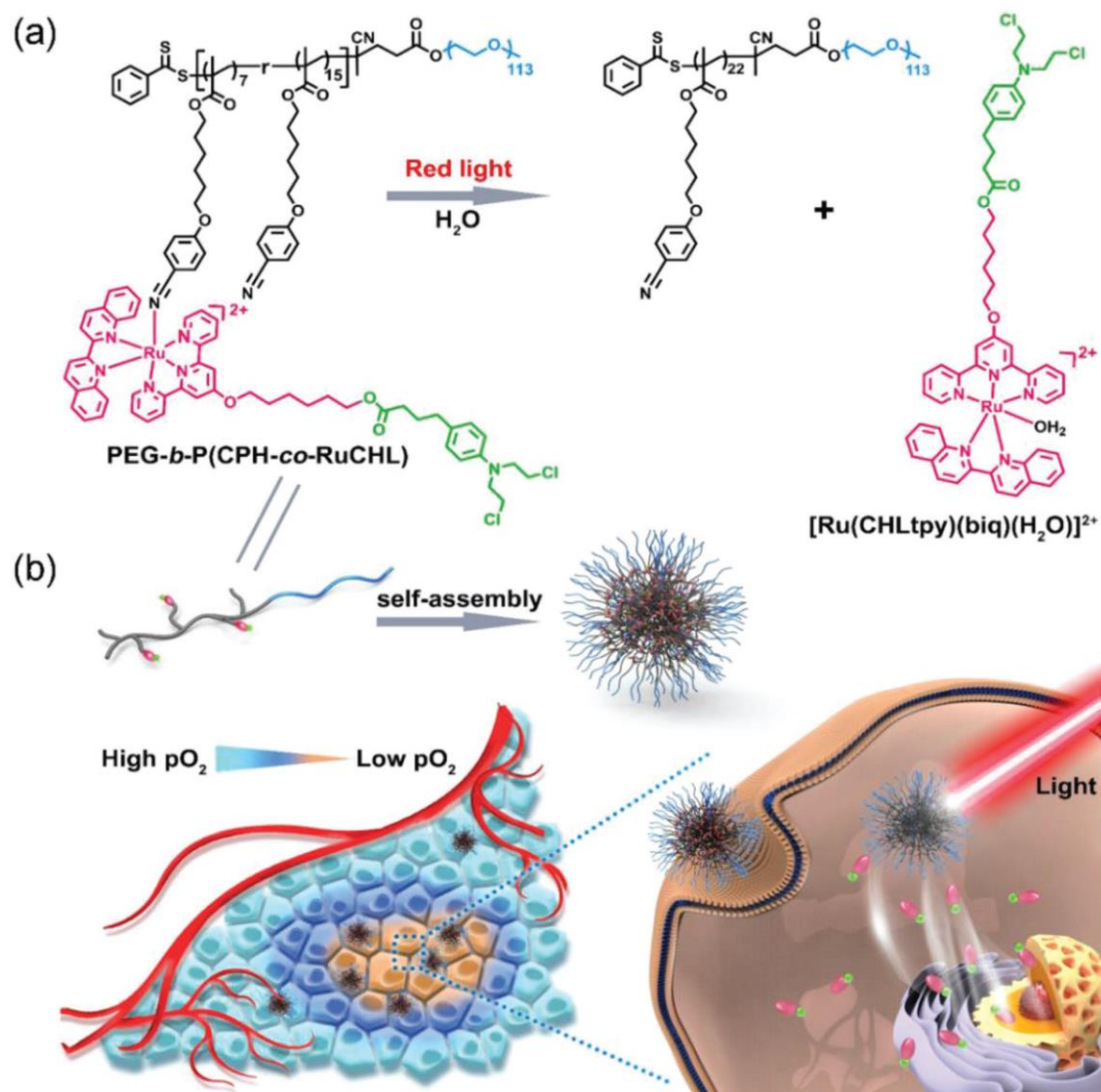


Figure B3.1. (a) Structure and photoreaction of the metallopolymer PEG-*b*-P(CPH-*co*-RuCHL). The green and purple parts in the chemical structures represent the drug (CHL) moiety and the Ru complex moiety. Red light induces the release of the drug-Ru complex conjugate $[\text{Ru}(\text{CHLtpy})(\text{biq})(\text{H}_2\text{O})]^{2+}$. (b) Self-assembly of PEG-*b*-P(CPH-*co*-RuCHL) and its phototherapy in hypoxic tumor environments.

B3.2. Results and discussion

We prepared block copolymer assemblies by adding water to a THF solution of PEG-*b*-P(CPH-*co*-RuCHL). The micelle solution was collected after removing the organic solvent *via* dialysis against water. Transmission electron microscopy (TEM) image showed that PEG-*b*-P(CPH-*co*-RuCHL) formed monodisperse micelles with a diameter of ~15 nm. Dynamic light scattering (DLS) showed that the micelles had a narrow size distribution and the average hydrodynamic diameter of the micelles was 22 nm. The micelles were well dispersed in water and physiological saline solution and had good stability. To achieve *in vivo* applications, we used red light in the therapeutic window (650 to 900 nm) to trigger the photoreaction. Red light irradiation (656 nm) of the micelles red-shifted the MLCT band from 519 nm (λ_{max} of PEG-*b*-P(CPH-*co*-RuCHL)) to 576 nm (λ_{max} of $[\text{Ru}(\text{CHLtpy})(\text{biq})(\text{H}_2\text{O})]^{2+}$). This detectable spectral change can be achieved less than 0.5 h and the change was identical to that of the photocleavage of similar Ru complexes, suggesting $[\text{Ru}(\text{CHLtpy})(\text{biq})(\text{H}_2\text{O})]^{2+}$ was cleaved from the polymer.^[B3-48,51] Additionally, the result from UV-Vis absorption spectroscopy indicated that the process of the photoreaction can be precisely controlled by the irradiation dose. Up to 84% of $[\text{Ru}(\text{CHLtpy})(\text{biq})(\text{H}_2\text{O})]^{2+}$ was released under light irradiation in our experimental condition. In comparison, only $\approx 7\%$ of $[\text{Ru}(\text{CHLtpy})(\text{biq})(\text{H}_2\text{O})]^{2+}$ was released in the dark after 24 h, suggesting the good stability of the micelles during long time incubation and the release was controlled by light (Results are not shown here, see **Publication [B3]**).

The released $[\text{Ru}(\text{CHLtpy})(\text{biq})(\text{H}_2\text{O})]^{2+}$ is a conjugate of a Ru complex and a commercial anticancer drug CHL, both of which can inhibit cancer cell growth. Thus, $[\text{Ru}(\text{CHLtpy})(\text{biq})(\text{H}_2\text{O})]^{2+}$ is expected to be an efficient anticancer agent. The cytotoxicity of $[\text{Ru}(\text{CHLtpy})(\text{biq})(\text{H}_2\text{O})]^{2+}$ was tested using HeLa cells, a commonly used model cancer cell line for evaluating anticancer activities of new anticancer materials (**Figure B3.1a**). HeLa cells were incubated with $[\text{Ru}(\text{CHLtpy})(\text{biq})(\text{H}_2\text{O})](\text{PF}_6)_2$ with a concentration from 1.25 to 50 $\mu\text{g mL}^{-1}$ for 24 h. Cell viability decreased as the concentration of $[\text{Ru}(\text{CHLtpy})(\text{biq})(\text{H}_2\text{O})]^{2+}$ increased. The half maximal effective concentration (EC_{50}) of $[\text{Ru}(\text{CHLtpy})(\text{biq})(\text{H}_2\text{O})]^{2+}$ to HeLa cell was $\approx 13.7 \mu\text{g mL}^{-1}$, much lower than those of both $[\text{Ru}(\text{tpy})(\text{biq})(\text{H}_2\text{O})](\text{PF}_6)_2$

($\approx 30 \mu\text{g mL}^{-1}$, **Figure B3.2**) and CHL ($\approx 150 \mu\text{g mL}^{-1}$).^[B3-52] The result indicated that the two anticancer moieties had synergistic effects and the conjugate $[\text{Ru}(\text{CHLtpy})(\text{biq})(\text{H}_2\text{O})]^{2+}$ had improved cytotoxicity toward cancer cells. The cytotoxicity of the complex after red light irradiation (671 nm , 120 J cm^{-2}) was also studied (**Figure B3.1a**). The EC_{50} value for HeLa cells after irradiation was $\approx 10.3 \mu\text{g mL}^{-1}$, which is close to that without irradiation. EC_{50} values under dark and light irradiation were similar because no $^1\text{O}_2$ was generated when $[\text{Ru}(\text{CHLtpy})(\text{biq})(\text{H}_2\text{O})]^{2+}$ was irradiated with light (**Figure B3.1b**).

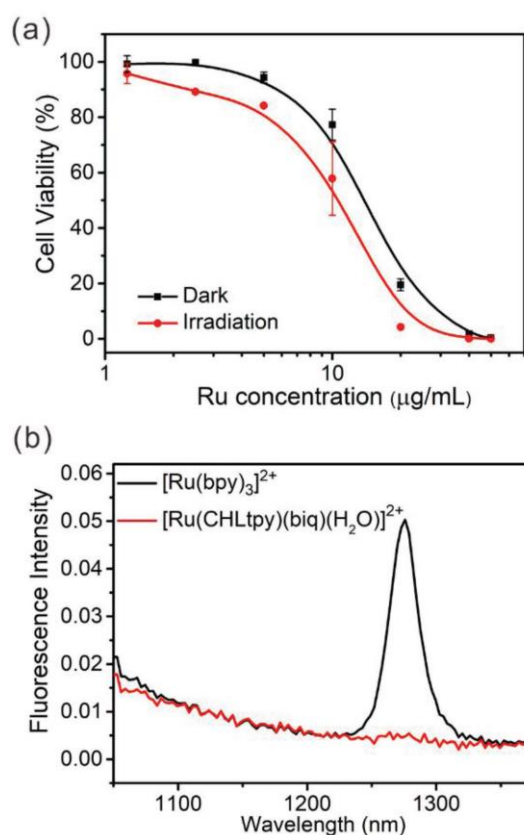


Figure B3.1. (a) Viability of HeLa cells incubated with $[\text{Ru}(\text{CHLtpy})(\text{biq})(\text{H}_2\text{O})](\text{PF}_6)_2$ with various concentrations for 24 h. HeLa cells were kept in the dark or under light irradiation (671 nm , 120 J cm^{-2}) at the beginning of the incubation. (b) Emission spectra of $^1\text{O}_2$ ($\lambda_{\text{em}} = 1275 \text{ nm}$) generated in the solutions of $[\text{Ru}(\text{CHLtpy})(\text{biq})(\text{H}_2\text{O})](\text{PF}_6)_2$ and $[\text{Ru}(\text{bpy})_3]\text{Cl}_2$ in CD_3OD after excitation at $\lambda_{\text{ex}} = 450 \text{ nm}$. $A_{450 \text{ nm}} = 0.1$ (4 mm path length) for all samples. $[\text{Ru}(\text{bpy})_3]\text{Cl}_2$ was used as a reference sample ($\Phi\Delta = 0.73$ in CD_3OD).^[B3-53]

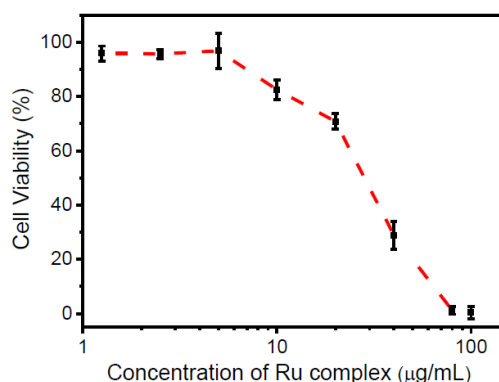


Figure B3.2. Viability of HeLa cells incubated for 24 h in the presence of $[\text{Ru}(\text{tpy})(\text{biq})(\text{H}_2\text{O})](\text{PF}_6)_2$ with different concentrations.

Encouraged by the improved anticancer efficiency of $[\text{Ru}(\text{CHLtpy})(\text{biq})(\text{H}_2\text{O})]^{2+}$ compared to CHL and $[\text{Ru}(\text{tpy})(\text{biq})(\text{H}_2\text{O})]^{2+}$, we used PEG-*b*-P(CPH-*co*-RuCHL) micelles as nanocarriers for PACT. First, we studied cellular uptake of PEG-*b*-P(CPH-*co*-RuCHL) micelles (**Figure B3.3a**). The micelles loaded with the dye were incubated with HeLa cells in the dark for 6 h. Subsequently, the cells were washed thoroughly and cell nuclei were stained with Hoechst 33342. Confocal laser scanning microscopy (cLSM) revealed green fluorescence from the micelles in the cytoplasm, indicating the micelles were taken up by the cancer cells (**Figure B3.3a**, top). We also imaged the cells without incubation with the micelles as a control experiment (**Figure B3.3a**, bottom). No green fluorescence was observed, suggesting the observed green fluorescence (**Figure B3.3a**, top) was from the micelles.

The cytotoxicity of PEG-*b*-P(CPH-*co*-RuCHL) micelles in the dark and after light irradiation was also studied (**Figure B3.3b**). In the dark, the micelles showed negligible toxic to HeLa cells, suggesting the micelles had good biocompatibility. In contrast, irradiating (656 nm , 60 J cm^{-2}) cancer cells incubated with PEG-*b*-P(CPH-*co*-RuCHL) micelles significantly decreased the cell viability (**Figure B3.3b**). The EC_{50} of polymeric micelles was less than $25 \mu\text{g mL}^{-1}$, which is much lower than that of CHL ($150 \mu\text{g mL}^{-1}$).^[B3-52] Because light irradiation (656 nm , 60 J cm^{-2}) on the micelles ($100 \mu\text{L}$, $200 \mu\text{g mL}^{-1}$) resulted in 90% conversion of the photoreaction, we interpret that the released $[\text{Ru}(\text{CHLtpy})(\text{biq})(\text{H}_2\text{O})]^{2+}$ from the micelles inhibited cancer cell growth. As a comparison, cytotoxicity of PEG-*b*-PCPH micelles without the drug–Ru complex

conjugate was also tested (**Figure B3.4**). The PEG-*b*-CPH polymer micelles showed no toxicity both in the dark and under light irradiation, which further proved that light-enhanced toxicity arose from the release of the drug–Ru complex conjugates.

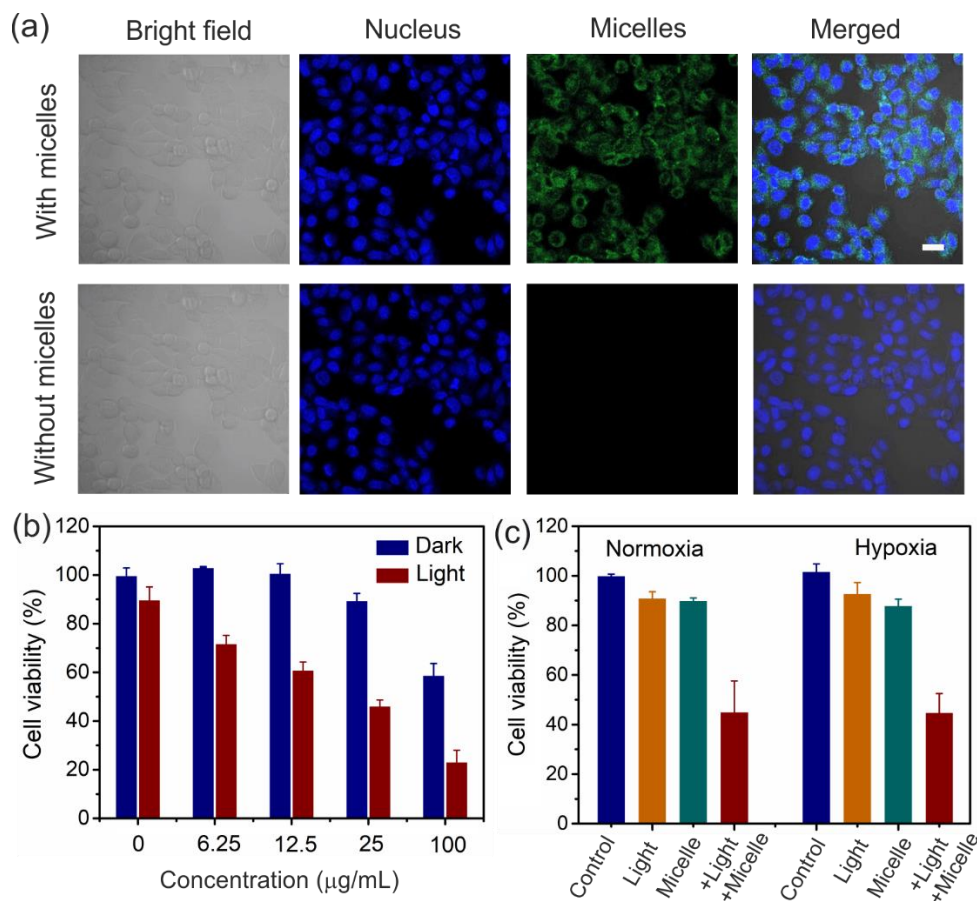


Figure B3.3. (a) Confocal laser scanning microscopy images of HeLa cells incubated with or without PEG-*b*-P(CPH-*co*-RuCHL) micelles. Nuclei were stained with Hoechst 33342 (blue). Scale bar: 20 µm. (b) Viability of HeLa cells incubated with different concentrations of the micelles in the dark and after irradiation (656 nm, 60 J cm⁻²). The cells were irradiated with red light (656 nm, 60 J cm⁻²) after incubation with the micelles for 6 h. Cell viability was tested after the cells were further incubated for 24 h. (c) Viability of HeLa cells after different treatments in normoxic and hypoxic conditions. Cells without any treatment were set as the Control group; Cells only irradiated with red light (671 nm, 120 J cm⁻²) were set as Light group; Cells only incubated with micelles were set as Micelle group; Cells irradiated with red light (671 nm, 120 J cm⁻²) after incubation with the micelles (25 µg mL⁻¹) for 6 h were set as Micelle + Light group. Cell viability was tested after incubating the cells for 24 h.

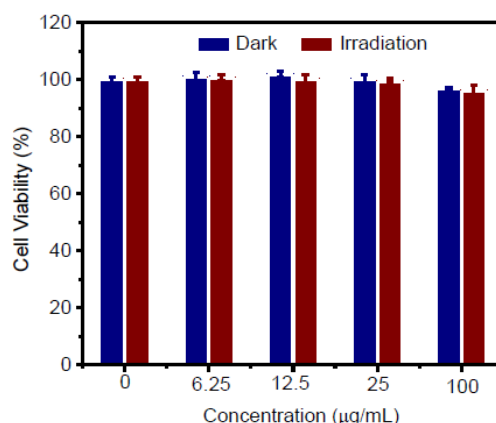


Figure B3.4. Viability of HeLa cells incubated with different concentrations of the micelles without the drug–Ru complex conjugate in the dark and after irradiation. The cells were irradiated with red light (671 nm, 120 J cm^{-2}) after incubation with the micelles for 6 h. After further incubated for 24 h, cell viability was tested.

In the next step, we compared cytotoxicity of PEG-*b*-P(CPH-*co*-RuCHL) micelles under normoxic and hypoxic conditions (**Figure B3.2c**). For the hypoxic group, cells were incubated in the culture medium containing CoCl_2 ($100 \times 10^{-6} \text{ M}$), which was used as the hypoxia inducer.^[B3-28] HeLa cells under normoxic conditions were also prepared simultaneously. Then, the cells were incubated with micelles ($25 \mu\text{g mL}^{-1}$) for 6 h prior to red light irradiation. In both normoxic and hypoxic conditions, only irradiating cancer cells (671 nm, 120 J cm^{-2}) (orange bars) or only incubating cancer cells with micelles ($25 \mu\text{g mL}^{-1}$) (green bars) cannot efficiently kill the cancer cells. Light irradiation in the presence of the micelles decreased the cell viability to 44.9% in the hypoxic condition and 45.1% in the normoxic condition (red bars). The results showed that the phototoxicity of the micelles was independent of oxygen level. Actually, PEG-*b*-P(CPH-*co*-RuCHL) cannot generate $^1\text{O}_2$ under light irradiation, suggesting that the inhibition of cancer cell growth was not due to $^1\text{O}_2$ generation but because of the released $[\text{Ru}(\text{CHLtpy})(\text{biq})(\text{H}_2\text{O})]^{2+}$.

The O_2 -independent phototoxicity of PEG-*b*-P(CPH-*co*-RuCHL) micelles *in vitro* motivated us to investigate PACT using the micelles *in vivo*. Photoactivated chemotherapy of the polymer micelles demonstrates efficient tumor growth inhibition

in a tumor-bearing mouse. Furthermore, the polymer micelles do not cause any toxic side effects to mice during the treatment, demonstrating their good biocompatibility to the blood and healthy tissues (Results are not shown here, see **Publication [B3]**).

B3.3. Conclusion

We reported the design of a Ru-containing amphiphilic polymer for PACT *in vivo*. The Ru-containing polymer, PEG-*b*-P(CPH*co*-RuCHL), contains novel red-light-cleavable drug–Ru conjugates. The drug–Ru complex conjugates bearing a very high content (≈ 45 wt%) in the polymer were carried by the polymer and can be released on-demand *via* red light irradiation. The Ru-containing polymer self-assembled into micelles and internalized into tumor cells. Light irradiation induced the release of drug–Ru complex conjugates, which inhibited tumor cell growth. Because the photoinduced drug release process is oxygen-independent, the polymer micelles are suited for PACT against tumor cells with hypoxic environments. The polymer micelles were further used for PACT in a tumor-bearing mouse model, which completely inhibited tumor growth. Moreover, the treatment using the polymer micelles eliminated substantial systemic toxicity in living animals. PACT based on our metallopolymers with red-light-cleavable drug–Ru complex conjugates is a new strategy to overcome the problem of conventional PDT in hypoxic environments. The development of polymers with drug–Ru complex conjugates opens up an avenue for the design of polymeric therapeutics for PACT against hypoxic tumors.

B3.4. References

- [B3-1] I. Romero-Canelon, P. J. Sadler, *Inorg. Chem.* **2013**, *52*, 12276.
- [B3-2] C. Mari, V. Pierroz, S. Ferrari, G. Gasser, *Chem. Sci.* **2015**, *6*, 2660.
- [B3-3] K. Vellaisamy, G. Li, C.-N. Ko, H.-J. Zhong, S. Fatima, H.-Y. Kwan, C.-Y. Wong, W.-J. Kwong, W. Tan, C.-H. Leung, D.-L. Ma, *Chem. Sci.* **2018**, *9*, 1119.
- [B3-4] K. M. Boyle, J. K. Barton, *J. Am. Chem. Soc.* **2018**, *140*, 5612.
- [B3-5] G. Yu, M. Zhang, M. L. Saha, Z. M. L. Saha, Z. Mao, J. Chen, Y. Yao, Z. Zhou, Y. Liu, C. Gao, F. Huang, X. Chen, P. J. Stang, *J. Am. Chem. Soc.* **2017**, *139*, 15940.
- [B3-6] C. S. Burke, A. Byrne, T. E. Keyes, *J. Am. Chem. Soc.* **2018**, *140*, 6945.
- [B3-7] J. D. Knoll, C. Turro, *Coord. Chem. Rev.* **2015**, *6*, 2660.

- [B3-8] B. A. Albani, B. Pena, N. A. Leed, N. A. B. G. de Paula, C. Pavani, M. S. Baptista, K. R. Dunbar, C. Turro, *J. Am. Chem. Soc.* **2014**, *136*, 17095.
- [B3-9] H. Huang, B. Yu, P. Zhang, J. Huang, Y. Chen, G. Gasser, L. Ji, H. Chao, *Angew. Chem., Int. Ed.* **2015**, *54*, 14049.
- [B3-10] N. W. Choi, S. S. Verbridge, R. M. Williams, J. Chen, J.-Y. Kim, R. Schmehl, C. E. Farnum, W. R. Zipfel, C. Fischbach, A. D. Stroock, *Biomaterials* **2012**, *33*, 2710.
- [B3-11] T. Sainuddin, J. McCain, M. Pinto, H. Yin, J. Gibson, M. Hetu, S. A. McFarland, *Inorg. Chem.* **2016**, *55*, 83.
- [B3-12] L. Kohler, L. Nease, P. Vo, J. Garofolo, D. K. Heidary, R. P. Thummel, E. C. Glazer, *Inorg. Chem.* **2017**, *56*, 12214.
- [B3-13] M. Wenzel, A. de Almeida, E. Bigaeva, P. Kavanagh, M. Picquet, P. L. Gendre, E. Bodio, A. Casini, *Inorg. Chem.* **2016**, *55*, 2544.
- [B3-14] C. Griffith, A. S. Dayoub, T. Jaranatne, N. Alatrash, A. Mohamedi, K. Abayan, Z. S. Breitbach, D. W. Armstrong, F. M. MacDonnell, *Chem. Sci.* **2017**, *8*, 3726.
- [B3-15] M. R. Gill, P. J. Jarman, S. Halder, M. G. Walker, H. K. Saeed, J. A. Thomas, C. Smythe, K. Ramadan, K. A. Vallis, *Chem. Sci.* **2018**, *9*, 841.
- [B3-16] M. Dickerson, B. Howerton, Y. Bae, E. C. Glazer, *J. Mater. Chem. B* **2016**, *4*, 394.
- [B3-17] E. Wachter, D. K. Heidary, B. S. Howerton, S. Parkin, E. C. Glazer, *Chem. Commun.* **2012**, *48*, 9649.
- [B3-18] B. S. Howerton, D. K. Heidary, E. C. Glazer, *J. Am. Chem. Soc.* **2012**, *134*, 8324.
- [B3-19] M. A. Sgambellone, A. David, R. N. Garner, K. R. Dunbar, C. Turro, *J. Am. Chem. Soc.* **2013**, *135*, 11274.
- [B3-20] L. N. Lameijer, D. Ernst, S. L. Hopkins, M. S. Meijer, S. H. C. Askes, S. E. Le Devedec, S. Bonnet, *Angew. Chem., Int. Ed.* **2017**, *56*, 11549.
- [B3-21] V. H. S. van Rixel, B. Siewert, S. L. Hopkins, S. H. C. Askes, A. Busemann, M. A. Siegler, S. Bonnet, *Chem. Sci.* **2016**, *7*, 4922.
- [B3-22] J. K. White, R. H. Schmehl, C. Turro, *Inorg. Chim. Acta* **2017**, *454*, 7.
- [B3-23] N. Karaoun, A. K. Renfrew, *Chem. Commun.* **2015**, *51*, 14038.
- [B3-24] A. N. Hidayatullah, E. Wachter, D. K. Heidary, S. Parkin, E. C. Glazer, *Inorg. Chem.* **2014**, *53*, 10030.
- [B3-25] E. Wachter, D. Moya, S. Parkin, E. C. Glazer, *Inorg. Chem.* **2011**, *50*, 9045.
- [B3-26] K. Liu, R. Xing, Q. Zou, G. Ma, H. Mohwald, X. Yan, *Angew. Chem., Int. Ed.* **2016**, *55*, 3036.
- [B3-27] S. S. Lucky, K. C. Soo, Y. Zhang, *Chem. Rev.* **2015**, *115*, 1990.
- [B3-28] S. Shen, C. Zhu, D. Huo, M. Yang, J. Xue, Y. Xia, *Angew. Chem., Int. Ed.* **2017**, *56*, 8801.
- [B3-29] B. A. Albani, C. B. Durr, C. Turro, *J. Phys. Chem. A* **2013**, *117*, 13885.
- [B3-30] R. Araya, V. Andino-Pavlovsky, R. Yuste, R. Etchenique, *ACS Chem. Neurosci.* **2013**, *4*, 1163.
- [B3-31] V. Nikolenko, R. Yuste, L. Zayat, L. M. Baraldo, R. Etchenique, *Chem. Commun.* **2005**, 1752.

- [B3-32] M. Huisman, J. K. White, V. G. Lewalski, I. Podgorski, C. Turro, J. M. Kodanko, *Chem. Commun.* **2016**, 52, 12590.
- [B3-33] W. Sun, X. Zeng, S. Wu, *Dalton Trans.* **2017**, 47, 283.
- [B3-34] W. Sun, M. Parowatkin, W. Steffen, H. J. Butt, V. Mailander, S. Wu, *Adv. Healthcare Mater.* **2016**, 5, 467.
- [B3-35] W. Sun, S. Li, B. Haupler, J. Liu, S. Jin, W. Steffen, U. S. Schubert, H. J. Butt, X.-J. Liang, S. Wu, *Adv. Mater.* **2017**, 29, 1603702.
- [B3-36] N. Lameijer, T. G. Breve, V. H. S. van Rixel, S. H. C. Askes, M. A. Siegler, S. Bonnet, *Chem. Eur. J.* **2018**, 24, 2709.
- [B3-37] L. M. Loftus, J. K. White, B. A. Albani, L. Kohler, J. J. Kodanko, R. P. Thummel, K. R. Dunbar, C. Turro, *Chem. Eur. J.* **2016**, 22, 3704.
- [B3-38] Y. Zhang, H. F. Chan, K. W. Leong, *Adv. Drug Delivery Rev.* **2013**, 65, 104.
- [B3-39] P. M. Kelly, C. Aberg, E. Polo, A. O'Connell, J. Cookman, J. Fallon, Z. Krpetić, K. A. Dawson, *Nat. Nanotechnol.* **2015**, 10, 472.
- [B3-40] F. Bertoli, D. Garry, M. P. Monopoli, A. Salvati, K. A. Dawson, *ACS Nano* **2016**, 10, 10471.
- [B3-41] G. Boeuf, G. V. Roullin, J. Moreau, L. V. Gulick, N. Z. Pineda, C. Terry, D. Ploton, M. C. Andry, F. Chuburu, S. Dukic, M. Molinari, G. Lemercier, *ChemPlusChem* **2014**, 79, 171.
- [B3-42] M. Abbas, Q. Zou, S. Li, X. Yan, *Adv. Mater.* **2017**, 29, 1605021.
- [B3-43] J. F. Gohy, Y. Zhao, *Chem. Soc. Rev.* **2013**, 42, 7117.
- [B3-44] K. Hildebrandt, K. Elies, D. R. D'hooge, J. P. Blinco, C. Barner-Kowollik, *J. Am. Chem. Soc.* **2016**, 138, 7048.
- [B3-45] Y. Zhao, *Macromolecules* **2012**, 45, 3647.
- [B3-46] J. P. Menzel, B. B. Noble, A. Lauer, M. L. Coote, J. P. Blinco, C. Barner-Kowollik, *J. Am. Chem. Soc.* **2017**, 139, 15812.
- [B3-47] C. H. Quek, K. W. Leong, *Nanomaterials* **2012**, 2, 92.
- [B3-48] W. Sun, R. Thiramanas, L. D. Slep, X. Zeng, V. Mailander, S. Wu, *Chem. Eur. J.* **2017**, 23, 10832.
- [B3-49] J. Yang, W. Liu, M. Sui, J. Tang, Y. Shen, *Biomaterials* **2011**, 32, 9136.
- [B3-50] S. Aryal, C.-M. J. Hu, L. Zhang, *ACS Nano* **2010**, 4, 251.
- [B3-51] L. Zayat, M. G. Noval, J. Campi, C. I. Calero, D. J. Calvo, R. Etchenique, *ChemBioChem* **2007**, 8, 2035.
- [B3-52] I. S. Vijayashree, P. Niranjana, G. Prabhu, V. V. Sureshbabu, J. Manjanna, *J. Cluster Sci.* **2017**, 28, 133.
- [B3-53] J.-A. Cuello-Garibo, M. S. Meijer, S. Bonnet, *Chem. Commun.* **2017**, 53, 6768.
- [B3-54] J. M. Brown, W. R. Wilson, *Nat. Rev. Cancer* **2004**, 4, 437.

CHAPTER C

NANOCAPSULE AS A TEMPERATURE SENSOR IN LIVING CELLS

This study developed polymeric upconversion nanocapsules for use as nanothermometers in living cells by employing temperature dependence of triplet-triplet annihilation upconversion (TTA-UC) phenomenon. A general introduction about human body temperature, the effects of temperature change and current nanotechnology used for temperature measurement is given. Afterwards, the study is presented.

(Note: The literature of the introduction can be found on page 138 at the end of the dissertation.)

[C1] [REDACTED], Rawewan Thiramanas, [REDACTED]. [REDACTED]. *Temperature Sensing in Cells by Polymeric Upconversion Nanocapsules*. (Manuscript in preparation).

C. Introduction

Human body temperature is normally around 35-37 °C, which is commonly measured by using a mercury thermometer. The internal core body temperature (T(c)) can be monitored from different sites of the body including oral, rectal and oesophageal temperatures. However, these measurement sites and the methods used to measure T(c) are not convenient and invasive, often causing irritation and discomfort.^[Z-74] Rectal temperature is not appropriate for use in many conditions due to its labor- and time-consuming response. However, rectal temperature is still considered to be the most correctly available method for measuring T(c) in thermal illness and also an indicator of systemic arterial temperature during whole body hyperthermia.^[Z-74-75] In fact, not only does the tissue temperature involve heterogeneity, but the temperature in tumors can be variable. Evidence indicates that most parts of the body can show similar

temperatures to rectal temperature, or T(c); however, higher and lower temperatures than T(c) can be observed in some parts of tumors.^[Z-75]

In cancer cells, a major temperature and pH change within the tumor microenvironment could easily affect them, which is not usually the case in normal cells as they have an effective buffering system to protect cells. There is about 1-2 degrees difference between the cancerous and normal cells, as typically mentioned in literature. It has been well known for at least 50 years that the tumor cells are slightly more sensitive to heat than normal cells, especially at temperatures between 42 and 45 °C. Thus, cancer cells could be killed by this range of temperature about one degree lower, causing irreversible damage to cancer cells but not affecting healthy cells. This fact motivated the establishment of hyperthermia as cancer therapy.^[Z-76]

Accumulating evidence indicates that temperature can play an important role in cancer therapy. Increased survival rate and more efficient chemotherapy after the cancer patient getting fever - resulting in T(c) increase - from infection have been found in many cases. Furthermore, temperature increase in tumor site can enhance permeability of therapeutic agents to cancer cells and can stimulate immune response.^[Z-77] Zhu et al.^[Z-78] found that culturing cancer cells at 39 °C slightly prevented cell growth by arresting the cells at the G1 phase of the cell cycle and by hampering of cell-cell interaction, and efficiently enhanced the killing effect of chemotherapy which can be long-lasting even after finishing of the treatment. Moreover, the morphology of the cancer cells was discovered to be temperature-dependent; when the temperature increased, the cell surface became smoother and cell height became higher, indicating that temperature can cause the alteration of cellular structures (such as cell surface and cell height), which may then lead to changes in the cellular mechanical properties.^[Z-79]

As the temperature changes inside cancer cells, from intra-metabolism or from external treatment, which have a significant impact on cancer therapy as mentioned above, the motivation to establish a new method to monitor temperature at the cellular level has increased intensively. This **Part [C1]** reported the development of light triggered-polymeric upconversion nanocapsules based on triplet-triplet annihilation upconversion (TTA-UC), which is a temperature dependent system for measurement

of cellular temperature in living cancerous cells. Here, recent advances in nanotechnology used for temperature measurement are described.

Considering the size of the cells, only nanoscale size of thermometer could overcome the intracellular temperature sensing and mapping, whereas a conventional thermometer could not achieve this. Development of nano-optic electronic device brought the thermocouples to precisely detect and reach the cellular temperature in nanoscale. However, this technique can interrupt cellular activity and morphology when coming into contact with the cells. Temperature sensing fluorescence microscopy can override the contacting issue and provide high spatiotemporal resolution. However, a limitation of this method is based on the properties of fluorophores such as cytotoxicity, photobleaching, and cellular environmental sensitiveness.

C.1 Fluorescent polymeric nano-thermometer

Polymers can be used to protect fluorescent probes from intracellular environment. Some of them have thermo-sensitive properties, which behave differently according to their critical solution temperatures such as the family of poly(*N*-isopropylacrylamide)s (PNIPAAms) and poly(2-oxazoline)s (POxs). Combined with fluorescent probes, fluorescent polymeric thermometers (FPT) have drawn significant interest because they provide accurate tracking of intracellular temperature with high spatial resolution. Instead of using thermo-responsive polymers for the controlled release of the drug, as mentioned in **Chapter B**, FPT uses temperature dependent morphology of the polymer to control fluorescence probes as a temperature reporter. For lower critical solution temperature (LCST)-type polymer, at a temperature below the LCST, the fluorescent polymer appears in coil state; at a temperature above the LCST, the fluorescent polymer turns from coil to globule state, allowing simple and fast detection of the fluorescent signal that is continuous, reversible and reusable.^[Z-80-81]

Gong et al.^[Z-82] developed a water soluble, visible excited and simple-structured copolymer hydrogel, poly(NIPAM-co-BODIPY-AA), containing *N*-isopropylacrylamide (NIPAM) and derivative of 4,4-difluoro-4-bora-3a,4a-diaza-s-indacene (BODIPY) units as thermo-responsive and polarity sensitive fluorescent

signaling parts, respectively. A linear increase of fluorescence intensity with increasing temperature could be obtained in a range of 37-42 °C in aqueous solution. The cLSM images showed the uptake of the copolymer inside BHK cells and exhibited temperature dependent fluorescent intensity at 35 and 42 °C.

C.2 DNA fluorescent thermometers

Thermo-sensitive DNA has several advantages including biocompatibility, a well-defined structure, nanoscale size and tunable temperature sensing properties. Therefore, it was applied for development of DNA fluorescent thermometers. The most common temperature sensitive-DNA based nanostructure is the molecular beacon (MB), which is a hairpin-shaped oligonucleotide containing a single-stranded loop and a double-stranded stem with end-labeled quencher and reporter fluorophores. MBs are highly sensitive, sequence specific, and are commonly used for sequence detection in qPCR. MBs are considered a smart temperature sensing material because the conformation of MBs can reversibly change between the hairpin shape and random coil state upon exposure to various temperatures. The relative distance changes between the fluorophore and quencher result in the quenching or emitting of fluorescence. The melting point (T_m) of MBs is defined as the temperature at which half of the MBs structure is open. It is also independent of concentration. Due to its fixed T_m for each MB, this led to a new design of multiplex MBs nanoassemblies for fluorescence thermometry with the resolution <0.5 °C for a wide range of temperatures from 15 to 60°C. MBs are widely used in fluorescence thermometry, including thermal mapping and temperature sensing in some living organisms.^[Z-83-84]

C.3 Gold nanoparticles

Gold nanoparticles (AuNPs) have several distinct properties such as high absorption coefficient, luminescence and conductivity, quenched or enhanced fluorescence, catalyzed reactions, chemically inert and excellent biocompatibility, which makes them more attractive for use as bio-nanosensors.^[Z-85] Shang et al. developed a gold nanocluster (AuNC)- based fluorescent nanothermometer introduced into HeLa cells by simple endocytosis and localized mainly in endosomes/lysosomes. The fluorescent lifetime of the AuNCs exhibited clearly excellent temperature

dependence. Interestingly, simultaneous intracellular temperature sensing and imaging of cells using fluorescence life time imaging microscopy (FLIM) was clearly shown and confirmed highly sensitive temperature dependent fluorescent emission.^[Z-86-87]

C.4 Nanodiamonds

Kucsko et al.^[Z-88] demonstrated a new approach for the nanothermometer by using coherent manipulation of the electronic spin associated with nitrogen-vacancy color centers in diamond nanocrystals (nanodiamond). The ground state of nanodiamonds is split into two energy levels. The energy gap between the two levels is temperature dependent. This technique uses nanowire to introduce nanodiamonds for local temperature sensing and AuNPs for heat transfer to the cells and achieves the detection of temperature fluctuations in living cells as small as 1.8 mK in an ultrapure bulk diamond sample at a small length scale as short as 200 nm. Using this technique, temperature-gradient control and mapping at the subcellular level in a human embryonic fibroblast were demonstrated. The adequate spatial resolution of this approach allows compatibility with tracking intracellular metabolic reaction in single cells. Although it is difficult and invasive to localize the nanodiamonds into the cells or subcellular organelles by microinjection or electroporation and this method involves laser which can cause photodamage to the cell, the incredible detection sensitivity is the highest among any thermometers developed so far.^[Z-89-90]

C.5 Quantum dots (QDs)

A quantum dot is a tiny inorganic nanoparticle with a typical size less than 10 nm. The unique optical properties are derived from the confinement of the electrons and produce changes in the electronic structure, leading to fluorescence enhancement with better brightness for detection, a broader excitation profile providing tunability, and greater photostability compared with organic dyes.^[Z-87] The well-known QDs include CdSe@ZnS (the @ symbol indicates a CdSe core surrounded by a ZnS shell) commonly used as fluorescent probes. They possess narrow emission lines with particle size dependent wavelengths. However, disadvantages such as potential cytotoxicity and fluorescence blinking can be problematic.^[Z-91]

Yang et al.^[Z-92] reported the cellular temperature response inside single living NIH/3T3 murine fibroblast cells upon external chemical and physical stimuli following Ca^{2+} stress and cold shock using quantum dots as nano-thermometers. The obtained photoluminescence spectral shifts used for intracellular heat generation mapping revealed inhomogeneous intracellular temperature progression, which supports the concept of subcellular temperature gradient signaling and regulation in cells.

C.6 Magnetic nanoparticles

Iron oxide nanoparticles (IONPs) and superparamagnetic iron oxide nanoparticles (SPIONs) have gained much attention in many bio-medical fields due to their intrinsic properties, such as internal magnetism, visualization by magnetic resonance (MR) imaging, biocompatibility, guidance to target sites by means of an external magnetic field, heating to provide hyperthermia for cancer therapy and degradation into nontoxic iron ions *in vivo*. SPIONs are composed of an inner magnetic particle core (usually magnetite, Fe_3O_4 , or maghemite, $\gamma\text{-Fe}_2\text{O}_3$) and a hydrophilic coating of polymers, such as polysaccharide, poly(ethylene glycol) (PEG), and poly(vinyl alcohol). The coating prevents agglomerations and protects them from the surrounding environment. They can also be modified by targeting ligands.^[Z-22,93]

Zhong et al.^[Z-94] reported a new non-invasive approach for remote temperature probing that provides accuracy as good as $0.017\text{ }^\circ\text{C}$ (0.0055% accuracy) by measuring the magnetization curve of a commercial oleic acid coated magnetic nanoparticles with a size around 10 nm. This method provides great significance in the potential establishment of safer and non-invasive protocols for hyperthermia therapy and intracellular temperature sensing. However, experimental evidence inside the living cells has not been proven so far.

Wang et al.^[Z-95] developed a magnetic fluorescent nano-thermometer consisting of magnetic nanoparticles (Fe_3O_4) encapsulated inside a silica layer. Then a poly(N-isopropylacrylamide)(pNIPAM) copolymer shell with Rhodamine B isothiocyanate (RhBITC) embedded inside was further coated. Finally, gold nanoparticles were introduced onto the copolymer shell by in-situ growth method and the nano-thermometer (denoted as $\text{Fe}_3\text{O}_4@\text{SiO}_2@(\text{pNIPAM-co-RhBITC})/\text{Au}$) was obtained.

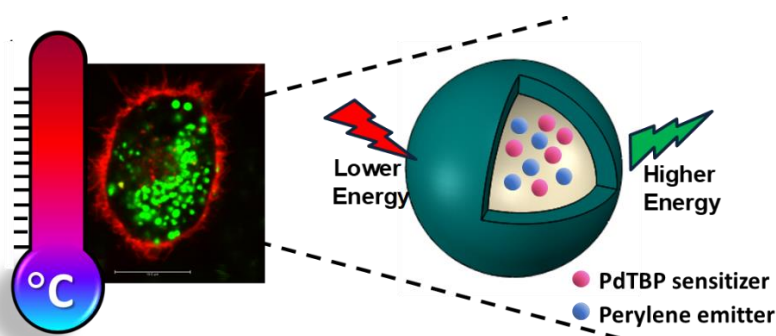
The dual responses to both magnetism and temperature nanothermometer, in which the fluorescence intensity of the nano-thermometer decreases as the temperature increases was demonstrated in HeLa at 26-41 °C with a sensitivity of $-4.84\% \text{ } ^\circ\text{C}^{-1}$.

C1: TEMPERATURE SENSING IN CELLS BY POLYMERIC UPCONVERSION NANOCAPSULES

(Note: The literature of the chapter C1 can be found on page 116 at the end of this chapter.)

Permission: The manuscript is under preparation.

Contribution: I carried out the biological part including cell preparation, cell toxicity, cellular uptake study by flow cytometry and cell imaging by cLSM. ██████████ synthesized and characterized the UCNCs. ██████████ performed upconversion measurements. ██████████ prepared the dyes. The project was supervised by ██████████.



TOC C1: Polymeric upconversion nanocapsules (UCNCs) utilized the temperature dependence of triplet-triplet annihilation upconversion (TTA-UC) phenomenon was developed for use as nanothermometers in living cells. The UCNCs consisted of a PMMA shell and a core containing oxygen scavenger rice bran oil with the PdTBP as sensitizer and perylene as emitter dyes, enabling the conversion of low energy photons ($\lambda_{\text{ex}} = 633 \text{ nm}$) into high energy photons ($\lambda_{\text{em}} = 520 \text{ nm}$). The UCNCs exhibited biocompatibility, efficient cellular uptake, and temperature dependent luminescence intensity in a range of 22-40 °C inside HeLa cells, which can be used for local temperature monitoring and is promising for metabolic study, therapy and diagnostics.

Aim: With the importance of local temperature monitoring, this study aimed to develop light-triggered polymeric upconversion nanocapsules based on triplet-triplet

annihilation upconversion (TTA-UC), which is a temperature dependent system for the measurement of cellular temperature in living HeLa cells.

Abstract: Monitoring local temperature in cells is crucial to interpret their biological activities since the enhanced cellular metabolism leads to higher heat productions as commonly correlated with the presence of diseases like cancer. For this purpose, herein, we reported polymeric upconversion nanocapsules that utilized temperature dependence of triplet-triplet annihilation upconversion (TTA-UC) phenomenon for use as nanothermometers in cells. The nanocapsules (NC) were synthesized by miniemulsion solvent evaporation technique that comprised a PMMA-shell and a liquid core of rice bran oil, hosting TTA-UC active dyes (sensitizer and emitter). The TTA-UC enables the conversion of lower energy photons ($\lambda_{\text{ex}} = 633 \text{ nm}$, low intensity laser excitation) into higher energy ones (with central emission wavelength of $\lambda_{\text{em}} = 520 \text{ nm}$), depends remarkably on the environment temperature. The sensitivity of the TTA-UC on the local oxygen concentration was overcome by oxygen reduction ability of the rice bran oil core and properly chosen temporal registration scheme. Therefore, TTA-UC process could be performed at different levels of oxygen amount including the ambient environment. By this, sustainable calibration curves, linking the local temperature (inside the NC, *in vitro*, for a temperature range $\Delta T \sim 22 \text{ }^\circ\text{C}$ up to $40 \text{ }^\circ\text{C}$) and the emission parameters of the TTA-UC signals, were obtained when UCNCs were uptaken by HeLa cells with a good cellular viability. Thus, the HeLa-cell temperatures approaching to their enhanced metabolic activity range led to a significant increase in the delayed fluorescence spectrum of the UCNCs that is promising for developing novel treatment and diagnostic tools in medicine.

C1.1. Introduction

Gathering information about local temperature in cells is useful for understanding their biological activities. It is well known that cellular events like enzyme reactions and cell division are strongly correlated with temperature changes.^[C1-1-3] For instance, continuously growing cancerous cells produce higher levels of heat in comparison with healthy cells due to their increased metabolism.^[C1-4, 5] Therefore, the determination of

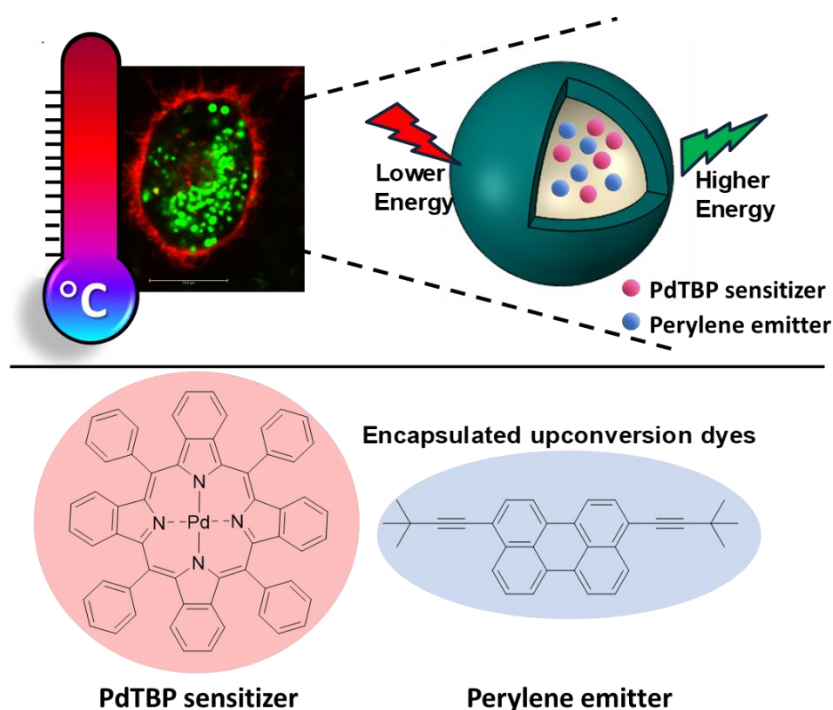
cell temperature can open up new opportunities for developing novel treatment and diagnostic tools in medicine. Nevertheless, there are significant technological challenges that need to be overcome. First, the temperature probe should be small in comparison with the cell-compartments, i.e. it must be in nanoscale size to enable the local heat monitoring, but also not to influence the real cell-temperature. Secondly, the sufficiently small size of the temperature probe is needed for a good cellular uptake to allow enough of them inside the cells. Third, the temperature probe needs to be entirely biocompatible and it should not interfere with the cell-metabolism processes during the temperature record.

Polymeric nanocapsules^[C1-6, 7] offer a solution to obtain the necessary above-mentioned functions through the ease of their flexible structure design for optimized shell / core balance and sufficient cellular uptake in a safe way. Besides, they can be constructed as temperature responsive by adding the corresponding sensitive units either to the polymer shell^[C1-8] or to the core through the right cargo combinations. In this context, a minimally-invasive strategy for providing the temperature-sensing response to the nanocapsules is to favor luminescent based-tools that are sensitive to temperature alterations when the light excitation proceeds.^[C1-9, 10]

Excitation light with wavelength shifted to biologically less-interacting optical region of deep-red or NIR-A is a harmless way of stimuli. Such light penetrates the tissue deep enough without significant side effects.^[C1-11, 12] Crucial benefit of using deep-red light is that the excitation light will not cause unwanted auto-fluorescence of the cell-culture and/or nutrition-mixtures. A promising tool to reach such target is to utilize photon energy upconverting processes, that can generate higher-energy photons *via* excitation of lower energy ones.^[C1-13] Various optical events such as two-photon absorption,^[C1-14] second harmonic generation,^[C1-15] rare-earth ions (e.g. lanthanide, Ln^{+3}) based upconversion (excited state absorption or energy transfer)^[C1-16] and triplet-triplet annihilation upconversion (TTA-UC)^[C1-17] exist for realizing upconversion processes. Among them, TTA-UC is the only UC-process performed with photons coming from a non-coherent optical source with very low excitation intensity (on the level of 20 mWcm^{-2}). Besides, the excitation and emission spectrum of the TTA-UC based system can be tuned freely by using suitable combination of sensitizer and emitter couples from a large molecular library.^[C1-13, 17]

The vast majority of the reported TTA-UC systems in the literature are hydrophobic; therefore, the transfer of the annihilation upconversion process into water environment is an unavoidable requirement when applications in the field of life-science are planned. This has been partially achieved by incorporating the UC-dyes into dendrimers,^[C1-18] micelles,^[C1-19] polymer,^[C1-20-23] silica^[C1-24] or protein^[C1-25] based nanoparticles. However, since the oxygen molecules penetrates into the nano-sized objects (even if the penetration rate is slowed-down), oxygen quenching in the process of TTA-UC optically excited triplet states still exists.^[C1-26] In this regard, core/shell structured nanoparticles (i.e. nanocapsules) enable an opportunity as their hydrophobic core can be enriched by incorporating oxygen-scavenging substances. At presence of molecular oxygen, the TTA-UC process is unavoidably related to generation of singlet oxygen, known as very aggressive species. If the rate of oxygen “consumption“ (i.e. the rate of covalent bonding of the singlet oxygen with the introduced singlet oxygen scavenging moiety) is higher than the rate of oxygen penetration through the NC-shell, it is possible to mimic “oxygen-free conditions”. So far, some examples of TTA-UC processing in the presence of oxygen have been shown^[C1-25, 27-30] and it should be further extended in order to utilize this technique in medical applications like the construction of nanothermometers.

To date, most reported luminescent nanothermometers are developed by use of lanthanide based upconversion nanoparticles (UCNPs).^[C1-31-33] In contrast, TTA-UC based nanocapsules are mainly fabricated for bio-imaging applications^[C1-22-25, 34] and the construction of solar cell devices.^[C1-29, 35] However, the intense developments of polymeric nanocapsules and high knowledge of their biosafety can be combined with the advantages of TTA-UC process for further advancement in this field. Thus, in this paper, we demonstrate the synthesis of polymeric upconversion nanocapsules and use them for temperature dependent *in vitro* TTA-UC process in HeLa cancer cells exposed to ambient environment for applicability as nanothermometer. The shell of the nanocapsules was selected as a biologically safe poly (methyl methacrylate) (PMMA) and the NC-core was rice bran oil (RBO), which serves as efficient singlet oxygen quencher. **Scheme C1** illustrates the general approach towards *in vitro* temperature-sensing in HeLa cells *via* TTA-UC, together with the chemical structures of the encapsulated sensitizer and emitter couple.



Scheme C1. Polymeric upconversion nanocapsules sensing the temperature in HeLa cells

C1.2. Results and discussion

C1.2.1 Cellular uptake and viability

After synthesis and characterization, the UCNCs were exposed to different temperatures and the typical luminescence spectra were recorded. The obtained luminescence intensity successfully demonstrated temperature dependence in the range of 20 to 50 °C in the aqueous solution. Prior to the assessment of *in vitro* temperature sensing, the cellular uptake and viability of the established nanocapsules were examined. Herein, HeLa cells were chosen for *in vitro* assay to mimic the cancer environment. First, cytotoxicity assay was performed to determine the optimal concentration of the UCNCs for further use as a potential nanothermometer. Various concentrations of the UCNCs ranging from 0.5 to 10 mg/mL were incubated with the cells for 24 h. After that, cell viability was determined, as shown in **Figure C1.1a**. The UCNCs decreased cell viability in a dose-dependent manner and their half-maximal effective concentrations (EC_{50}) were similar at 6.95 and 6.22 mg/mL, respectively. This indicates that the established nanocapsules are highly biocompatible.

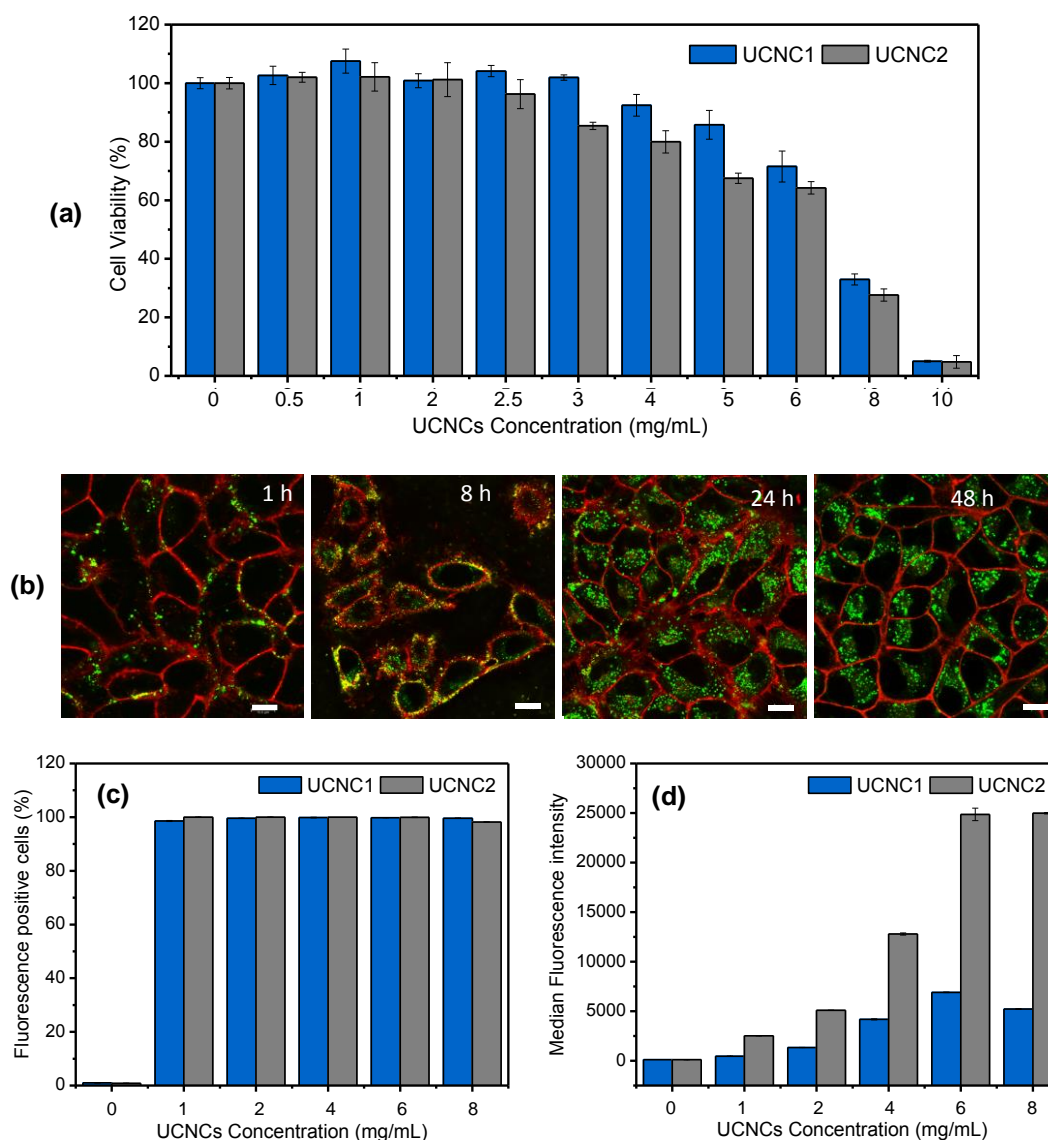


Figure C1.1. (a) Cell viability assay of HeLa cells after treatment with the UCNCs for 24 h. (b) Confocal laser scanning microscopy (cLSM) images of HeLa cells incubated with UCNC2 at 6 mg/mL for various incubation times. The cell membrane was stained with CellMask™Orange and pseudocolored in red. The direct fluorescence emission from encapsulated perylene dye was detected and pseudocolored in green. The scale bar is 10 μm. Flow cytometry analysis showing (c) the percentage of fluorescence-positive cells and (d) median fluorescence intensity (MFI) obtained from the direct fluorescence emission of encapsulated perylene dye in UCNC1 and UCNC2 incubated in HeLa cells after 24 h.

The next step was to study the cellular uptake of the corresponding nanocapsules to select the sufficient loading amount for a good upconversion signal from the HeLa cells. For this purpose, flow cytometry analysis was performed by following the direct fluorescence emission of BDMBP dye as already present in UCNPs that was taken up by the cells after 24 h. **Figure C1.1c** showed 100% of fluorescence positive-cells when the concentration of the UCNPs has reached to 1 mg/mL. However, the median fluorescence intensity (MFI) obtained from the cells treated with UCNC2 (containing more amount of BDMBP dye) was higher than those from UCNC1 at the same concentration of the nanocapsules as shown in **Figure C1.1d**. This stronger signal exhibits the high potential of those nanocapsules to be used as a reporter in physiological temperature measurement. Moreover, the MFI value was reached its maximum level at 6 mg/mL which was not increased more in the case of higher concentrations as observed for 8 mg/mL in **Figure C1.1d**. Therefore, the maximum concentration that gave the highest fluorescence signal and still less toxic to the cell at 6 mg/mL for both UCNC1 and UCNC2 was selected for further temperature sensing investigations in HeLa cells. Nevertheless, before proceeding to that final part, the cellular uptake of UCNC2 at 6 mg/mL in HeLa cells was further investigated by imaging with confocal laser scanning microscopy (cLSM) at different times of incubation. **Figure C1.1b** showed the progress of cellular uptake process. At 1 h of incubation, small amount of UCNPs surrounded the HeLa cells. Later at 8 h, more nanocapsules were co-localized with the membrane and some of them were already inside of the HeLa cells. After 24 h, high amount of the nanocapsules were taken up by every cell and this status was still stable even after 48 h of incubation. Thus, this confirmed not only the higher efficiency for the cellular uptake of the nanocapsules, but also supported their biocompatibility to the cells.

C1.2.2 Temperature Sensing in HeLa Cells

After the confirmation of good cellular uptake and biocompatibility to the cells, we have continued with the *in vitro* TTA-UC measurements to evaluate the potential of our PMMA nanocapsules as a thermometer. Thus, the first investigation was to ensure the sufficient upconversion efficiency at mild excitation power for acquiring the temperature-sensing response when UCNCs are inside the HeLa cells. As mentioned previously, 6 mg/mL of the UCNC1 and UCNC2 nanocapsules were uptaken by the

HeLa cells, which was then followed by excitation with 633 nm HeNe laser by increasing the excitation intensity stepwise from 40 mWcm^{-2} to 320 mWcm^{-2} at a fixed temperature ($22 \text{ }^\circ\text{C}$, **Figure C1.2**). Herein, we could not obtain an enough UC signal from UCNC1 nanocapsules in HeLa cells at this range of the excitation intensity. It should be noted that the loss is obviously related with the lesser concentration of the nanocapsules since about 7 times dilution was applied to incubate them within the cells. On the other hand, the higher dye loaded nanocapsules (UCNC2) in HeLa cells can function good at varied light excitation intensities as shown in **Figure C1.2**. Again, almost 7 times dilution leads to lower efficiencies (**Figure C1.2**) than the whole bulk status of the nanocapsules but the obtained UC efficiency of nanocapsules in cells was sufficient for testing the *in vitro* temperature response of the UCNCs (**Figure C1.3**). In addition, residual phosphorescence signal was in a lesser amount and was spectrally overlapped with the auto-fluorescence of the cell medium. The cell medium auto-fluorescence was investigated by parallel experiments using control HeLa cell dishes having no nanocapsules inside (**Figure C1.4**). Additional proof for this was that the strong temperature dependence of the observed optical signal with local maximum at $\lambda = 660 \text{ nm}$. This signal decreases strongly with the increase of the sample temperature.

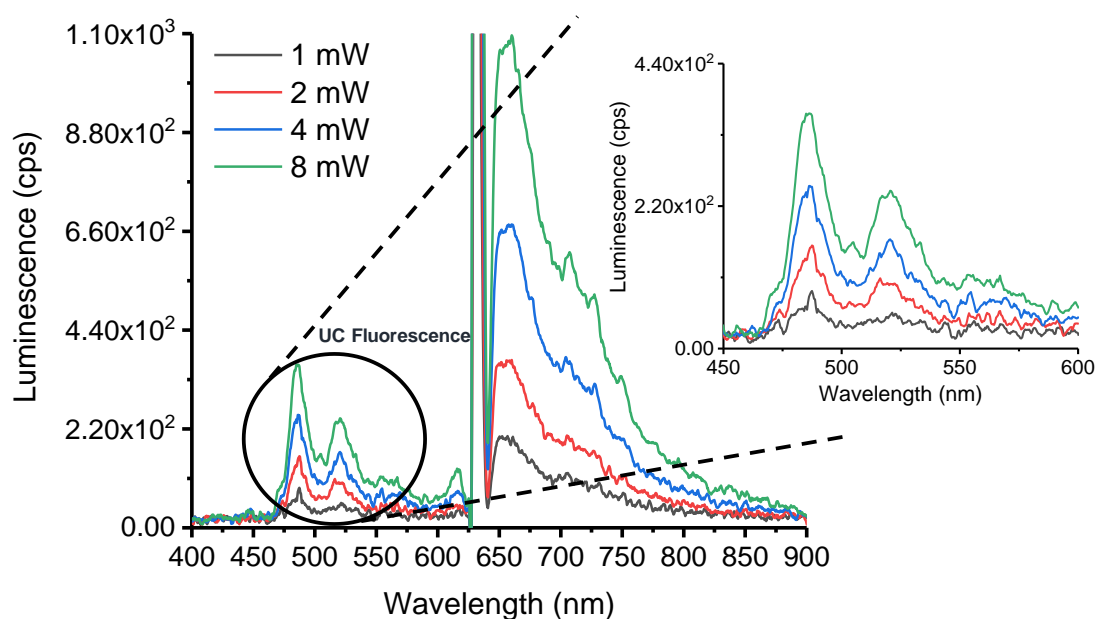


Figure C1.2. Power dependent luminescence spectra of HeLa cells incubated with UCNC2 (6 mg/mL) at $22 \text{ }^\circ\text{C}$, excited at $\lambda_{\text{ex}} = 633 \text{ nm}$, with HeNe laser.

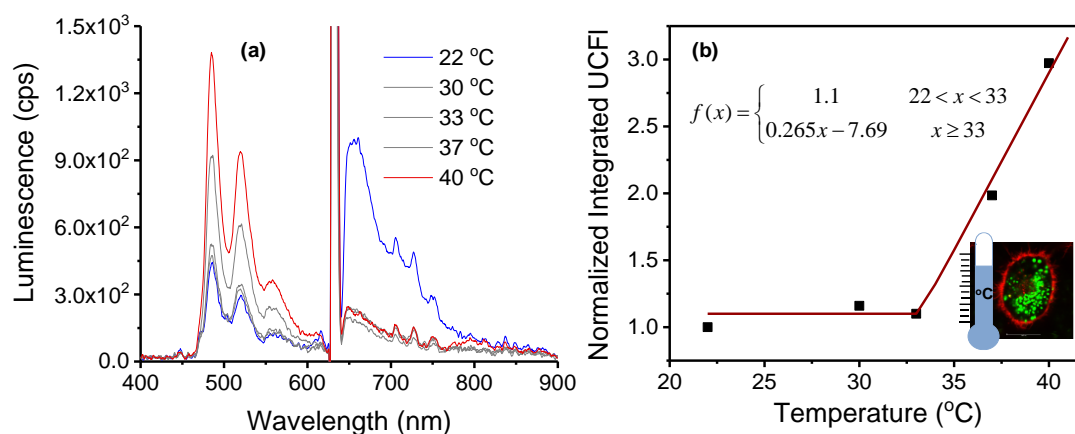


Figure C1.3. Temperature dependent luminescent spectra of UCNC2 nanocapsules uptaken by HeLa cells – excitation at $\lambda_{\text{ex}} = 633 \text{ nm}$, 320 mWcm^{-2} HeNe laser. **(b)** Temperature dependence of the normalized integral UC Fluorescence (UCFI) defined from the spectra in part b of this figure (Integral region is from $\lambda_0 = 460 \text{ nm}$ to $\lambda_f = 620 \text{ nm}$) to use as a potential calibration curve (Residual phosphorescence is small but almost constant). Inset: Confocal image of HeLa cells with UCNCs for illustrating the employment as nanothermometer.

In **Figure C1.3a**, temperature dependent luminescent spectra of living HeLa cells incubated with UCNC2 nanocapsules are reported. The studied temperature interval was on purpose limited to $22 \text{ }^\circ\text{C}$ to $40 \text{ }^\circ\text{C}$ not to impair the HeLa cell metabolism. In this temperature range, almost constant intensity of the residual phosphorescence signal (at $\lambda_{\text{max}} = 800 \text{ nm}$, **Figure C1.3a**) was observed. On the other side, UC Fluorescence increased monotonically with the increase of the sample temperature. Here, an important outcome is that the increase of HeLa cell temperature obviously showed more pronounced effect on the intensity of the UC signal for $T > 33 \text{ }^\circ\text{C}$, than for the range of $20 \text{ }^\circ\text{C} - 33 \text{ }^\circ\text{C}$. This is most probably attributed with the enhanced cellular activity at higher temperatures which in turn leads to an increased oxygen consumption at this condition. HeLa cells utilized O_2 of about 26.9 amol/cell.s [C1-44] at $37 \text{ }^\circ\text{C}$ and this becomes as a supporting reaction to the RBO oxygenation when compared with the case of bulk nanocapsules in dispersions. Herein, the cells act as a self-helper for the TTA-UC process happening in their vicinity and mimics more likely the situation we have seen in UCNC1 nanocapsules in which the UC fluorescence increases with

temperature. This also confirms that the oxygen presence and all further physical/chemical events together forms the unique condition. Briefly, combination of all these events leads to lesser oxygen at a certain time at higher temperatures which results in the enhanced UC-fluorescence by the temperature increase. **Figure C1.3b** reflects this behaviour by showing that the UC signal is increased more than 3 times when it reaches to 40 °C. This result is also comparable with the data obtained for UCNC1 nanocapsules as the enhancement was also in this range. This showed us that together with the oxygen reduction, the varied nanocapsule concentration also have an effect on this result. Obviously, the irradiated area covers 7 times lesser amounts of nanocapsules in HeLa cells (uptaken at 6 mg/mL condition). This leads to the same reduction in the total dye concentrations contributing to the final luminescence spectra. If we have a closer look, these local dye amounts embedded in the nanocapsules are of about 1.4 times more than the bulk UCNC1 nanocapsules whereas about 7 times lesser than in the case of UCNC2 nanocapsules. Thus, it is not a surprising outcome that TTA-UC processing with UCNC1 nanocapsules mimic the *in vitro* TTA-UC process inside the HeLa cells more closely. By this, the temperature sensing in HeLa cells by use of a PMMA based upconversion nanocapsules were shown with a minimally-invasive way.

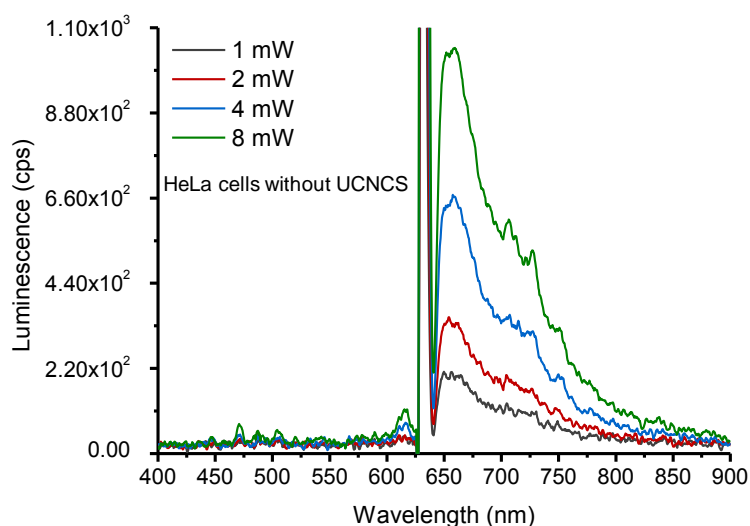


Figure C1.4. Power dependent luminescence spectra of HeLa cells without UCNCs at 22 °C, excited at $\lambda_{ex} = 633$ nm, with HeNe laser, control experiments performed in parallel to the *in vitro* TTA-UC process.

C1.3. Conclusion

In the present work, we have demonstrated polymeric upconversion nanocapsules that utilized TTA-UC based temperature responsivity for potential use as minimally-invasive nanothermometers in living cells. The established nanocapsules consist of a PMMA shell and a RBO core hosting the PdTBP sensitizer and BDMBP emitter. Different amounts of dye encapsulation were shown to perform TTA-UC at aqueous medium and for further applications in temperature probing of a biological environment. The UCNCs can function at different levels of oxygen presence including the fully air saturated condition that supports the antioxidant capacity with the aid of an unsaturated fatty acids in the RBO core. In addition, the good cellular uptake and biocompatibility towards HeLa cancer cells and further temperature sensing through *in vitro* TTA-UC process with a mild excitation intensity by red light opens up new opportunities for the design of nanothermometers to gain information about the cellular activities. This exhibits further advances in medical applications for especially early diagnosis and treatment of the diseases like cancer.

C1.4. References

- [C1-1] Hildebrandt, B.; Wust, P.; Ahlers, O.; Dieing, A.; Sreenivasa, G.; Kerner, T.; Felix, R.; Riess, H., The cellular and molecular basis of hyperthermia. *Critical Reviews in Oncology/Hematology* 2002, 43, 33-56.
- [C1-2] Lowell, B. B.; Spiegelman, B. M., Towards a molecular understanding of adaptive thermogenesis. *Nature* 2000, 404, 652.
- [C1-3] Rao, P. N.; Engelberg, J., HeLa Cells: Effects of Temperature on the Life Cycle. *Science* 1965, 148, 1092-1094.
- [C1-4] Monti, M.; Brandt, L.; Ikomi-Kumm, J.; Olsson, H., Microcalorimetric investigation of cell metabolism in tumour cells from patients with non-Hodgkin lymphoma (NHL). *Scandinavian Journal of Haematology* 1986, 36, 353-357.
- [C1-5] Karnebogen, M.; Singer, D.; Kallerhoff, M.; Ringert, R. H., Microcalorimetric investigations on isolated tumorous and non-tumorous tissue samples. *Thermochim. Acta* 1993, 229, 147-155.
- [C1-6] Cui, J.; van Koeverden, M. P.; Müllner, M.; Kempe, K.; Caruso, F., Emerging methods for the fabrication of polymer capsules. *Adv. Colloid Interface Sci.* 2014, 207, 14-31.
- [C1-7] Musyanovych, A.; Landfester, K., Polymer Micro- and Nanocapsules as Biological Carriers with Multifunctional Properties. *Macromolecular Bioscience* 2014, 14, 458-477.

- [C1-8] Schmaljohann, D., Thermo- and pH-responsive polymers in drug delivery. *Advanced Drug Delivery Reviews* 2006, 58, 1655-1670.
- [C1-9] Jaque, D.; Rosal, B. d.; Rodríguez, E. M.; Maestro, L. M.; Haro-González, P.; Solé, J. G., Fluorescent nanothermometers for intracellular thermal sensing. *Nanomedicine* 2014, 9, 1047-1062.
- [C1-10] Jaque, D.; Vetrone, F., Luminescence nanothermometry. *Nanoscale* 2012, 4, 4301-4326.
- [C1-11] Frangioni, J. V., In vivo near-infrared fluorescence imaging. *Curr. Opin. Chem. Biol.* 2003, 7, 626-634.
- [C1-12] Stolik, S.; Delgado, J. A.; Pérez, A.; Anasagasti, L., Measurement of the penetration depths of red and near infrared light in human “ex vivo” tissues. *Journal of Photochemistry and Photobiology B: Biology* 2000, 57, 90-93.
- [C1-13] Zhou, J.; Liu, Q.; Feng, W.; Sun, Y.; Li, F., Upconversion Luminescent Materials: Advances and Applications. *Chem. Rev.* 2015, 115, 395-465.
- [C1-14] Denk, W.; Strickler, J.; Webb, W., Two-photon laser scanning fluorescence microscopy. *Science* 1990, 248, 73-76.
- [C1-15] Clark, H. A.; Campagnola, P. J.; Wuskell, J. P.; Lewis, A.; Loew, L. M., Second Harmonic Generation Properties of Fluorescent Polymer-Encapsulated Gold Nanoparticles. *J. Am. Chem. Soc.* 2000, 122, 10234-10235.
- [C1-16] Chen, G.; Qiu, H.; Prasad, P. N.; Chen, X., Upconversion Nanoparticles: Design, Nanochemistry, and Applications in Theranostics. *Chem. Rev.* 2014, 114, 5161-5214.
- [C1-17] Simon, Y. C.; Weder, C., Low-power photon upconversion through triplet-triplet annihilation in polymers. *J. Mater. Chem.* 2012, 22, 20817-20830.
- [C1-18] Roussakis, E.; Li, Z.; Nowell, N. H.; Nichols, A. J.; Evans, C. L., Bright, “Clickable” Porphyrins for the Visualization of Oxygenation under Ambient Light. *Angew. Chem. Int. Ed.* 2015, 54, 14728-14731.
- [C1-19] Andrey, T.; Dmitry, B.; Stanislav, B.; Tzenka, M.; Katharina, L., Micellar carrier for triplet-triplet annihilation-assisted photon energy upconversion in a water environment. *New Journal of Physics* 2011, 13, 083035.
- [C1-20] Monguzzi, A.; Frigoli, M.; Larpent, C.; Tubino, R.; Meinardi, F., Low-Power-Photon Up-Conversion in Dual-Dye-Loaded Polymer Nanoparticles. *Adv. Funct. Mater.* 2012, 22, 139-143.
- [C1-21] Thévenaz, D. C.; Monguzzi, A.; Vanhecke, D.; Vadrucci, R.; Meinardi, F.; Simon, Y. C.; Weder, C., Thermoresponsive low-power light upconverting polymer nanoparticles. *Materials Horizons* 2016, 3, 602-607.
- [C1-22] Wohnhaas, C.; Turshatov, A.; Mailänder, V.; Lorenz, S.; Balushev, S.; Miteva, T.; Landfester, K., Annihilation Upconversion in Cells by Embedding the Dye System in Polymeric Nanocapsules. *Macromolecular Bioscience* 2011, 11, 772-778.

- [C1-23] Wohnhaas, C.; Mailänder, V.; Dröge, M.; Filatov, M. A.; Busko, D.; Avlasevich, Y.; Balushev, S.; Miteva, T.; Landfester, K.; Turshatov, A., Triplet–Triplet Annihilation Upconversion Based Nanocapsules for Bioimaging Under Excitation by Red and Deep-Red Light. *Macromolecular Bioscience* 2013, 13, 1422-1430.
- [C1-24] Kwon, O. S.; Song, H. S.; Conde, J.; Kim, H.-i.; Artzi, N.; Kim, J.-H., Dual-Color Emissive Upconversion Nanocapsules for Differential Cancer Bioimaging In Vivo. *ACS Nano* 2016, 10, 1512-1521.
- [C1-25] Liu, Q.; Yin, B.; Yang, T.; Yang, Y.; Shen, Z.; Yao, P.; Li, F., A General Strategy for Biocompatible, High-Effective Upconversion Nanocapsules Based on Triplet–Triplet Annihilation. *J. Am. Chem. Soc.* 2013, 135, 5029-5037.
- [C1-26] Balushev, S.; Katta, K.; Avlasevich, Y.; Landfester, K., Annihilation upconversion in nanoconfinement: solving the oxygen quenching problem. *Materials Horizons* 2016, 3, 478-486.
- [C1-27] Kim, J.-H.; Kim, J.-H., Encapsulated Triplet–Triplet Annihilation-Based Upconversion in the Aqueous Phase for Sub-Band-Gap Semiconductor Photocatalysis. *J. Am. Chem. Soc.* 2012, 134, 17478-17481.
- [C1-28] Ye, C.; Wang, B.; Hao, R.; Wang, X.; Ding, P.; Tao, X.; Chen, Z.; Liang, Z.; Zhou, Y., Oil-in-water microemulsion: an effective medium for triplet–triplet annihilated upconversion with efficient triplet acceptors. *Journal of Materials Chemistry C* 2014, 2, 8507-8514.
- [C1-29] Svagan, A. J.; Busko, D.; Avlasevich, Y.; Glasser, G.; Balushev, S.; Landfester, K., Photon Energy Upconverting Nanopaper: A Bioinspired Oxygen Protection Strategy. *ACS Nano* 2014, 8, 8198-8207.
- [C1-30] Marsico, F.; Turshatov, A.; Peköz, R.; Avlasevich, Y.; Wagner, M.; Weber, K.; Donadio, D.; Landfester, K.; Balushev, S.; Wurm, F. R., Hyperbranched Unsaturated Polyphosphates as a Protective Matrix for Long-Term Photon Upconversion in Air. *J. Am. Chem. Soc.* 2014, 136, 11057-11064.
- [C1-31] Vetrone, F.; Naccache, R.; Zamarrón, A.; Juarranz de la Fuente, A.; Sanz-Rodríguez, F.; Martínez Maestro, L.; Martín Rodríguez, E.; Jaque, D.; García Solé, J.; Capobianco, J. A., Temperature Sensing Using Fluorescent Nanothermometers. *ACS Nano* 2010, 4, 3254-3258.
- [C1-32] Sedlmeier, A.; Achatz, D. E.; Fischer, L. H.; Gorris, H. H.; Wolfbeis, O. S., Photon upconverting nanoparticles for luminescent sensing of temperature. *Nanoscale* 2012, 4, 7090-7096.
- [C1-33] Fischer, L. H.; Harms, G. S.; Wolfbeis, O. S., Upconverting Nanoparticles for Nanoscale Thermometry. *Angew. Chem. Int. Ed.* 2011, 50, 4546-4551.
- [C1-34] Tian, B.; Wang, Q.; Su, Q.; Feng, W.; Li, F., In vivo biodistribution and toxicity assessment of triplet-triplet annihilation-based upconversion nanocapsules. *Biomaterials* 2017, 112, 10-19.

- [C1-35] Wohnhaas, C.; Friedemann, K.; Busko, D.; Landfester, K.; Balushev, S.; Crespy, D.; Turshatov, A., All Organic Nanofibers As Ultralight Versatile Support for Triplet–Triplet Annihilation Upconversion. *ACS Macro Letters* 2013, 2, 446-450.
- [C1-36] Ju, Y.-H.; Vali, S. R., Rice bran oil as a potential resource for biodiesel: a review. 2005.
- [C1-37] Bettencourt, A.; Almeida, A. J., Poly(methyl methacrylate) particulate carriers in drug delivery. *J. Microencapsulation* 2012, 29, 353-367.
- [C1-38] Keivanidis, P. E.; Balushev, S.; Lieser, G.; Wegner, G., Inherent Photon Energy Recycling Effects in the Up-Converted Delayed Luminescence Dynamics of Poly(fluorene)–PtIIoctaethyl Porphyrin Blends. *ChemPhysChem* 2009, 10, 2316-2326.
- [C1-39] Nazarova, N. V.; Avlasevich, Y. S.; Landfester, K.; Balushev, S., Stimuli-responsive protection of optically excited triplet ensembles against deactivation by molecular oxygen. *Dalton Transactions* 2018, 47, 8605-8610.
- [C1-40] Stich, M. I. J.; Fischer, L. H.; Wolfbeis, O. S., Multiple fluorescent chemical sensing and imaging. *Chem. Soc. Rev.* 2010, 39, 3102-3114.
- [C1-41] Filatov, M. A.; Heinrich, E.; Busko, D.; Ilieva, I. Z.; Landfester, K.; Balushev, S., Reversible oxygen addition on a triplet sensitizer molecule: protection from excited state depopulation. *PCCP* 2015, 17, 6501-6510.
- [C1-42] Pope, M.; Swenberg, C. E., *Electronic processes in organic crystals and polymers.* Oxford University Press New York: 1999; Vol. 2.
- [C1-43] Duan, P.; Yanai, N.; Nagatomi, H.; Kimizuka, N., Photon Upconversion in Supramolecular Gel Matrixes: Spontaneous Accumulation of Light-Harvesting Donor–Acceptor Arrays in Nanofibers and Acquired Air Stability. *J. Am. Chem. Soc.* 2015, 137, 1887-1894.
- [C1-44] Wagner, B. A.; Venkataraman, S.; Buettner, G. R., The rate of oxygen utilization by cells. *Free Radical Biol. Med.* 2011, 51, 700-712.
- [C1-45] Filatov, M. A.; Balushev, S.; Ilieva, I. Z.; Enkelmann, V.; Miteva, T.; Landfester, K.; Aleshchenkov, S. E.; Cheprakov, A. V., Tetraaryltetraanthra[2,3]porphyrins: Synthesis, Structure, and Optical Properties. *The Journal of Organic Chemistry* 2012, 77, 11119-11131.
- [C1-46] Cheprakov, A. V.; Filatov, M. A., The dihydroisoindole approach to linearly annelated π -extended porphyrins. *J. Porphyrins Phthalocyanines* 2009, 13, 291-303.

Materials and Methods

General protocols applied in all chapters are combined and specific protocols needed for each chapter are separately described. The other experimental methods that was done by the collaborators can be found in the original online publications.

GENERAL PROTOCOLS FOR ALL CHAPTERS

1. Adherent Cell Culture

Adherent cells including HeLa, LNCaP, PC3 and SAOS-2 were obtained from DSMZ (Deutsche Sammlung von Mikroorganismen und Zellkulturen, Germany). They were cultured in Dulbecco's Modified Eagle's Medium (DMEM, Gibco, USA) complete medium containing 10% fetal bovine serum (FBS, Gibco, USA), 1% L-glutamine (Gibco, USA) and 1% penicillin/streptomycin (Gibco, USA) and incubated at 37 °C in CO₂-incubator with 95% humidity and 5% CO₂ (C200, Labotect, Germany). To dissociate adherent cells, the cells were trypsinized with 0.25% trypsin (Gibco, USA) for 3 min as general procedure. The cell pellet was collected by centrifugation at 130 g for 3 min, resuspended in DMEM complete medium and used for further assays. Viable cells were determined by trypan blue exclusion method and counted by using TC10™ automated cell counter (Bio-Rad, USA).

For uptake and toxicity study, adherent cells resuspended in DMEM complete medium were seeded at a density of 6,400 cells per well in 96-well plate or 8×10^4 cells per well in 24-well plate for 48 h. For cLSM imaging, adherent cells were seeded at a density of 2×10^4 cells per well in μ -Slide 8 well with a glass coverslip bottom (Ibidi, Germany) and cultured for 24 h in DMEM complete medium (Phenol red free).

2. Cell Viability Assay determined by CellTiter-Glo® Luminescent Assay

After cell preparation, the cells were treated with various concentrations of the corresponding samples for 24 h. Sample without any treatment was used as a negative control and calculated as 100% cell viability, while 20% DMSO added sample was used as a positive control. After cell treatment, cell viability was evaluated by using the CellTiter-Glo® luminescent cell viability assay (Promega, USA) according to the manufacturer's protocol. This assay is based on the amount of ATP present, which

reflect the presence of metabolically active cells. Luminescence was recorded 10 minutes after reagent addition using plate reader (Infinite® M1000, Tecan, Germany). The half maximal effective concentration (EC₅₀) values were calculated by fitting a curve with non-linear regression using GraphPad Program.

3. Cellular Uptake Study by Flow Cytometry

After cell treatment, the cells were washed and resuspended in PBS. Flow cytometry measurements were performed on a Attune™ NxT Flow Cytometer (Invitrogen, USA). Zombie Aqua™ dye (BioLegend, USA) was used for live cell gating with the excitation of the violet laser (405 nm) and detected in channel VL-2. All fluorophores labeling nanocapsules and dyes conjugating antibodies are excited and recorded according to their excitation and emission profiles. Data analysis was performed using Attune™ NxT software (Invitrogen, USA) by selecting the cells on a forward/sideward scatter plot, thereby excluding cell debris. These gated events were shown by the histogram of fluorescent signal. Percentages of cell viability were recorded from living cells (Zombie Aqua negative-cells) compared to dead cells (Zombie Aqua positive-cells). After gating for living cells, percentages of fluorescence positive-cells or their median fluorescence intensities (MFI) were reported.

4. Cell Imaging by Confocal Laser Scanning Microscopy (cLSM)

After cell treatment, adherent cells were washed twice with DMEM to remove the remaining nanocapsules outside of the cells. T-cells were collected from the plate, washed and transferred to μ -Slide 8 well with a glass coverslip bottom (Ibidi, Germany). Then the cells were stained subcellular organs with fluorescent dyes and finally suspended in DMEM. Live cell images were taken with a commercial setup (LSM SP5 STED Leica Laser Scanning Confocal Microscope, Leica, Germany), consisting of an inverse fluorescence microscope DMI 6000 CS equipped with a multi-laser combination, five detectors operating in the range of 400-800 nm. A HCX PL APO CS 63 x 1.4 oil objective was used in this study. The excitation and detection conditions in a sequential mode were described as follows: green fluorescence labeling such as FITC or Perylene dye were excited with an Ar laser (488 nm), detected at 510-540 nm; The cell membrane was stained with CellMask™Orange (5 μ g/mL, Life

technologies, USA), excited with a DPSS laser (561 nm), detected at 570-600 nm; The cell nucleus was stained with DraQ[®]5 (5 μ M, Cell signaling technology, USA) or red fluorescence labeling such as Cy5, excited with a HeNe laser (633 nm), detected at 650-710 nm.

5. Co-Localization Assay with Lysosome visualized by cLSM

To provide more evidences for cellular uptake, co-localization assay of nanocapsules and lysosome was investigated. After cell treatment, LysoTracker[®] Green DND-26 or LysoTracker[®] Red DND-99 (50 nM diluted in DMEM, Life Technologies, USA) was used to stain lysosome for 1 h. Then the subcellular organs were stained with fluorescent dyes and live cell images were taken as described above.

SPECIFIC PROTOCOLS FOR CHAPTER A

A.1. T-cell Isolation and Culture

Peripheral blood mononuclear cells (PBMCs) were collected from blood of healthy donors by using lymphocyte separation medium (Histopaque[®]-1077, Sigma-Aldrich, USA). Human PBMCs were co-stimulated with immobilized 0.1 μ g/mL of anti-human CD3 (Clone OKT3, functional grade, eBioscience, Germany) and 100 U/mL recombinant human IL-2 (Novartis, Switzerland) in Roswell Park Memorial Institute (RPMI, Gibco, USA) complete medium containing 10% fetal bovine serum (FBS, Gibco, USA), 1% L-Glutamine (Gibco, USA) and 1% penicillin/streptomycin (Gibco, USA) according to T-cell activation, *in vitro* protocol from eBioscience. After cell aggregation was formed on the bottom of the flask, CD8⁺ T-cells were harvested from the culture by CD8 MicroBead and separated through immunomagnetically MACS separation column (Miltenyi Biotec, Germany). CD8⁺ T-cells were cultured in RPMI complete medium and restimulated with anti-CD3 and IL-2 as mentioned above and incubated at 37°C in CO₂-incubator (C200, Labotect, Germany). The cell pellet was collected by centrifugation at 500 g for 5 min, resuspended in RPMI medium and used for further assays. Viable cells were determined by trypan blue exclusion method and counted by using TC10[™] automated cell counter (Bio-Rad, USA).

For uptake and toxicity study, CD8⁺ T-cells resuspended in RPMI medium containing 1% FBS and 100 U/mL IL-2 without antibiotics were added into 0.1 µg/mL of anti-CD3 immobilized 24-well plate at a density of 200,000 cells per well. Then, various concentrations of SiNCs were incubated with the cells for 24 h. Then, the samples were analyzed by flow cytometer and further confirmed by cLSM.

SPECIFIC PROTOCOLS FOR CHAPTER A1

A1.1. Synthesis of silica nanocapsules (synthesized by ██████████)

Silica nanocapsules were synthesized in an oil-in-water miniemulsion by using the surface of oil nanodroplets as template for the hydrolysis and condensation of alkoxy silanes. Specifically, 2.0 g (9.6 mmol) of TEOS was first mixed with 125 mg of hexadecane and 1 g of organic solvent (olive oil or chloroform) to form the oil phase for the synthesis of NCs with hydrodynamic diameter of ~150 nm. In order to tune the size of NCs, 400 vol%, 200 vol%, 50 vol%, or 25 vol% of the above solution was used as oil phase. In the second step, 30 mL of 0.77 mg·mL⁻¹ aqueous solution of CTMA-Cl was poured into the oil mixture under stirring. After a pre-emulsification step by stirring at 1000 rpm for 1 h, the obtained emulsion was sonicated by using a Branson 450 W sonifier with a 1/2'' tip at 70% amplitude for 180 s (30 s of sonication, 10 s of pause) with ice cooling. The resulting miniemulsion was stirred at 1000 rpm for 12 h at room temperature to obtain an aqueous dispersion of SiNCs. In the case of nanocapsules containing chloroform as core liquid, the dispersion was further stirred at air for 24 h to evaporate the chloroform, during which the water diffuses in for filling the core.

To obtain NCs stabilized with nonionic surfactant Lutensol AT50, 40 mg of Lutensol AT50 was added to 2 mL of NC dispersion. The mixture was stirred at 1000 rpm for 2 h and then dialyzed against water within a dialysis tube with MWCO of 1000 g/mol. In this case, CTMA-Cl ($M_w = 320$ g/mol) could diffuse through the dialysis membrane into the aqueous dialysis medium while Lutensol AT50 ($M_w = 2460$ g/mol) was kept inside.

For amino functionalization of SiNCs, 0.5 mL dispersion of SiNC-LUT was first diluted by 2 mL of 0.1vol% acetic acid solution. Calculated amount of APTES (1wt% in acetic acid solution, pH ~3.5) was added to the dispersion. Afterward, the dispersion was stirred at 50 °C for 2 days. For fluorescent labeling of SiNCs, Cy5-NHS was first coupled with APTES at a molar ratio of 1:1.1 to obtain fluorescently labeled silica precursors. The APTES-Cy5 conjugates were then mixed with TEOS as the silica source. The molar ratio of fluorescent molecules with TEOS was 1:14000.

A1.2. Protein Corona Effect on Cellular Uptake

To study the effect of protein corona on cellular uptake, SiNCs were pre-incubated with human serum prior to incubate with CD8⁺ T-cells. Human serum was thawed and centrifuged at 20,000 g under 4°C for 30 min. The supernatant (1 mL) was transferred to a new 1.5 mL-Protein Lobind tube (Eppendorf, Germany) containing calculated volume of SiNC solution with the amount of capsule that provide a surface area of 0.05 m² per reaction according to the following equations (1-3).

$$V_{dispersion \text{ for } 0.05 \text{ m}^2 \text{ NC surface}} = \frac{N_{NC} \cdot m_{dry \text{ NC}}}{\rho_{dispersion} \cdot \text{Solid content(wt\%)}} \quad (1)$$

$$N_{NC} = \frac{0.05 \text{ m}^2}{S_{NC}} = \frac{0.05 \text{ m}^2}{4\pi r^2} \quad (2)$$

$$m_{dry \text{ NC}} = m_{HD} + m_{SiO_2} = m_{HD} + \frac{Mw_{SiO_2}}{Mw_{TEOS}} \cdot m_{TEOS} = \rho_{HD} \cdot V_{HD} + \frac{Mw_{SiO_2}}{Mw_{TEOS}} \rho_{TEOS} V_{TEOS} = \rho_{HD} \cdot V_{droplet} \cdot \frac{V_{HD}}{V_{TEOS} + V_{HD} + V_{CHCl_3}} + \frac{Mw_{SiO_2}}{Mw_{TEOS}} \rho_{TEOS} V_{droplet} \cdot \frac{V_{TEOS}}{V_{TEOS} + V_{HD} + V_{CHCl_3}} \quad (3)$$

where N_{NC} is the number of NCs in the dispersion, $m_{dry \text{ NC}}$ is the mass of single NC at dried state, $\rho_{dispersion}$ is the density of NC dispersion, and S_{NC} is the surface area per NC.

The SiNC-serum mixture was incubated at 37°C for 1 h with 300 rpm shaking in ThermoMixer (HLC Heating, MHR 23, DITABIS, Germany). After that, hard corona SiNCs were separated by centrifugation at 20,000 g 4°C for 1 h and resuspended in 1 mL PBS. The samples were continued to wash 3 times more, resuspended in 1 mL PBS and finally added to 0.1 µg/mL of anti-CD3 pre-coated 24-well plate containing 200,000 cells per well of CD8⁺ T-cells resuspended in RPMI medium containing 100

U/mL IL-2 without antibiotics in the presence of different concentrations of human serum at 0%, 1% and 10%. To keep the cells in a good condition, the human serum was added to the group of 0% to obtain 1% final concentration after 6 h. The uptake of uncoated SiNC in the presence of 1% FBS was used to compare with the pre-coated SiNCs uptake in the presence of 0%, 1% and 10% human serum. After 24 h of incubation, the cells were collected and determined for cell viability and Cy5 positive-cells by flow cytometer as described above.

A1.3. Protein Pattern Analysis by SDS-PAGE

After separating and 3 times washing of hard corona SiNCs, the capsule pellet was resuspended in 100 μ L of desorption buffer containing 2% SDS, 62.5 mM Tris-HCl and incubated at 95°C for 5 min. After centrifugation at 20,000 g 4°C for 1 h, the supernatant containing the protein absorbed on the surface of the capsules was collected and kept at -20°C until used. The protein concentration was determined by Pierce™ 660nm Protein Assay (Pierce, USA) according to the manufacturer's instruction. The total amount of protein at 1.5 μ g of each sample was loaded onto pre-cast Bolt™ 10% Bis-Tris Plus Gel (Invitrogen, USA) and separated in MES SDS running buffer (Invitrogen, USA) at 100 volts for 1 h 15 min. Then, the gel was stained with SilverQuest™ Silver Staining Kit (Invitrogen, USA) according to the manufacturer's protocol.

SPECIFIC PROTOCOLS FOR CHAPTER A2

A2.1. Synthesis of silica nanocapsules (synthesized by ██████████)

The silica nanocapsules were synthesized in a water-in-oil miniemulsion. For NC-1, 7 mg of NaCl and 20 μ L of 25 wt% CTMA-Cl aqueous solution were dissolved in 0.5 mL of milli-Q water as dispersed (water) phase. For continuous (oil) phase, 5 mg of dodecylamine and 35 mg of P(E/B-*b*-EO) were dissolved in 7.5 mL of cyclohexane and the mixture was added to the aqueous phase under stirring at 500 rpm for 10 min at room temperature. The emulsion was then sonicated under ice cooling for 180 s at 70% amplitude in a pulse regime (20 s sonication, 10 s pause) using a Branson 450 W

sonifier and a 1/2" tip. A cyclohexane solution containing 10 mg of P(E/B-*b*-EO) and 250 μ L TEOS in 5 mL of cyclohexane was then added dropwise over a period of 20 min to the miniemulsion. The mixture was stirred at 25 °C for 24 h. For NC-2, an aqueous solution (0.5 mL) with pH 10.3 tuned by ammonia and containing 0.5 mg/mL of NaCl was used as the dispersed phase. A cyclohexane solution (6 mL) containing 160 mg PGPR surfactant was added to the water phase under stirring at 500 rpm for 10 min. The following sonication process for NC-2 is the same as that for NC-1.

The synthesized nanocapsules were purified by repetitive centrifugation (3 times for 20 min, RCF 1664) and redispersion in cyclohexane to remove the excess amount of surfactant. For transferring the nanocapsules into aqueous media, 600 μ L of nanocapsule dispersion in cyclohexane were added dropwise to 5 mL of Lutensol AT50 aqueous solution (1 wt%) under mechanical stirring, and the samples were placed in an ultrasound bath for 3 min at 25 °C (25 kHz). Subsequently, the samples were stirred openly at 25 °C for 24 h to evaporate cyclohexane.

A2.2. Materials

All siRNAs and primers were purchased from Sigma. The sequences were as follows: PD-L1 siRNAs (sense: 5'-GGAUAAGAACAUAUUCAA[dT][dT]-3', antisense: 5'-UUGAAUAAUGUUCUUAUCC[dT][dT]-3'), PD-L1 primers (forward: 5'-TATGGTGGTGCCGACTACAA-3', reverse: 5'-TGCTTGTCAGATGACTTCG-3') and actin primers (forward: 5'-TTGCCGACAGGATGCAGAA-3', reverse: 5'-GCCGATCCACACGGAGTACT-3'). MISSION® siRNA Universal Negative Control #1 was used as siRNA control. All antibodies were purchased from BioLegend (USA): anti-CD274-APC (anti-PD-L1, clone 29E.2A3), anti-CD25-FITC (clone BC96,) and anti-CD71-APC (clone CY1G4).

A2.3. PD-L1 Knockdown Study by Flow Cytometry

After T-cells preparation as mentioned above, the cells were treated with SiNCs encapsulated with siRNA target that specific to PD-L1 mRNA (siRNA target SiNC) or SiNCs encapsulated with siRNA control which has no specific sequences to human mRNA (siRNA control SiNC) compared to the cell control (without any capsule). After

24 h, FBS was added to the culture to obtain a final concentration at 20%. The cells were daily collected from the plate, washed and stained with Zombie Aqua™ for live cell gating and anti-CD274-APC or anti-CD25-FITC or anti-CD71-APC antibodies at 4°C for 30 min. Subsequently, the cells were washed, resuspended in PBS and analyzed by flow cytometer as described above. After gating for living cells, their median fluorescence intensities were used to calculate relative expression of each cell surface marker.

A2.4. Quantitative Polymerase Chain Reaction (qPCR) Analysis

After 2 days of cell treatment with SiNCs containing siRNA as described earlier, the cells were collected and total RNA was extracted using RNeasy Mini Kit (Qiagen, USA). RNA concentration of extracted RNA samples was measured by Nanodrop (NanoDrop™ 8000 Spectrophotometer, Thermo Fisher Scientific, USA). RT-PCR grade water (Invitrogen, USA) was used throughout the experiment. Then, cDNA was synthesized using iScript™ cDNA Synthesis Kit (Bio-Rad, USA) and qPCR reaction was performed using iQ™ SYBR® Green Supermix (Bio-Rad, USA) in a Thermal cycler (C1000, CFX96 Real-time PCR detection system, Bio-Rad, USA). The qPCR data was analyzed using $2^{-(\Delta\Delta C(T))}$ method. Results are expressed as relative expression of two independent experiments compared to the cell control.

A2.5. Cell Proliferation Assay

For cell proliferation assay, CD8⁺ T-cells treated with siRNA target SiNC or siRNA control SiNC was compared to the cell control to follow the proliferation of the cells at day 1 and day 3 using the same protocol for *CellTiter-Glo® Luminescent Cell Viability Assay* as described above. Sample without any treatment in each day was used as a control and calculated as 100% cell proliferation.

SPECIFIC PROTOCOLS FOR CHAPTER B1

B1.1. Cell Viability after NIR Light Treatment

To study effects of NIR irradiation, the cells were exposed to 974 nm light at 1 W/cm² (L4-9897510-100M, JDS Uniphase Corporation) for 0, 15 and 30 min with and

without RuEI&UCNP@hmSiO₂ (150 µg/mL) and then incubated at 37 °C in a CO₂ incubator for 24 h. The samples without NIR irradiation were covered with a black plate. For each cell type, all control and treatments were performed in the same plate. After that, cell viability was evaluated by MTS assay using CellTiter 96[®] aqueous one solution cell proliferation assay (Promega, USA) according to the manufacturer's protocol. This assay is based on NADPH or NADH produced by dehydrogenase enzymes in metabolically active cells that can reduce MTS tetrazolium compound [3-(4,5-dimethylthiazol-2-yl)-5-(3-carboxymethoxyphenyl)-2-(4-sulfophenyl)-2H-tetrazolium, inner salt] into a soluble-colored formazan product which can be detected at 490 nm by plate reader (Infinite[®] M1000, Tecan, Germany).

B1.2. Cathepsin K Inhibition Assay with EI and RuEI

The cathepsin K activity assay was performed in a 96-well plate at a total volume of 100 µL and incubated at 37 °C. Recombinant human cathepsin K (Enzo Life Sciences, USA) with a final concentration of 2 nM was used to study the catalytic activity of 100 µM Z-Gly-Pro-Arg(GPR)-AMC, which is a fluorogenic substrate specific for cathepsin K, (Enzo Life Sciences, USA) with or without EI. Commercial cathepsin K was diluted from a stock solution to 8 nM as the working concentration with enzymatic assay buffer containing 100 mM sodium acetate buffer (pH 5.5), 8 mM DTT, 4 mM EDTA, 0.01% Triton X-100, and 1% DMSO. The enzyme solution (25 µL) and additional buffer (15 µL) were activated at 37 °C for 15 min prior to the addition of the substrate and/or EI. EI or RuEI at concentrations ranging from 0.001 to 10 µM were prepared in a reaction buffer (50 mM sodium acetate buffer pH 5.5, 2.5 mM DTT, 2.5 mM EDTA) containing 10% DMSO. Then, the EI solution (10 µL) was added to the activated enzyme solution to obtain a final DMSO concentration of 1%. Finally, the Z-GPR-AMC substrate, which was dissolved in the enzymatic assay buffer (200 µM, 50 µL), was added to the mixture and gently mixed. The fluorescent signals were kinetically measured every 3 min for 30 min by a plate reader with excitation at 365 nm and emission at 440 nm. The fluorescent intensities were converted to the percentage of enzyme activity by setting the signal obtained from the control experiment without EI as 100%. The IC₅₀ values were calculated at a reaction time of 15 min by fitting a curve with non-linear regression using the GraphPad program.

B1.3. NIR Photoinhibition of Cathepsin K

RuEI&UCNP@hmSiO₂ was prepared in a reaction buffer containing 10% DMSO. Then, the RuEI&UCNP@hmSiO₂ suspension (10 μL) was added to the activated enzyme solution to obtain a final concentration of 10 μg/mL. The samples were irradiated with an NIR laser at 974 nm (1 W/cm²) without or through a slice of chicken tissue (1 mm thick) at various exposure times (0, 7, 15, and 30 min). The plate was placed in a cold-water bath during irradiation. Finally, the Z-GPR-AMC substrate (200 μM, 50 μL) was added, and the fluorescent signal was kinetically measured every 3 min for 30 min as previously mentioned. The enzyme activity is expressed as percentage of the activity. The percentage of the activity at 100% was calculated from the control experiment without RuEI&UCNP@hmSiO₂ and NIR treatment, which were performed in parallel.

B1.4. Cathepsin K Activity Assay of Live Cells

100 μL of live cells (2-days culture starting from approximately 10⁶ cells/mL per well) were incubated with 5 μM of Abz-HPGGPQ-EDDnp, a highly cathepsin K specific fluorogenic substrate (Anaspec) at 37 °C in a 96-well plate. Abz-HPGGPQ-EDDnp substrate was dissolved in dimethylformamide at a concentration of 1 mM stock solution, kept at -20 °C until used and diluted to 0.1 mM working substrate solution in the reaction buffer. The fluorescent signals of enzymatic hydrolysis were monitored until 24 h. *Cathepsin K inhibition assay with EI in live cells*: All cell lines resuspended in DMEM complete medium were seeded at a density of 5,000 cell per well in a 96-well plate for 48 h. After medium removal, the reaction was carried out in the absence or presence of EI at concentration in a range of 0.1-1000 μM in the reaction buffer containing 1 % DMSO. The inhibition was allowed to occur for 1 h at 37 °C before adding Abz-HPGGPQ-EDDnp substrate at final concentration of 5 μM. After that, the fluorescent signals were measured at 5 h of incubation. The IC₅₀ values were calculated at 15 min of reaction time by fitting a curve with non-linear regression using GraphPad Program.

B1.5. NIR Photoinhibition of Cathepsin K in Live Cells

To perform NIR-controlled inhibition assay in cells, all cell lines resuspended in DMEM complete medium were seeded at a density of 5,000 cells per well in a 96-well plate for 72 h. After medium removal, the reaction was carried out in the absence or presence of RuEI&UCNP@hmSiO₂ (150 µg/mL). RuEI&UCNP@hmSiO₂ and cells were incubated for 1 h at 37 °C prior to treatment with NIR at 0, 7, and 15 min. The inhibition was then allowed to occur for 1 h at 37 °C before adding Abz-HPGGPQ-EDDnp substrate at final concentration of 5 µM. The fluorescent signals were measured at 3 h after incubation. Enzyme activity was exhibited as percentage of activity. The percentage of activity at 100% was calculated from the control experiment without the NPs and NIR treatment which were performed in parallel.

SPECIFIC PROTOCOLS FOR CHAPTER B2

B2.1. Cell Viability after Red Light Treatment

After cell preparation, the cells were treated with Ru4 solutions at final concentration of 10 and 20 µg/mL for 4 h prior to irradiation with laser (671 nm) through a sliced piece of 8 mm-pork tissue for 30 min and further incubated at 37°C in CO₂-incubator for 24 h. Samples without light treatment were covered with aluminium foil and performed parallelly. After that, cell viability was evaluated by using the CellTiter-Glo® luminescent cell viability assay (Promega, USA) as described above.

SPECIFIC PROTOCOLS FOR CHAPTER B3

B3.1. Cell Viability after Red Light Treatment in Hypoxic condition

After cell preparation, the cells were incubated with various concentrations of Ru complex from 1.25-50 µg mL⁻¹ for 4 h before irradiation or with various concentrations of micelles from 6.25 to 150 µg mL⁻¹ for 6 h before irradiation. To investigate the toxic effect of micelles under hypoxia, the cells were prepared as described above except for using the medium containing 100 × 10⁻⁶ M of cobalt chloride (CoCl₂) to switch on hypoxic cellular response for 24 h. Then, the cells were treated with 25 µg mL⁻¹ of micelles for 6 h before irradiation. After exposed to the light,

the cells were incubated at 37 °C for 24 h. Samples without being treated with light were covered with a piece of Al foil and performed in parallel. After that, cell viability was evaluated by using the CellTiter-Glo® luminescent assay as described above.

SPECIFIC PROTOCOLS FOR CHAPTER C1

C1.1. Cell Preparation

For the *in vitro* TTA-UC measurements, HeLa cells were seeded at a density of 6×10^4 cells in 35 mm Petri-dish with a glass coverslip bottom (μ -Dish, 7 mm walls, Ibidi, Germany) and cultured for 24 h in DMEM complete medium. After that, the cells were further incubated for 24 h with the nanocapsules at 6 mg/mL (UCNC1, UCNC2). Then, the cells were washed 5 times with 500 μ L of DMEM to remove the remaining nanocapsules outside of the cells and finally suspended in 1 mL DMEM. Subsequently, the HeLa cells incubated with UCNCs were placed into temperature-controlled sample holder and the variation of the temperature starting from 22 °C to 40 °C was controlled.

Summary and Outlook

Advances in nanotechnology have brought together different scientific fields to join and create a wide variety of nanocapsules, which can be beneficially applied in many bio-applications including diagnostics, therapy, imaging and sensors. However, the broad ranges of either commercial or lab-made nanocapsules do not match every kind of application and also fail to match every type of cell. Therefore, nanocapsules firstly need to be tested for their safe use in each application and for various cell types. Subsequently, internalization will be the second basic biological question that needs to be answered if they show proven biocompatibility. The rest of the experiments are mainly performed to support their potential use *in vitro* or *in vivo* according to specific purposes.

Chapter A points out the importance of uptake studies in the very well-known “hard to transfect cell – T-cell”. Starting from **Part [A1]**, the study emphasizes investigation of the crucial physicochemical properties of the silica nanocapsules (SiNCs) that affect cellular uptake and toxicity in T-cells. The major impact of cellular uptake and viability was found to be dose and size dependence. The findings suggest the critical criteria have to be carefully taken into account for SiNC design and also *in vitro* culture conditions, especially serum concentrations that are able to maintain cell viability and facilitate uptake. Applying all knowledge to the next **Part [A2]**, this study used optimally designed SiNCs as nanocarriers containing siRNA to knockdown PD-L1, a potent T-cell exhausting factor. The PD-L1 knockdown efficiency in T-cells at mRNA level was higher than at the protein level due to the background protein. However, the knockdown effect was strong enough to increase cell proliferation and cell function biomarkers. This result can be improved by blocking the pre-existing PD-L1 using anti-PD-L1 antibody, either directly applied in the culture or attached to the SiNCs surface, which provides a double inhibition system both at the mRNA level by siRNA and the protein level by antibody. Because T-cells are highly sensitive immune cells, many factors can affect not only their cell viability, but also their immune responses e.g. cytokine secretion, specific biomarker expression and activation state. It is worth noting that the nanocarriers used in T-cells have to be considered carefully in

terms of the possible immune reaction consequences before applying *in vivo* T-cell immunotherapy.

Chapters B and C employ the advantage of light as a responsive stimulus to trigger the light sensitive system for different purposes: control the release of enzyme inhibitors or anti-cancer drugs in **Chapter B**; report cellular temperature in **Chapter C**.

In **Publication [B1]**, NIR light was used to activate the upconversion nanoparticle, which was loaded inside mesoporous silica nanocapsules resulting in the emission of blue light, which is able to cleave the light-sensitive bond of ruthenium (Ru) complex, then uncaging the Cathepsin K enzyme inhibitor and finally inhibiting enzyme activity. Red light was used instead of NIR light in **Publications [B2] and [B3]** because the wavelength of red light is in the region of the therapeutic window and stronger than NIR light. Red light was used to trigger the Ru complex in **Publication [B2]** and showed deep penetration through the thickness of the tissue, which is still able to cleave the light sensitive bond, uncage the toxic product and finally kill cancer cells. In **Publication [B3]**, the Ru complex conjugated anti-cancer drug chlorambucil was released from micelles by red light stimulation and efficiently killed cancer cells, even under hypoxia simulated *in vitro* and tumor-bearing mouse *in vivo*. All light sensitive releasing systems here exhibited promising results that could be beneficially applied in various kinds of therapeutic agents and cancer cells for cancer therapy through a non-invasive strategy and spatiotemporal control.

Similar to **Publication [B1]**, light triggered-polymeric upconversion nanocapsules (UCNCs) were developed in **Part [C1]**. The system utilized the temperature dependence of triplet-triplet annihilation upconversion (TTA-UC) phenomenon for use as a nanothermometer in living cells, which was successfully obtained in the range of 22 to 40°C. At high temperatures in the range of 40-45°C, a difference in cellular temperature of only 1°C is enough to kill cancer cells while not affecting healthy cells. Therefore, it is of great interest to develop a highly sensitive real-time temperature detection system at the cellular level that could be used to track the metabolic reaction before and after drug treatment or distinguish cancer cells from

non-cancerous cells. This has led to the development of novel therapy and diagnostic tools in medicine.

Zusammenfassung

Durch Fortschritte in der Nanotechnologie werden verschiedene wissenschaftliche Bereiche zusammengebracht. Eine Vielzahl von Nanokapseln werden in unterschiedlichen Bioapplikationen u.a. in der medizinischen Diagnostik, der Therapie, dem Imaging oder Sensoring angewendet. Jedoch kann nicht jede Nanokapsel für jede Anwendung und jeden Zelltyp eingesetzt werden. Daher müssen die Nanokapseln für jede spezielle Anwendung und jeden Zelltyp zunächst hinsichtlich ihrer biologische Verträglichkeit untersucht werden. Wenn diese biokompatibel sind, ist die Internalisierung der Nanokapseln in verschiedene Zelltypen die zweite grundlegende biologische Frage.

In **Kapitel A** wurden Aufnahme studie in die sehr bekannten "schwer zu transfizierenden" T-Zellen untersucht. In der **Teil [A1]** wurden die physikochemischen Eigenschaften von Siliciumdioxid-Nanokapseln (SiNCs) und deren Einfluss auf die zelluläre Aufnahme und Toxizität in T-Zellen analysiert. Es zeigte sich, dass sowohl die Dosis als auch die Größe die Zellaufnahme und Toxizität erheblich beeinflussen. Diese Ergebnisse beschreiben kritische Faktoren, die für die Entwicklung von SiNC sorgfältig berücksichtigen werden sollten. Weiterhin, wurde in diesen Versuchen der Einfluss von Serum auf die Zellinteraktion *in vitro* untersucht. Es zeigte sich, dass Serum einen signifikanten Einfluss auf die Zellaufnahme und Toxizität hat. In der **Teil [A2]** wurden siRNA beladene SiNC verwendet, wodurch ein Knock-Down von PD-L1, einem T-Zell-Erschöpfungsmarker, hervorgerufen werden sollte. Die PD-L1-Knockdown-Effizienz in T-Zellen war auf mRNA-Ebene höher als auf Proteinebene. Der Knockdown Effekt war jedoch ausreichend um die Zellproliferation und Zellfunktion zu erhöhen. Diese Ergebnisse könnten durch das Blocken des PD-L1 Rezeptors (bsp. in Form von anti-PD-L1-Antikörpern) verbessert werden. Die Antikörper können entweder direkt in der Zellkultur zugesetzt werden oder könnten auf die Oberfläche der SiNCs angebracht werden. Dadurch entsteht ein Doppelinhibitionssystem auf mRNA-Ebene (siRNA) und Protein-Ebene (Antikörper). Da T-Zellen hochempfindliche Immunzellen sind, können viele Faktoren nicht nur ihre Lebensfähigkeit beeinflussen, sondern auch ihre Immunantworten z.B. Zytokinsekretion, Biomarker-Expression und ihren Aktivierungszustand. Deshalb ist

es von großer Bedeutung, dass bevor Nanocarrier *in vivo* für die T-Zell-Immuntherapie eingesetzt werden können, diese erst hinsichtlich ihrer immunologischen Reaktion untersucht werden.

In den **Kapiteln B** und **C** wurden lichtempfindliche nanodimensionale Trägersystem in verschiedenen Anwendungen wie z.B für die lichtgesteuerte Freisetzung von Enzymhemmern und Krebsmedikamenten oder für das Monitoring der Zelltemperatur (**Kapitel C**) verwendet.

In Publikation **[B1]** wurden mesoporöse Silica-Nanokapseln mit so genannten "Upconversion-Nanopartikeln" beladen. Durch NIR-Licht konnten diese aktiviert werden, wodurch es zur Emission von blauem Licht kam. Dadurch wurde die Bindung an den Ruthenium (Ru)-Komplex gespalten und es konnte der Cathepsin-K-Enzym Inhibitor freigesetzt werden, welcher die Enzymaktivität hemmte. Rotes Licht wurde in **Publikationen [B2]** und **[B3]** anstelle von NIR-Licht verwendet, da die Wellenlänge des roten Lichts in einem therapeutisch relevanten Bereich liegt und stärker ist als das NIR-Licht. Rotes Licht wurde als Trigger für das Anregen des Ru-Komplexes in Publikation **[B2]** verwendet. Durch rotes Licht kam es zum Eindringen in dickes Gewebe. Auch dort konnte die lichtempfindliche Bindung gespalten werden, wodurch das toxische Produkt freigesetzt wurde und die Krebszelle schließlich abgetötet werden konnte. In Publikation **[B3]** wurde das mit Ru-Komplex konjugierte Antikrebsmedikament Chlorambucil durch Rotlichtstimulation aus Mizellen freigesetzt und tötete Krebszellen selbst unter Hypoxie *in vitro*, und auch intumortragenden Mäusen *in vivo*. Alle lichtempfindlichen Freisetzungssysteme zeigten hier vielversprechende Ergebnisse, die aufgrund der nichtinvasiven Anwendung und der räumlich-zeitlichen Kontrolle in verschiedenen Arten von Therapeutika und für die Krebstherapie eingesetzt werden können.

Ähnlich wie in der **Publikation [B1]** wurden in der **Teil [C1]** lichtgesteuerte polymere Upconversion-Nanokapseln (UCNCs) entwickelt. Das System nutzte die Temperaturabhängigkeit des Phänomens der Triplett-Triplett-Annihilations-Aufwärtskonvertierung (TTA-UC) zur Verwendung von Nanokapseln als Nanothermometer in lebenden Zellen in einem Bereich von 22°C bis 40°C. Bei höheren Temperaturen in einem Bereich von 40°C bis 45°C reichte bereits ein Unterschied von

1°C in der Zelltemperatur aus, um Krebszellen abzutöten, nicht jedoch gesunde Zellen. Daher ist es von großem Interesse, ein hochempfindliches Echtzeit-Temperaturerfassungssystem auf zellulärer Ebene zu entwickeln, das zum Beispiel die Stoffwechselreaktion vor und nach der Medikamentenbehandlung verfolgt oder Krebszellen von gesunden Zellen unterscheidet. Dies könnte Fortschritte in Krebstherapie bringen oder auch als Diagnosewerkzeuge in der Medizin genutzt werden.

Literature

Combined references from the general introduction (page 4-7) and the individual introduction parts in chapter A, B and C.

- [Z-1] Vert, M., Doi, Y., Hellwich, K.-H., Hess, M., Hodge, P., Kubisa, P., Rinaudo, M., & Schué, F. (2012). Terminology for biorelated polymers and applications (IUPAC Recommendations 2012) (Vol. 84). *Pure Appl. Chem.* 84, 377–410.
- [Z-2] Lee, B. K., Yun, Y. H., & Park, K. (2015). Smart nanoparticles for drug delivery: boundaries and opportunities. *Chem Eng Sci.*, 125, 158-164.
- [Z-3] Mohanraj, V.J. and Chen, Y. (2007). Nanoparticles - A review. *Trop J Pharm Res.* 5 (1), 561-573.
- [Z-4] Jeevanandam, J., Barhoum, A., Chan, Y. S., Dufresne, A., & Danquah, M. K. (2018). Review on nanoparticles and nanostructured materials: history, sources, toxicity and regulations. *Beilstein J Nanotechnol*, 9, 1050-1074.
- [Z-5] Klaessig, F., Marrapese, M., & Abe, S. (2011). Chapter 2 - Current Perspectives in Nanotechnology Terminology and Nomenclature. In V. Murashov and J. Howard (Eds.), *Nanotechnology Standards, Nanostructure Science and Technology* (pp. 21-52). Pennsylvania: Springer Science+Business Media.
- [Z-6] House of Lords Science and Technology Committee: Nanotechnologies and Food, vol. I and II. (2010). Available from: <http://www.publications.parliament.uk/pa/ld200910/ldselect/ldsctech/22/22i.pdf>. Accessed 27 Jan 2019.
- [Z-7] Yu, X., Valmikinathan, C. M., Rogers, A., & Wang, J. (2007). Chapter 5 - Nanotechnology and Drug Delivery. In K. E. Gonsalves, C. R. Halberstadt, C. T. Laurencin & L. S. Nair (Eds.), *Biomedical Nanostructures* (pp. 93-113). New Jersey: John Wiley & Sons
- [Z-8] Richards, D. A., Maruani, A., & Chudasama, V. (2017). Antibody fragments as nanoparticle targeting ligands: a step in the right direction. *Chem Sci*, 8(1), 63-77.
- [Z-9] Baghaban-Eslaminejad, M., Oryan, A., Kamali, A., & Moshiri, A. (2017). Chapter 25 - The role of nanomedicine, nanotechnology, and nanostructures on oral bone healing, modeling, and remodeling. In E. Andronescu & A. M. Grumezescu (Eds.), *Nanostructures for Oral Medicine* (pp. 777-832). Amsterdam: Elsevier.
- [Z-10] Kothamasu, P., Kanumur, H., Ravur, N., Maddu, C., Parasuramrajam, R., & Thangavel, S. (2012). Nanocapsules: the weapons for novel drug delivery systems. *Bioimpacts*, 2(2), 71-81.

-
- [Z-11] Christoforidis, J. B., Chang, S., Jiang, A., Wang, J., & Cebulla, C. M. (2012). Intravitreal devices for the treatment of vitreous inflammation. *Mediators Inflamm*, 2012, 126463.
- [Z-12] Zhu, X., Anquillare, E. L. B., Farokhzad, O. C., & Shi, J. (2014). Chapter 22 - Polymer- and Protein-Based Nanotechnologies for Cancer Theranostics. In X. Chen & S. Wong (Eds.), *Cancer Theranostics* (pp. 419-436). Amsterdam: Elsevier.
- [Z-13] Houot, R., Schultz, L. M., Marabelle, A., & Kohrt, H. (2015). T-cell-based immunotherapy: adoptive cell transfer and checkpoint inhibition. *Cancer Immunol Res.*, 3(10), 1115-1122.
- [Z-14] Perica, K., Varela, J. C., Oelke, M., & Schneck, J. (2015). Adoptive T cell immunotherapy for cancer. *Rambam Maimonides Med J*, 6(1), e0004.
- [Z-15] Wang, M., Yin, B., Wang, H. Y., & Wang, R.-F. (2014). Current advances in T-cell-based cancer immunotherapy. *Immunotherapy*, 6(12), 1265-1278.
- [Z-16] Baruch, E. N., Berg, A. L., Besser, M. J., Schachter, J., & Markel, G. (2017). Adoptive T cell therapy: An overview of obstacles and opportunities. *Cancer*, 123(S11), 2154-2162.
- [Z-17] Li, S. Y., Liu, Y., Xu, C. F., Shen, S., Sun, R., Du, X. J., Xia, J. X., Zhu Y. H., & Wang, J. (2016). Restoring anti-tumor functions of T cells via nanoparticle-mediated immune checkpoint modulation. *J Control Release*, 231, 17-28.
- [Z-18] Zhang, Y., Hsu, B. Y., Ren, C., Li, X., & Wang, J. (2015). Silica-based nanocapsules: synthesis, structure control and biomedical applications. *Chem Soc Rev*, 44(1), 315-335.
- [Z-19] Freeley, M., & Long, A. (2013). Advances in siRNA delivery to T-cells: potential clinical applications for inflammatory disease, cancer and infection. *Biochem J*, 455(2), 133-147.
- [Z-20] Alberts, B., Johnson, A., Lewis, J., Raff, M., Roberts, K., & Walter, P. (2002). Chapter 25 - Pathogens, Infection, and Innate Immunity. In *Molecular Biology of the Cell*. (Forth Edition). New York: Garland Science. Available from: <https://www.ncbi.nlm.nih.gov/books/NBK26846/>
- [Z-21] Porcelli, S. A. (2017). Chapter 17 - Innate Immunity. In G. S. Firestein, R. C. Budd, S. E. Gabriel, I. B. McInnes, & J. R. O'Dell (Eds.), *Kelley and Firestein's Textbook of Rheumatology (Tenth Edition)* (pp. 274-287): Elsevier.
- [Z-22] Bonilla, F. A., & Oettgen, H. C. (2010). Adaptive immunity. *J Allergy Clin Immunol*, 125(2 Suppl 2), S33-40.
- [Z-23] Merlo, L. M. F., & Mandik-Nayak, L. (2013). Chapter 3 - Adaptive Immunity: B Cells and Antibodies. In G. C. Prendergast & E. M. Jaffee (Eds.), *Cancer Immunotherapy (Second Edition)* (pp. 25-40). San Diego: Academic Press.
- [Z-24] Alberts, B., Johnson, A., Lewis, J., Raff, M., Roberts, K., & Walter, P. (2002). Chapter 24 - The Adaptive Immune System. In *Molecular Biology of the Cell*.

- (Forth Edition). New York: Garland Science. Available from: <https://www.ncbi.nlm.nih.gov/books/NBK21070/>
- [Z-25] Fontenot, A. P., & Simonian, P. L. (2016). 13 - Adaptive Immunity. In V. C. Broaddus, R. J. Mason, J. D. Ernst, T. E. King, S. C. Lazarus, J. F. Murray, J. A. Nadel, A. S. Slutsky, & M. B. Gotway (Eds.), *Murray and Nadel's Textbook of Respiratory Medicine (Sixth Edition)* (pp. 206-224.e203). Philadelphia: W.B. Saunders.
- [Z-26] Moticka, E. J. (2016). Chapter 2 - Hallmarks of the Adaptive Immune Responses. In E. J. Moticka (Ed.), *A Historical Perspective on Evidence-Based Immunology* (pp. 9-19). Amsterdam: Elsevier.
- [Z-27] Chen, D. S., & Mellman, I. (2013). Oncology meets immunology: the cancer-immunity cycle. *Immunity*, 39(1), 1-10.
- [Z-28] Larsson, M., Messmer, D., Somersan, S., Fonteneau, J.-F., Donahoe, S. M., Lee, M., Dunbar, P. R., Cerundolo, V., Julkunen, I., Nixon, D. F. & Bhardwaj, N. (2000). Requirement of Mature Dendritic Cells for Efficient Activation of Influenza A-Specific Memory CD8⁺ T Cells. *J Immunol*, 165(3), 1182-1190.
- [Z-29] Albert, M. L., Jegathesan, M., & Darnell, R. B. (2001). Dendritic cell maturation is required for the cross-tolerization of CD8⁺ T cells. *Nat Immunol*, 2(11), 1010-1017.
- [Z-30] Nagai, T. (2017). Difference between Immature Dendritic Cells (imDCs) and Mature Dendritic Cells (mDCs) Derived from Human Monocytes. *J Immunol*, 198(1 Supplement), 201.16.
- [Z-31] Peter, M. E., Hadji, A., Murmann, A. E., Brockway, S., Putzbach, W., Pattanayak, A., & Ceppi, P. (2015). The role of CD95 and CD95 ligand in cancer. *Cell Death Differ*, 22(4), 549-559.
- [Z-32] Volpe, E., Sambucci, M., Battistini, L., & Borsellino, G. (2016). Fas-Fas ligand: checkpoint of t cell functions in multiple sclerosis. *Front Immunol*, 7, 382.
- [Z-33] Messerschmidt, J. L., Prendergast, G. C., & Messerschmidt, G. L. (2016). How cancers escape immune destruction and mechanisms of action for the new significantly active immune therapies: helping nonimmunologists decipher recent advances. *Oncologist*, 21(2), 233-243.
- [Z-34] Bhatia, A., & Kumar, Y. (2011). Cancer-immune equilibrium: questions unanswered. *Cancer Microenviron*, 4(2), 209-217.
- [Z-35] Pitt, J. M., Vetizou, M., Daillere, R., Roberti, M. P., Yamazaki, T., Routy, B., Lepage, P., Boneca, I. G., Chamaillard, M., Kroemer G., & Zitvogel, L. (2016). Resistance mechanisms to immune-checkpoint blockade in cancer: tumor-intrinsic and -extrinsic factors. *Immunity*, 44(6), 1255-1269.
- [Z-36] Topalian, S. L., Drake, C. G., & Pardoll, D. M. (2015). Immune checkpoint blockade: a common denominator approach to cancer therapy. *Cancer Cell*, 27(4), 450-461.

-
- [Z-37] Sharma, P., & Allison, J. P. (2015). Immune checkpoint targeting in cancer therapy: toward combination strategies with curative potential. *Cell*, 161(2), 205-214.
- [Z-38] Shin, D. S., & Ribas, A. (2015). The evolution of checkpoint blockade as a cancer therapy: what's here, what's next? *Curr Opin Immunol*, 33, 23-35.
- [Z-39] Cohen, J. E., Merims, S., Frank, S., Engelstein, R., Peretz, T., & Lotem, M. (2017). Adoptive cell therapy: past, present and future. *Immunotherapy*, 9(2), 183-196.
- [Z-40] Maus, M. V., Fraietta, J. A., Levine, B. L., Kalos, M., Zhao, Y., & June, C. H. (2014). Adoptive immunotherapy for cancer or viruses. *Annu Rev Immunol*, 32, 189-225.
- [Z-41] Shalek, A. K., Gaublomme, J. T., Wang, L., Yosef, N., Chevrier, N., Andersen, M. S., Robinson, J. T., Pochet, N., Neuberg, D., Gertner, R. S., Amit, I., Brown, J. R., Hacohen, N., Regev, A., Wu C. J., & Park, H. (2012). Nanowire-mediated delivery enables functional interrogation of primary immune cells: application to the analysis of chronic lymphocytic leukemia. *Nano Lett*, 12(12), 6498-6504.
- [Z-42] Dardalhon, V., Herpers, B., Noraz, N., Pflumio, F., Guetard, D., Leveau, C., Dubart-Kupperschmitt, A., Charneau, P., & Taylor, N. (2001). Lentivirus-mediated gene transfer in primary T cells is enhanced by a central DNA flap. *Gene Therapy*, 8, 190-198.
- [Z-43] McManus, M. T., Haines, B. B., Dillon, C. P., Whitehurst, C. E., van Parijs, L., Chen, J., & Sharp, P. A. (2002). Small interfering RNA-mediated gene silencing in T lymphocytes. *J Immunol*, 169(10), 5754-5760.
- [Z-44] Liu, Z., Winters, M., Holodniy, M., & Dai, H. (2007). siRNA delivery into human T cells and primary cells with carbon-nanotube transporters. *Angew Chem Int Ed Engl*, 46(12), 2023-2027.
- [Z-45] Lee, J., Yun, K. S., Choi, C. S., Shin, S. H., Ban, H. S., Rhim, T., Lee, S. K., & Lee, K. Y. (2012). T cell-specific siRNA delivery using antibody-conjugated chitosan nanoparticles. *Bioconjug Chem*, 23(6), 1174-1180.
- [Z-46] Yosef, N., Shalek, A. K., Gaublomme, J. T., Jin, H., Lee, Y., Awasthi, A., Wu, C., Karwacz, K., Xiao, S., Jorgolli, M., Gennert, D., Satija, R., Shakya, A., Lu, D. Y., Trombetta, J. J., Pillai, M. R., Ratcliffe, P. J., Coleman, M. L., Bix, M., Tantin, D., Park, H., Kuchroo, V. K., & Regev, A. (2013). Dynamic regulatory network controlling TH17 cell differentiation. *Nature*, 496(7446), 461-468.
- [Z-47] Weber, N., Ortega, P., Clemente, M. I., Shcharbin, D., Bryszewska, M., de la Mata, F. J., Gomez, R., & Munoz-Fernandez, M. A. (2008). Characterization of carbosilane dendrimers as effective carriers of siRNA to HIV-infected lymphocytes. *J Control Release*, 132(1), 55-64.
- [Z-48] Zhou, J., Neff, C. P., Liu, X., Zhang, J., Li, H., Smith, D. D., Swiderski, P., Aboellail, T., Huang, Y., Du, Q., Liang, Z., Peng, L., Akkina R., & Rossi, J. J. (2011). Systemic administration of combinatorial dsRNAs via nanoparticles

- efficiently suppresses HIV-1 infection in humanized mice. *Mol Ther*, 19(12), 2228-2238.
- [Z-49] Felber, A. E., Castagner, B., Elsabahy, M., Deleavey, G. F., Damha, M. J., & Leroux, J. C. (2011). siRNA nanocarriers based on methacrylic acid copolymers. *J Control Release*, 152(1), 159-167.
- [Z-50] Peer, D., Park, E. J., Morishita, Y., Carman, C. V., & Shimaoka, M. (2008). Systemic leukocyte-directed siRNA delivery revealing cyclin D1 as an anti-inflammatory target. *Science (New York, N.Y.)*, 319(5863), 627-630.
- [Z-51] Frick, S. U., Domogalla, M. P., Baier, G., Wurm, F. R., Mailänder, V., Landfester, K., & Steinbrink, K. (2016). Interleukin-2 functionalized nanocapsules for T cell-based immunotherapy. *ACS Nano*, 10(10), 9216-9226.
- [Z-52] Chakraborty, S., & Rahman, T. (2012). The difficulties in cancer treatment. *Ecancermedalscience*, 6, ed16.
- [Z-53] Vinay, D. S., Ryan, E. P., Pawelec, G., Talib, W. H., Stagg, J., Elkord, E., Lichtor, T., Decker, W. K., Whelan, R. L., Kumara, H. M. C. S., Signori, E., Honoki, K., Georgakilas, A. G., Amin, A., Helferich, W. G., Boosani, C. S., Guha, G., Ciriolo, M. R., Chen, S., Mohammed, S. I., Azmi, A. S., Keith, W. N., Bilslund, A., Bhakta, D., Halicka, D., Fujii, H., Aquilano, K., Ashraf, S. S., Nowsheen, S., Yang, X., Choi, B. K., Kwon, B.S. (2015). Immune evasion in cancer: Mechanistic basis and therapeutic strategies. *Semin Cancer Biol*, 35 Suppl, S185-S198.
- [Z-54] Lyratzopoulos, G., Wardle, J., & Rubin, G. (2014). Rethinking diagnostic delay in cancer: how difficult is the diagnosis? *BMJ*, 349, g7400.
- [Z-55] Dhani, N., Fyles, A., Hedley, D., & Milosevic, M. (2015). The clinical significance of hypoxia in human cancers. *Semin Nucl Med*, 45(2), 110-121.
- [Z-56] Patel, A., & Sant, S. (2016). Hypoxic tumor microenvironment: Opportunities to develop targeted therapies. *Biotechnol Adv*, 34(5), 803-812.
- [Z-57] Petrova, V., Annicchiarico-Petruzzelli, M., Melino, G., & Amelio, I. (2018). The hypoxic tumour microenvironment. *Oncogenesis*, 7(1), 10.
- [Z-58] Shen, S., Zhu, C., Huo, D., Yang, M., Xue, J., & Xia, Y. (2017). A hybrid nanomaterial for the controlled generation of free radicals and oxidative destruction of hypoxic cancer cells. *Angew Chem Int Ed Engl*, 56(30), 8801-8804.
- [Z-59] Hu, Q., Sun, W., Wang, C., & Gu, Z. (2016). Recent advances of cocktail chemotherapy by combination drug delivery systems. *Adv Drug Deliv Rev*, 98, 19-34.
- [Z-60] Liu, B., Ezeogu, L., Zellmer, L., Yu, B., Xu, N., & Joshua Liao, D. (2015). Protecting the normal in order to better kill the cancer. *Cancer Med*, 4(9), 1394-1403.
- [Z-61] McDermott, M., Eustace, A. J., Busschots, S., Breen, L., Crown, J., Clynes, M., O'Donovan N., & Stordal, B. (2014). In vitro development of chemotherapy and

- targeted therapy drug-resistant cancer cell lines: a practical guide with case studies. *Front Oncol*, 4, 40.
- [Z-62] Kushwaha, S. K. S., Rastogi, A., Rai, A. K. & Singh, S. (2012). Novel drug delivery system for anticancer drug: A review. *Int J Pharmtech Res.* 4. 542-553.
- [Z-63] Cheng, L., Wang, C., Feng, L., Yang, K., & Liu, Z. (2014). Functional nanomaterials for phototherapies of cancer. *Chem Rev*, 114(21), 10869-10939.
- [Z-64] Avci, P., Gupta, A., Sadasivam, M., Vecchio, D., Pam, Z., Pam, N., & Hamblin, M. R. (2013). Low-level laser (light) therapy (LLLT) in skin: stimulating, healing, restoring. *Seminars in cutaneous medicine and surgery*, 32(1), 41-52.
- [Z-65] Linsley, C. S., & Wu, B. M. (2017). Recent advances in light-responsive on-demand drug-delivery systems. *Ther deliv*, 8(2), 89-107.
- [Z-66] Ding, C., Tong, L., Feng, J., & Fu, J. (2016). Recent advances in stimuli-responsive release function drug delivery systems for tumor treatment. *Molecules*, 21, 1715.
- [Z-67] Schwalfenberg, G. K. (2012). The alkaline diet: is there evidence that an alkaline pH diet benefits health? *J Environ Public Health*, 2012, 727630.
- [Z-68] Lisanti, M. P., Martinez-Outschoorn, U. E., Lin, Z., Pavlides, S., Whitaker-Menezes, D., Pestell, R. G., Howell, A., & Sotgia, F. (2011). Hydrogen peroxide fuels aging, inflammation, cancer metabolism and metastasis: the seed and soil also needs "fertilizer". *Cell Cycle*, 10(15), 2440-2449.
- [Z-69] Sharifzadeh, G., & Hosseinkhani, H. (2017). Biomolecule-responsive hydrogels in medicine. *Adv Healthc Mater*, 6(24), 1700801.
- [Z-70] Kim, Y.-J., & Matsunaga, Y. T. (2017). Thermo-responsive polymers and their application as smart biomaterials. *J Mater Chem B*, 5(23), 4307-4321.
- [Z-71] Senapati, S., Mahanta, A. K., Kumar, S., & Maiti, P. (2018). Controlled drug delivery vehicles for cancer treatment and their performance. *Signal Transduct Target Ther*, 3, 7.
- [Z-72] Raza, A., Hayat, U., Rasheed, T., Bilal, M., & Iqbal, H. M. N. (2018). "Smart" materials-based near-infrared light-responsive drug delivery systems for cancer treatment: A review. *J Mater Res Technol.* doi:<https://doi.org/10.1016/j.jmrt.2018.03.007>
- [Z-73] Cui, L., Zhang, F., Wang, Q., Lin, H., Yang, C., Zhang, T., Tong, R., An, N., & Qu, F. (2015). NIR light responsive core-shell nanocontainers for drug delivery. *Journal of Materials Chemistry B*, 3(35), 7046-7054.
- [Z-74] Moran, D. S., & Mendal, L. (2002). Core temperature measurement. *Sports Medicine*, 32(14), 879-885.
- [Z-75] Thrall, D. E., Page, R. L., Dewhirst, M. W., Meyer, R. E., Hoopes, P. J., & Kornegay, J. N. (1986). Temperature Measurements in Normal and Tumor Tissue of Dogs Undergoing Whole Body Hyperthermia. *Cancer Research*, 46(12 Part 1), 6229.

-
- [Z-76] Storm, F. K., & Morton, D. L. (1982) Localized hyperthermia in the treatment of cancer. *Int Adv Surg Oncol*, 5: 261-275.
- [Z-77] Repasky, E. A., Evans, S. S., & Dewhirst, M. W. (2013). Temperature matters! And why it should matter to tumor immunologists. *Cancer Immunol Res*, 1(4), 210-216.
- [Z-78] Zhu, S., Wang, J., Xie, B., Luo, Z., Lin, X., & Liao, D. J. (2015). Culture at a higher temperature mildly inhibits cancer cell growth but enhances chemotherapeutic effects by inhibiting cell-cell collaboration. *PLoS One*, 10(10), e0137042.
- [Z-79] Li, M., Liu, L., Xi, N., Wang, Y., Xiao, X., & Zhang, W. (2015). Effects of temperature and cellular interactions on the mechanics and morphology of human cancer cells investigated by atomic force microscopy. *Sci China Life Sci*, 58(9), 889-901.
- [Z-80] Qiao, J., Mu, X., & Qi, L. (2016). Construction of fluorescent polymeric nanothermometers for intracellular temperature imaging: A review. *Biosens Bioelectron*, 85, 403-413.
- [Z-81] Kim, Y.-J., & Matsunaga, Y. T. (2017). Thermo-responsive polymers and their application as smart biomaterials. *J Mater Chem B*, 5(23), 4307-4321.
- [Z-82] Gong, D., Cao, T., Han, S.-C., Zhu, X., Iqbal, A., Liu, W., Qin, W., & Guo, H. (2017). Fluorescence enhancement thermoresponsive polymer luminescent sensors based on BODIPY for intracellular temperature. *Sensors and Actuators B: Chemical*, 252, 577-583.
- [Z-83] Qin, T., Liu, B., Zhu, K., Luo, Z., Huang, Y., Pan, C., & Wang, L. (2018). Organic fluorescent thermometers: Highlights from 2013 to 2017. 102, 259-271.
- [Z-84] Ebrahimi, S., Akhlaghi, Y., Kompany-Zareh, M., & Rinnan, Å. (2014). Nucleic Acid Based Fluorescent Nanothermometers. *ACS Nano*, 8(10), 10372-10382.
- [Z-85] Maysinger, D., Ji, J., Hutter, E., & Cooper, E. (2015). Nanoparticle-based and bioengineered probes and sensors to detect physiological and pathological biomarkers in neural cells. *Front Neurosci*, 9, 480.
- [Z-86] Shang, L., Stockmar, F., Azadfar, N., & Nienhaus, G. U. (2013). Intracellular thermometry by using fluorescent gold nanoclusters. *Angew Chem Int Ed Engl*, 52(42), 11154-11157.
- [Z-87] Nakano, M., & Nagai, T. (2017). Thermometers for monitoring cellular temperature. *Journal of Photochemistry and Photobiology C: Photochemistry Reviews*, 30, 2-9.
- [Z-88] Kucsko, G., Maurer, P. C., Yao, N. Y., Kubo, M., Noh, H. J., Lo, P. K., Park, H., & Lukin, M. D. (2013). Nanometre-scale thermometry in a living cell. *Nature*, 500(7460), 54-58.

-
- [Z-89] Wang, D., Zhao, X., & Gu, Z. (2017). Advanced optoelectronic nanodevices and nanomaterials for sensing inside single living cell. *Optics Communications*, 395, 3-15.
- [Z-90] Sakaguchi, R., Kiyonaka, S., & Mori, Y. (2015). Fluorescent sensors reveal subcellular thermal changes. *Curr Opin Biotechnol*, 31, 57-64.
- [Z-91] Dowd, A., Pissuwan, D., & Cortie, M. B. (2014). Optical readout of the intracellular environment using nanoparticle transducers. *Trends Biotechnol*, 32(11), 571-577.
- [Z-92] Yang, J.-M., Yang, H., & Lin, L. (2011). Quantum dot nano thermometers reveal heterogeneous local thermogenesis in living cells. *ACS Nano*, 5(6), 5067-5071.
- [Z-93] Manatunga, D. C., de Silva, R. M., de Silva, K. M. N., de Silva, N., Bhandari, S., Yap, Y. K., & Costha, N. P. (2017). pH responsive controlled release of anti-cancer hydrophobic drugs from sodium alginate and hydroxyapatite bi-coated iron oxide nanoparticles. *Eur J Pharm Biopharm*, 117, 29-38.
- [Z-94] Zhong, J., Liu, W., Kong, L., & Morais, P. C. (2014). A new approach for highly accurate, remote temperature probing using magnetic nanoparticles. *Sci Rep*, 4, 6338.
- [Z-95] Wang, Z., Ma, X., Zong, S., Wang, Y., Chen, H., & Cui, Y. (2015). Preparation of a magnetofluorescent nano-thermometer and its targeted temperature sensing applications in living cells. *Talanta*, 131, 259-265.

Declaration

I hereby declare that I wrote the dissertation submitted without any unauthorized external assistance and used only sources acknowledged in this work. All textual passages which are appropriate verbatim or paraphrased from published and unpublished texts, as well as all information obtained from oral sources, are duly indicated and listed in accordance with bibliographical rules. In carrying out this research, I complied with the rules of standard scientific practice as formulated in the statutes of Johannes Gutenberg-University Mainz to insure standard scientific practice.

.....

(Rawewan Thiramanas)

Publication List

- [1] Zhijun Chen⁺, **Rawewan Thiramanas**⁺, Mischa Schwendy, Chaoming Xie, Sapun H. Parekh, Volker Mailänder,* and Si Wu*. *Upconversion Nanocarriers Encapsulated with Photoactivatable Ru Complexes for Near-Infrared Light-Regulated Enzyme Activity*. *Small* **2017**, 13, 1700997. (+ **Shared first**)
- [2] Wen Sun⁺, **Rawewan Thiramanas**⁺, Leonardo D. Slep, Xiaolong Zeng, Volker Mailänder,* and Si Wu*. *Photoactivation of Anticancer Ru Complexes in Deep Tissue: How Deep Can We Go?* *Chem. Eur. J.* **2017**, 23, 10832-10837. (+ **Shared first**)
- [3] Wen Sun⁺, Yan Wen⁺, **Rawewan Thiramanas**⁺, Mingjia Chen, Jianxiong Han, Ningqiang Gong, Manfred Wagner, Shuai Jiang, Michael S. Meijer, Sylvestre Bonnet, Hans-Jürgen Butt, Volker Mailänder,* Xing-Jie Liang,* Si Wu*. *Red-Light-Controlled Release of Drug-Ru Complex Conjugates from Metallopolymer Micelles for Phototherapy in Hypoxic Tumor Environments*. *Adv. Funct. Mater.* **2018**, 28, 1804227. (+ **Shared first**)
- [4] **Rawewan Thiramanas**, Shuai Jiang,* Jorge Pereira, Katharina Landfester,* Volker Mailänder.* *Silica Nanocapsule as a Suitable Nanocarrier: Uptake and Toxicity Study in T-cell*. (Manuscript in preparation).
- [5] **Rawewan Thiramanas**, Mengyi Li, Shuai Jiang, Katharina Landfester,* Volker Mailänder*. *Cellular Uptake of siRNA Loaded Nanocarrier to Knockdown PD-L1: Strategies to Improve T-cell Functions*. (Manuscript in preparation).
- [6] Banu Iyisan, **Rawewan Thiramanas**, Nadya Nazarova, Yuri Avlasevich, Volker Mailänder*, Stanislav Balouchev*, Katharina Landfester*. *Temperature Sensing in Cells by Polymeric Upconversion Nanocapsules*. (Manuscript in preparation).

Acknowledgement

[Redacted text block containing multiple paragraphs of blacked-out content]